Technische Universität München

Fakultät Wissenschaftszentrum Weihenstephan für Ernährung, Landnutzung und Umwelt

Lehrstuhl für Systembiologie der Pflanzen

Identification and characterization of
vacuolar fusion defective (*vfd*) mutants
in *Arabidopsis thaliana*

Cornelia Kolb

Vollständiger Abdruck der von der Fakultät Wissenschaftszentrum Weihenstephan für Ernährung, Landnutzung und Umwelt der Technischen Universität München zur Erlangung des akademisches Grades eines

Doktors der Naturwissenschaften

genehmigten Dissertation.

Vorsitzende: Prof. Dr. B. Poppenberger-Sieberer
Prüfer der Dissertation: 1.   Prof. Dr. C. Schwechheimer
                                        2.   Prof. Dr. R. Hückelhoven

Die Dissertation wurde am 13.03.2017 bei der Technischen Universität München eingereicht und durch die Fakultät Wissenschaftszentrum Weihenstephan für Ernährung, Landnutzung und Umwelt am 15.05.2017 angenommen.

Table of contents

List of Figures

List of Tables

List of Abbreviations

AAA	ATPase associated with a variety of cellular activities, triple A
ABA	abscisic acid
agg	large aggregates
Amp	ampicillin
AMSH	ASSOCIATED MOLECULE WITH THE SH3 DOMAIN OF STAM
ARF	ADP ribosylation factor
At	*Arabidopsis thaliana*
ATG	AUTOPHAGY
ATP	adenosine triphosphate
BFA	Brefeldin A
bub	bubble-bath
Ca	calcium
CCV	clathrin-coated vesicle(s)
cDNA	complementary DNA (copy DNA)
CDPK	calcium/calmodulin-dependent protein kinase
CHMP	CHROMATIN MODIFYING PROTEINS/ CHARGED MULTIVESICULAR BODY PROTEIN
CIPK	CBL-interacting protein kinase
CLC	CLATHRIN LIGHT CHAIN
Col	Columbia
COP	coat protein
DAG, dag	days after germination
DG	diacylglycerol
DGK	diacylglycerol kinase
DMSO	dimethyl sulfoxide
DNA	deoxyribonucleic acid
dNTP	deoxy-nucleoside triphosphate
DTT	dithiothreitol
DUB	deubiquitinating enzyme
E	glutamic acid, Glu
EEA1	EARLY ENDOSOME ANTIGEN 1
EAP	ELL-associated proteins
ELC	ELCH
EMS	ethyl methane sulfonate
ER	endoplasmic reticulum

ESCRT	ENDOSOMAL SORTING COMPLEX REQUIRED FOR TRANSPORT
Fab1	formation of aploid and binucleates
FYVE	Fab1, YOTB, Vac1, and EEA1
GA	gibberellic acid, Gibberellin A3
GAT	GGA and TOM1 domain
GEF	guanine nucleotide exchange factor
GGA	Golgi-localized, gamma adaptin ear-containing, ARF-binding protein
GFP	GREEN FLUORESCENT PROTEIN
GM	growth medium
Gln	glutamine, Q
Glu	glutamic acid, E
HGF	HEPATOCYTE GROWTH FACTOR
HRP	HORSERADISH PEROXIDASE
HRS	HGF-REGULATED TYROSINE KINASE SUBSTRATE (HGS)
HSE1	HEAT SHOCK ELEMENT 1
Hyg	hygromycin B
IAA	indole-3-acetic acid
ILV	intraluminal vesicle
IP_3	inositol tri-phosphate
IP_6	phytic acid, inositol hexakisphosphate
IPK	inositol polyphosphate multikinase
IRT1	IRON-REGULATED TRANSPORTER 1
JAMM	JAB1/MPN/MOV34 domain; MPN+
K	lysine, Lys
Kan	kanamycin
kDa	kilo Dalton
L	leucine, Leu
L*er*	Landsberg *erecta*
Leu	leucine, L
LV	lytic vacuole
Lys	lysine, K
MES	2-(N-morpholino)ethanesulfonic acid
MIM	MIT interacting motif
MIT	microtubule interacting and trafficking
MJDs	MACHADO-JOSEPH DISEASE PROTEIN DOMAIN PROTEASES
MPN+/JAMM	MPR1, PAD1 N-terminal+/JAB1/MPN/MOV34
mRNA	messenger RNA

MS	Murashige & Skoog medium
MVB	multivesicular body
MVB12	MULTIVESICULAR BODY SORTING FACTOR OF 12kDa
MVE	multivesicular endosome (=MVB)
MVP	modified vacuole phenotype
MyAP	myrosinase-associated protein
NGS	Next generation sequencing
NLS	nuclear localization signal
P	proline, Pro
PA	phosphatidic acid
PAGE	polyacrylamide gel electrophoresis
PC	phosphatidylcholine
PCR	polymerase chain reaction
PE	phosphatidylethanolamine
PEG 4000	polyethylene glycol 4000
PH	pleckstrin homology
PI	phosphoinositol
PI3K	phosphatidylinositol 3-kinase
PIP	phosphatidylinositol phosphate
PI(3)P	phosphatidylinositol-3-phosphate
PI(4)P	phosphatidylinositol-4-phosphate
PI(4,5)P$_2$	phosphatidylinositol-4,5-bisphosphate
PI(3,4,5)P$_3$	phosphatidylinositol-3,4,5-trisphosphate
PIN	PIN-FORMED
PKC	protein kinase C
PLC	phospholipase C
PLD	phospholipase D
PM	plasma membrane
PPI	polyphosphoinositide
PRAF	PH domain, RCC and FYVE
Pro	proline, P
PSV	protein storage vacuole
PVC	prevacuolar compartment
Q	glutamine, Gln
RCC	regulator of chromosome condensation
RFP	RED FLUORESCENT PROTEIN
RING	REALLY INTERESTING NEW GENE

RNA ribonucleic acid

RPN REGULATORY PARTICLE NON-ATPASE

SBM STAM binding motif

SDS sodium dodecyl sulfate

SH3 SRC-HOMOLOGY DOMAIN 3

SKD1 SUPPRESSOR OF K(+) TRANSPORT GROWTH DEFECT1

SNARE N-ETHYLMALEIMIDE-SENSITIVE FUSION (NSF) ATTACHMENT PROTEIN RECEPTOR

SNF7 SUCROSE NON-FERMENTING 7

sqRT-PCR semiquantitative real time PCR

STAM SIGNAL TRANSDUCING ADAPTOR MOLECULE

SYP SYNTAXIN OF PLANTS

T-DNA transfer DNA

TEMED tetramethylethylenediamine

TGN *trans*-Golgi network

TIP TONOPLAST INTRINSIC PROTEIN

TOM TRANSLOCASES OF THE OUTER MEMBRANE

Trp tryptophan, W

TSG101 TUMOR SUSCEPTIBILITY GENE 101

TVS, tvs transvacuolar strands

Ub, UB, UBQ ubiquitin

UBC UBIQUITIN-CONJUGATING ENZYME

UBD ubiquitin binding domain

UIM ubiquitin-interacting motif

Vac1 vacuole 1

VAMP, VAM VESICLE-ASSOCIATED MEMBRANE PROTEIN

VCL1 VACUOLELESS 1

vfd, VFD VACUOLAR FUSION DEFECTIVE

VHS Vps27p, HRS, STAM domain

VPS VACUOLAR PROTEIN SORTING

VSS vacuolar sorting signal

VSR vacuolar sorting receptor

W tryptophan, Trp

wt, WT wild-type

YOTB hypothetical *C. elegans* protein ZK632.12

Y2H yeast two-hybrid

Zn zinc

Summary

Proteins destined to the vacuole (lysosome) are transported through the endomembrane system of the cell. Proteins originating from the plasma membrane (PM) or endoplasmic reticulum (ER) are targeted to the vacuole either for degradation or storage purposes. The small protein ubiquitin is attached to cargo proteins via a post-translational modification process called ubiquitination. Ubiquitination is a reversible process and can be counteracted by deubiquitinating enzymes (DUBs), by which a free ubiquitin pool is maintained. ASSOCIATED MOLECULE WITH THE SH3 DOMAIN OF STAM (AMSH) is a deubiquitinating enzyme and belongs to the JAB1/MPN/MOV34/MPR1, PAD1 N-terminal+ (JAMM/MPN+) domain-containing DUB family. The *Arabidopsis thaliana* genome encodes three AMSH proteins. In a previous study, the *amsh3* mutant, a knockout mutant of the *AtAMSH3* gene, was identified (Isono et al., 2010). The transposon insertion in the *AtAMSH3* gene leads to seedling lethality, indicating that AMSH3 is essential for plant growth. The *amsh3* mutants lack central vacuoles, instead containing small round vacuolar structures surrounded by tonoplast membrane. Furthermore, the mutants accumulate ubiquitinated proteins, leading to the conclusion that AMSH3 is a major DUB in plants.

At the beginning of this project, a forward genetic screen by EMS mutagenesis was conducted, to identify factors that act together with or downstream of AMSH3. Mutated plant lines were selected for *amsh3*-like attributes at the seedling stage. This study presents the identification and initial characterization of *vacuolar fusion defective* (*vfd*) mutants. The *vfd* mutants show a seedling lethal phenotype, lack the central vacuole and accumulate ubiquitinated proteins. Combining classical mapping with next generation sequencing, the causative gene for the *vfd1* mutant was identified to be *FYVE1*. The *FYVE1* gene encodes a FYVE (Fab1, YOTB, Vac1, and EEA1) domain-containing protein. This result was confirmed by complementation with the wild-type gene and phenotypic rescue.

FYVE domains contain zinc finger-binding motifs and have been characterized as lipid-binding domains that are specific for phosphatidylinositol 3-phosphate. The fusion protein GFP-FYVE1 is localized to the cytosol, the nucleus and endosomal vesicles. GFP-FYVE1 is colocalising with subpopulations of the endocytosis marker protein CLATHRIN LIGHT CHAIN (CLC) and ARA7, a marker protein for late endosomes. The artificial cargo protein GFP-CT24 was missorted in the *fyve1-1* mutant embryos, indicating an influence of FYVE1 already at early steps of plant development in protein transport to protein storage vacuoles (PSVs). Experiments with the lipophilic marker dye FM4-64 and the GFP fusion protein of the plasma membrane auxin efflux transporter PIN-FORMED 2 (PIN2-GFP) showed that the *fyve1-1* mutant is impaired in endocytosis.

In conclusion, this study shows that the FYVE1 protein is a novel and essential protein in endomembrane trafficking during plant development.

Zusammenfassung

Proteine, deren Ziel die Vakuole (das Lysosom) ist, werden durch das Endomembransystem der Zelle transportiert. Proteine, die von der Plasmamembran (PM) oder dem endoplasmatischen Retikulum (ER) stammen, werden gezielt zur Vakuole transportiert, um dort entweder abgebaut oder gespeichert zu werden. Das kleine Protein Ubiquitin wird über eine posttranslationale Modifikation, genannt Ubiquitinierung, an Cargo-Proteine gebunden. Ubiquitinierung ist ein reversibler Prozess, der durch die Aktivität von deubiquitinierenden Enzymen (DUBs) aufgehoben werden kann, die dadurch einen Vorrat an freiem Ubiquitin aufrechterhalten. ASSOCIATED MOLECULE WITH THE SH3 DOMAIN OF STAM (AMSH) ist ein deubiquitinierendes Enzym und gehört zur Familie der JAB1/MPN/MOV34/MPR1, PAD1 N-terminal+ (JAMM/MPN+)-Domäne enthaltenden DUBs. Das Genom von *Arabidopsis thaliana* kodiert für drei AMSH Proteine. In einer vorhergehenden Studie wurde die *amsh3* Mutante, eine Knock-out-Mutante des *AtAMSH3* Gens identifiziert (Isono et al., 2010). Die Insertion des Transposons im *AtAMSH3* Gen führt zu Keimlingssterblichkeit und ist ein Hinweis darauf, dass AMSH3 für das Pflanzenwachstum essentiell ist. Die *amsh3* Mutante besitzt keine zentrale Vakuole, sondern enthält stattdessen kleine runde vakuoläre Strukturen, die von einer Tonoplastmembran umgeben sind. Darüber hinaus akkumulieren die Mutanten ubiquitinierte Proteine, woraus zu schließen ist, dass AMSH3 ein wichtiges DUB in Pflanzen ist.

Zu Beginn dieses Projekts wurde nach der EMS-Mutagenese ein vorwärtsgerichteter, genetischer Screen durchgeführt, um Faktoren zu identifizieren, die mit AMSH3 zusammen oder *downstream* davon agieren. Mutierte Pflanzenlinien wurden auf Keimlingsebene aufgrund von *amsh3*-ähnlichen Attributen selektiert. Diese Arbeit präsentiert die Identifizierung und die erste Charakterisierung von *vacuolar fusion defective* (*vfd*) Mutanten. Die *vfd* Mutanten zeigen einen keimlingsletalen Phänotyp, besitzen keine Zentralvakuole und akkumulieren ubiquitinierte Proteine. Durch Verbindung von klassischem Mapping und Next Generation Sequencing wurde das mutierte Gen der *vfd1* Mutante als *FYVE1* identifiziert. Das *FYVE1*-Gen kodiert für ein Protein mit einer FYVE (Fab1, YOTB, Vac1 und EEA1) Domäne. Dieses Ergebnis wurde durch Komplementation der *vfd1* Mutante mit dem Wildtyp-Gen und Wiederherstellung des Wildtyp-Phänotyps bestätigt.

FYVE-Domänen enthalten Zink-Finger-bindende Motive und wurden bereits als Lipidbindedomänen, die für Phosphatidylinositol 3-Phosphat spezifisch sind, charakterisiert. Das Fusionsprotein GFP-FYVE1 ist im Zytosol, im Nukleus und an endosomalen Vesikeln lokalisiert. GFP-FYVE1 kolokalisiert mit Subpopulationen des Endozytose-Markers CLATHRIN LIGHT CHAIN (CLC) und ARA7, einem Markerprotein für späte Endosomen. Das künstliche Cargo-Protein GFP-CT24 wurde in *fyve1-1* Mutanten-Embryos fehlsortiert, was bereits auf einen Einfluss von FYVE1 in frühen Stufen der Pflanzenentwicklung im

Proteintransport zu den Proteinspeichervakuolen (PSVs) hindeutet. Experimente mit dem lipophilen Farbstoff FM4-64 und dem Fusionsprotein des Auxineffluxtransporter PIN-FORMED2 (PIN2-GFP) zeigen, dass die *fyve1-1* Mutante generelle Defekte in der Endozytose aufweist.

Zusammenfassend demonstriert diese Studie, dass das FYVE1 Protein ein neues und essentielles Protein im Endomembransystem und in der Pflanzenentwicklung ist.

1. Introduction

1.1 The vacuole in plant cells

In plants, the vacuole is an essential organelle that has important physiological functions (Figure 1). Vacuole function is necessary for maintenance of the turgor pressure against the cell wall, which supports the structural stability of the cell and the surrounding tissue. This hydrostatic pressure is required for cell elongation during plant growth.

The vacuole also serves as an important storage organ for sugars, metabolites, carbohydrates, lipids, amino acids, enzymes, proteins and anthocyanins. The stored materials in plant vacuoles are often of special interest for human uses: seed and fruit quality are of major importance in agriculture and in both tissues, the vacuole is the organelle that harbors the desirable ingredients. For instance, the sap of the rubber tree stored in the vacuole of lacifier cells is of economic importance in the chemical industry. The alkaloid nicotine, which is stored in vacuoles of tobacco leaves, acts as a natural stimulant of economic significance in tobacco industry. Plant components, like morphine and salicylic acid, are also interesting for medicinal uses and there is a whole sector evolving that utilizes phyto-engineering to breed and modify plants to harvest specific useful pharmaceuticals of medicinal plants. In addition, the vacuole stores toxic ions and compounds that play a role in bacterial pathogen and herbivore defense of plants that can be manipulated for increasing resistance against biotic stress. Therefore, understanding the biogenesis and function of plant vacuoles touches many topics of interest for humans. In future years, climate changes will increase droughts and water shortage, leading to decreased harvesting yields. The focus of crop breeders is shifting to drought resistant plants with adapted abilities in vacuole function (Martinoia et al., 2012; Zhang et al., 2014).
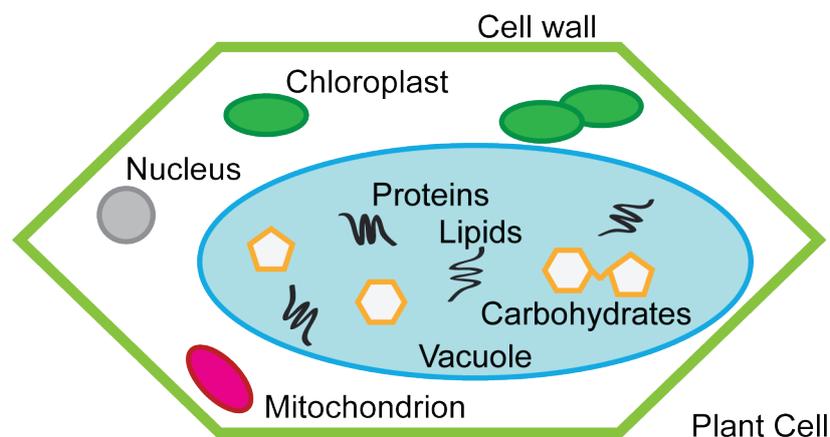
Figure 1. The main organelles of a plant cell include the cell wall, nucleus, chloroplast, mitochondrion and the vacuole. The vacuole as the storage organelle of the plant cell contains proteins, lipids, carbohydrates and sugars.

Vacuoles or lysosomes exist in all eukaryotic organisms and have evolved several times during evolution (Becker, 2007). In plant and fungal cells, vacuoles have similar functions. The designation "lysosome" is primarily used for the functional counterpart in animal cells. Interestingly, vacuoles also exist in several sulfur bacteria that use vacuoles as storage organelles for sulfide and nitrate. Cyanobacteria contain gas vacuoles to control their buoyancy to maximize the efficiency of photosynthesis (Walsby and Nichols, 1969; Schulz-Vogt, 2006).

Plant vacuoles can be functionally classified into two types. In seeds and storage organs, protein storage vacuoles (PSVs) serve as protein storage organelles in addition to protein bodies. PSVs contain storage proteins like albumins, prolamins and globulins, which are needed during embryo maturation and seed germination (Robinson and Hinz, 1997; Herman and Larkins, 1999). In fully differentiated cells of the vegetative tissue, lytic vacuoles (LVs) are dominant, which form the central vacuole and contain hydrolytic enzymes for protein degradation (Aubert et al., 1996; Moriyasu and Ohsumi, 1996; Jauh et al., 1999; Marty, 1999).

The vacuole is encased by a single membrane called vacuolar membrane or tonoplast and varies in form, size, number per cell, content and functional dynamics depending on the developmental stage and organ or cell type (Marty, 1999). Vacuoles can make up 30 to 90 % of the volume of a plant cell and the majority of differentiated cells have one large central vacuole. In meristem cells smaller vacuoles or structures called provacuoles, that mature into a central vacuole, can be found (Marty, 1999).

The vacuole contributes to the osmoregulation of a plant cell mainly by means of the vacuolar water channel aquaporin TONOPLAST INTRINSIC PROTEIN (TIPs), through which water molecules are selectively transported. The vacuolar membrane also contains other integral membrane proteins, such as the vacuolar H^+-ATPases (V-ATPases) and the vacuolar H^+-pyrophosphatases (V-PPases) as well as different ion transporters. By the action of these ATPases as proton pumps, the lumen of the vacuole maintains its acidic pH, whereas the surrounding cytosol remains neutral (Bethke and Jones, 2000). In stomatal guard cells, this dynamic process of water input and output is the driving force to control the opening of the stomata, which is regulated by the osmotic pressure of the adjacent vacuoles (Gao et al., 2005).

The lytic vacuole is necessary for degradative processes. The acidic pH activates vacuolar hydrolases and other degradative enzymes, that are necessary for the degradation and recycling of diverse biomolecules. Proteins are transported to the vacuole by membrane trafficking and together with the 26S proteasome, the vacuole serves as an essential compartment for proteolysis.

1.2 The biosynthetic vacuolar transport pathway for *de novo* synthesized proteins

The vacuolar system, consisting of endosomal vesicles and vacuoles, derives from three pathways: (a) the intracellular biosynthetic pathway via the secretory system, (b) the endocytotic pathway and (c) the autophagic pathway (Figure 2).

The vacuole is the destination for newly synthesized vacuolar proteins from the endoplasmic reticulum (ER) via the vacuolar biosynthesis pathway. Newly synthesized proteins destined to the vacuole contain a transient N-terminal signal peptide. These pre-proproteins are translocated from the ER to the Golgi apparatus. At the *trans*-Golgi network (TGN), the vacuolar sorting signal (VSS) is recognized by a vesicle-associated receptor. Proteins get sorted according to their destination and vacuolar proteins are translocated to endosomes or the prevacuolar compartment (PVC). Proteins without a signal peptide are secreted via the default pathway to the extracellular space. The PVC (also referred to as provacuole) is an intermediate compartment between the TGN and the mature vacuole and buds from the TGN (Marty, 1999).
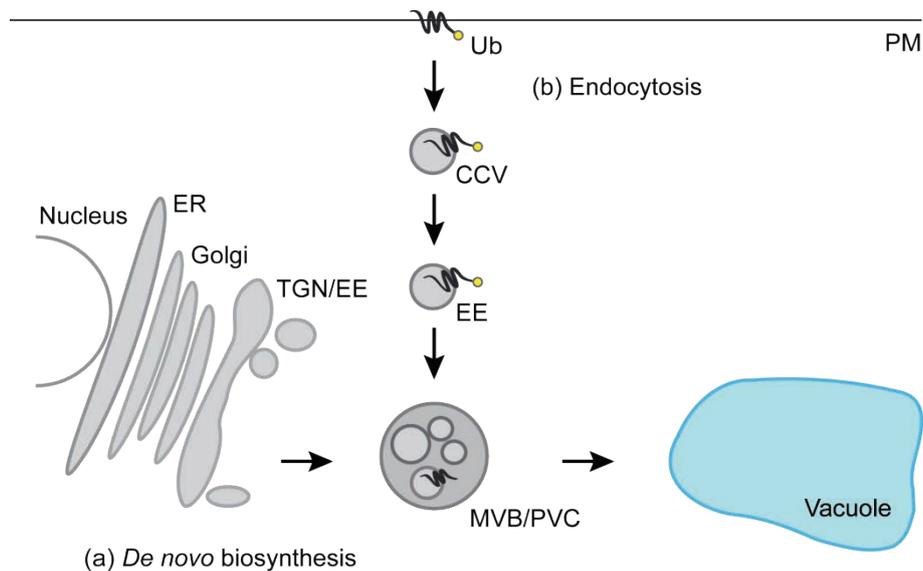
Figure 2. Protein biosynthesis and endocytosis are the main transport pathways to the vacuole. **(a)** The *de novo* biosynthesis pathway leads newly synthesized proteins from the origin of synthesis at the ER via the Golgi apparatus and the MVB/PVC to the vacuole. **(b)** Endocytosis is the uptake of membrane material or proteins from the plasma membrane via CCVs, EE and MVB to the vacuole. Autophagic pathway (c) not shown. Ub: Ubiquitin, CCV: clathrin-coated vesicle, EE: early endosome, MVB: multivesicular body, PVC: prevacuolar compartment, ER: endosomal reticulum, TGN: *trans*-Golgi network, PM: plasma membrane.

If there is a VSS, there is also a specific vacuolar sorting receptor (VSR). One VSR of plants is the 80 kDa protein BP-80 (binding protein) from pea (Kirsch et al., 1994). BP-80 is an integral membrane protein located in the Golgi apparatus. The other plant VSR is *ARABIDOPSIS THALIANA* EPIDERMAL GROWTH FACTOR RECEPTOR-LIKE PROTEIN (AtELP), which is located at the TGN, in clathrin-coated vesicles (CCVs) and on the PVC of *Arabidopsis* (Ahmed et al., 1997).

In maturing seeds of pumpkin and castor bean, the precursor-accumulating (PAC) vesicles, which are similar to protein bodies, transport storage proteins from the rough ER to the PSV and can bypass the Golgi apparatus (Hara-Nishimura et al., 1998). The PAC-specific VSR in pumpkin is PV72. PACs have not been identified in *Arabidopsis*.

The final fusion events in the vacuolar pathway are still unclear. Two reasonable possibilities are that either the PVC is directly fusing by heterotypic membrane fusion with the vacuole or it is engulfed by an autophagic event into the vacuole (Marty, 1999).

There are three distinct vesicles, which transport proteins from the Golgi or ER to the vacuole: dense vesicles (DVs), clathrin-coated vesicles (CCVs) and precursor-accumulating PAC vesicles (Hinz et al., 1999; Bethke and Jones, 2000). DVs in pea transport storage proteins to PSVs, CCVs traffic other proteins to lytic vacuoles (Hinz et al., 1999).

Pre- or provacuoles are defined as organelles that receive cargo from transport vesicles and subsequently deliver that cargo to the vacuole by fusion with the tonoplast (Bethke and Jones, 2000). Multivesicular bodies (MVBs) are late endosomal organelles with internalized, intraluminal vesicles (ILVs). Since MVBs lie *en-route* to the vacuole, they are also referred to as prevacuolar compartment (PVC). MVBs can fuse with the lytic or storage vacuole, upon which the content of the ILVs is released into the lumen of the vacuole. Therefore, MVBs play an intermediary role in protein sorting and targeting to the vacuole, protein degradation, secretion and intracellular recycling.

1.3 The endocytic degradation pathway of plasma membrane proteins

The vacuole is also the final destination of the endocytic degradation pathway. Plasma membrane localized transmembrane receptors and transporters are known to be transported to the vacuole for degradation through the endocytic degradation pathway. This pathway is essential for plant cells during growth and development, hormonal signaling and detection of environmental changes, such as sensing of nutrients, toxins and pathogens (Chen et al., 2011). The endocytosis of receptor-ligand complexes is crucial for signal transduction processes (Battey et al., 1999).

In most of the cases, the membrane proteins are first endocytosed from the plasma membrane into the cell in the form of clathrin coated vesicles (CCV). Clathrin and adaptor

proteins are assembled from the cytosol to form a coat complex and attach to the vesicle membrane. The second step is the docking of the transport vesicle to the target membrane by means of diverse soluble N-ethylmaleimide-sensitive factor attachment protein receptors (SNAREs) (Robinson et al., 1998; Sanderfoot and Raikhel, 1999). Vesicle SNAREs (v-SNAREs) interact with SNAREs on the target membrane (t-SNAREs) and build a v-SNARE/t-SNARE complex.

Ubiquitin is a small regulatory protein of 8.5 kDa. Ubiquitin is ubiquitously expressed and highly conserved in eukaryotic organisms. This small protein can be covalently attached to the protein substrates and acts as a posttranslational signal in many pathways. Modification by ubiquitin or ubiquitination can alter protein location, activity and interaction with binding partners and thereby regulate protein homeostasis, turnover, abundance and quality control (Schnell and Hicke, 2003).

Cytosolic proteins modified with ubiquitin are mostly targeted to and degraded by the 26S proteasome, whereas ubiquitinated plasma membrane proteins are sent to the vacuole for degradation (Hershko and Ciechanover, 1992). The transport of ubiquitinated proteins to the vacuole is mediated by Endosomal Sorting Complex Required for Transport (ESCRT), which are heteromeric protein clusters that function sequentially in the sorting of proteins (Winter and Hauser, 2006; Iwaki et al., 2007).

Classical examples of endocytosed cargo proteins are the auxin efflux transporter PIN-FORMED proteins (PINs). PINs are constitutively endocytosed from the plasma membrane and are either targeted to the vacuole for degradation or recycled back via CCVs to the plasma membrane (Dhonukshe et al., 2007).

In yeast and mammals, ubiquitinated membrane proteins are first recognized by the ubiquitin-binding proteins of the ESCRT-0 complex (Bowers and Stevens, 2005). The ESCRT-0 protein Vps27p/Hrs has a N-terminal VHS domain with an ubiquitin-binding domain (UIM), as well as a FYVE domain necessary for binding to endosome specific phospholipids (Hayakawa and Kitamura, 2000). ESCRT-0 then recruits ESCRT-I from the cytosol by the interaction of Vps27p/Hrs with the ESCRT-I subunit Vps23/Tsg101 (Figure 3 A). Upon which Vps23/Tsg101 recruits the secondary ESCRT-I components Vps28 and Vps37. After binding of ESCRT-I, the ESCRT-II complex is activated. The cargo protein is transferred to the ubiquitin-binding subunit Vps23/Tsg101 of ESCRT-I and subsequently to the ubiquitin-binding Vps36/Eap45 of ESCRT-II. The ESCRT-II subunits Vps22/Eap30, Vps36 and Vps25 interact with the ESCRT-III subunit Vps20/Chmp6. ESCRT-III functions to concentrate the cargo proteins on the limiting membrane of the MVB, prior to sorting into the intraluminal vesicles (ILVs). ESCRT-III is continuously assembled and disassembled and for the disassembly, the activity of the AAA ATPase Vps4p/SKD1 is required (Figure 3).
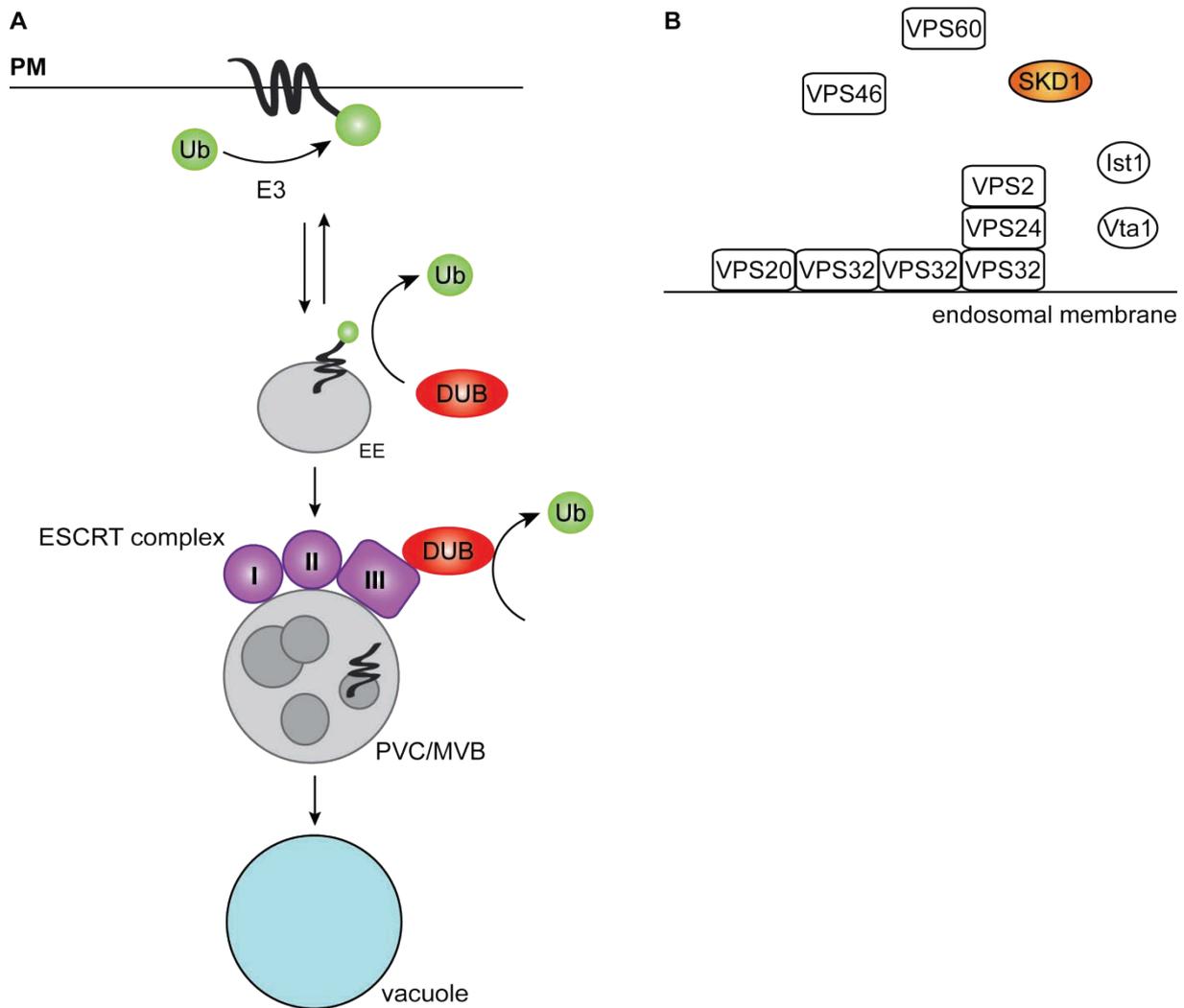
Figure 3. The ESCRT complexes play an important role in the intracellular transport of membrane proteins to the vacuole.
(A) Plasma membrane (PM) proteins are ubiquitinated by an E3 ligase, marked for endocytosis and subsequently internalized. The ubiquitinated protein is transported to early endosomes (EE), where the ubiquitin-tag can be removed by action of deubiquitinating enzymes (DUBs), thereby releasing the protein from the degradation pathway and recycling it back to the plasma membrane. The ubiquitinated protein is recognized by ESCRT (endosomal sorting complex required for transport) subunits. DUBs remove the ubiquitin tag, upon which the target protein is internalized in intraluminal vesicles of the multivesicular body (MVB). The MVB fuses with the vacuole and transported proteins are degraded. **(B)** The ESCRT-III complex consists of the core subunits VPS20, VPS32 (SNF7), VPS24 and VPS2. Additional subunits are VPS46 and VPS60, as well as Ist1 and Vta1. The AAA-ATPase SKD1 (VPS4) is essential for the ATP-dependent disassembly of the complex.

In plants, all ESCRT and ESCRT-related components, except for the two subunits of ESCRT-0, are conserved (Winter and Hauser, 2006). It was suggested that other ubiquitin-binding proteins, such as TOM1-LIKE (TOLs), take over the ubiquitin adaptor function in plants (Winter and Hauser, 2006).

Ubiquitination of target proteins is in general mediated by the activity of ubiquitin-activating enzymes (E1), ubiquitin-conjugating enzymes (E2) and target-specific ubiquitin-protein ligases (E3). The combination of E2 and E3 determines the ubiquitin chain type,

among which K63-linked ubiquitin chains are suggested to be the major chain type for proteins of the endosomal degradation pathway (Figure 4 A).

Ubiquitination can be reversed by deubiquitinating enzymes (DUBs) (Figure 4 B). They hydrolyze the covalent bond between ubiquitin and the cargo protein and can thus regulate the ubiquitination status of proteins and substrate stability. The activity of DUBs is also essential for processing pre-ubiquitin molecules and for maintaining a pool of free ubiquitin in the cell.
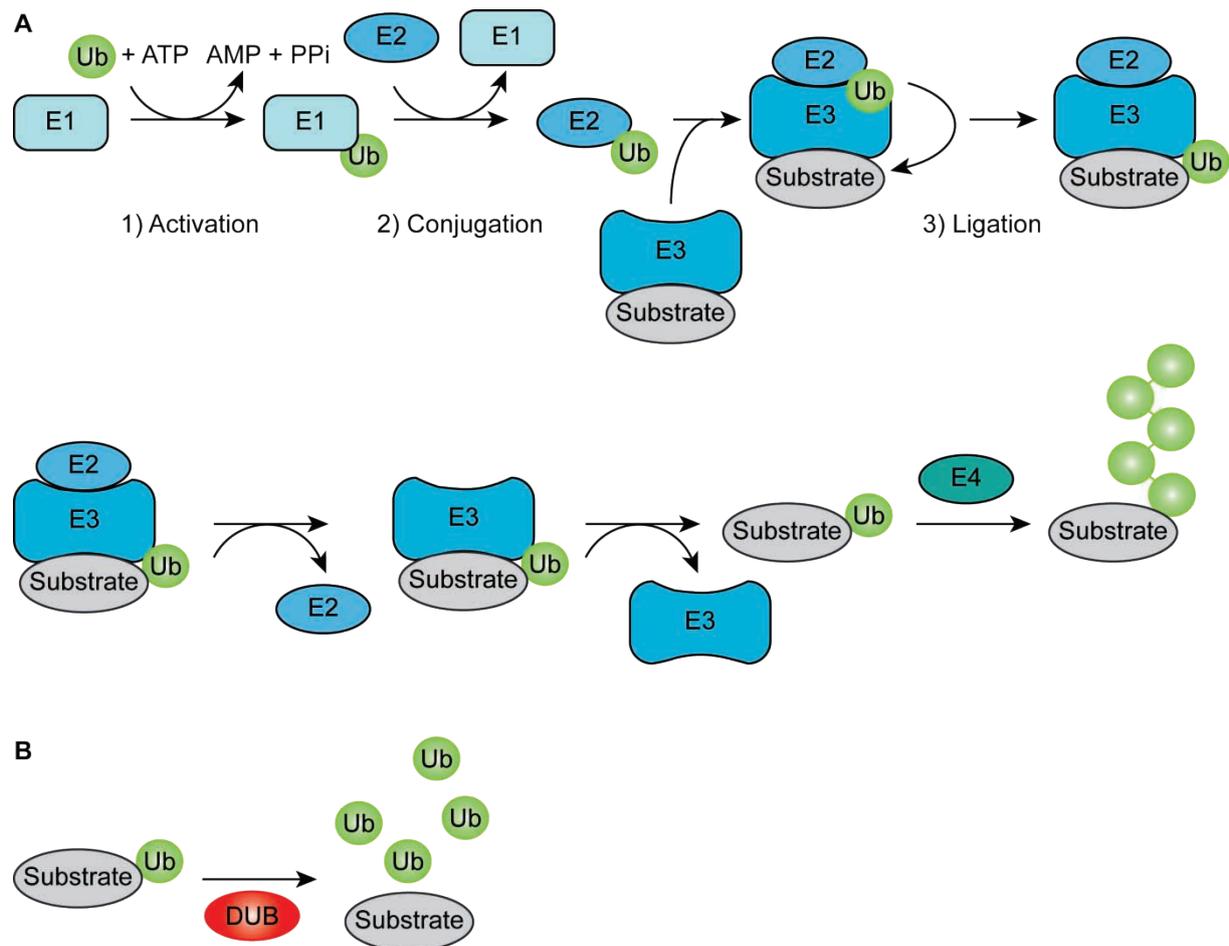
Figure 4. Ubiquitination and deubiquitination of a protein are conducted by a specific set of enzymes. **(A)** Ubiquitin (Ub) is activated by an E1 ubiquitin-activating enzyme in an ATP-dependent manner. The E2 ubiquitin-conjugating enzyme catalyses the transfer of ubiquitin from E1 to E2. The E3 ubiquitin ligase recognizes the substrate protein. It transports the substrate protein to the complex, binds to E2 and transfers the ubiquitin to the bound substrate protein. After disassembly of E2 and E3, the substrate protein can be further ubiquitinated or the ubiquitin chain can be elongated to a polyubiquitin chain by action of the E4 ubiquitin factors. **(B)** Deubiquitination is the antagonistic process to the E1-E2-E3 cascade. Deubiquitinating enzymes (DUBs) can hydrolyze the isopeptide bonds and remove ubiquitin from its substrate, thereby releasing free ubiquitin molecules.

1.4 Role of AMSH proteins in endocytosis and autophagy

ASSOCIATED MOLECULE WITH THE SH3 DOMAIN OF STAM (AMSH) is a deubiquitinating enzyme that belongs to the Jab1/Mov34/Mpr1 Pad1 N-terminal+ (JAMM/MPN+) domain-containing metalloprotease DUB family. It also has a SRC HOMOLOGY 3 (SH3) domain, the nuclear localization signal (NLS), the clathrin-binding site (CBS) and the STAM-binding motif (SBM). STAM is a component of the ESCRT-0 complex necessary for endocytosis.

The genome of *Arabidopsis thaliana* encodes three homologs of *AMSH* named *AMSH1*, *AMSH2* and *AMSH3*, which were identified by their sequence homology of the MPN+ domain. The amino acid sequence homology between the plant AMSH1 and AMSH3 proteins and the animal AMSH proteins is restricted to the N-terminal microtubule-interacting and trafficking (MIT) domain and the C-terminal MPN+ domain (Figure 5). Since plants do not have homologs of the ESCRT-0 subunit STAM/HRS, the SBM seems to be obsolete for AMSH function. Both AMSH1 and AMSH3 interact directly with VPS2.1 and VPS24.1, two components of the ESCRT-III complex in plants, through their N-terminal MIT domain (Katsiarimpa et al., 2011).

The *Arabidopsis amsh3* mutant is a recessive null allele of the deubiquitinating enzyme AMSH3 (Isono et al., 2010). The mutant is seedling lethal and cells lack the large central lytic vacuole (Figure 6 A and B). Transmission electron microscopy (TEM) pictures show small round vacuoles or prevacuoles (Figure 6 C). On the molecular level, *amsh3* mutants show accumulation of ubiquitinated proteins (Figure 6 D), suggesting that the DUB function of AMSH3 is necessary for degradation of ubiquitinated cargo in endosomal trafficking. Endocytosis of the lipophilic dye FM4-64 and the plasma membrane protein PIN-FORMED 2 (PIN2) is impaired (Figure 6 E). Vacuolar protein cargos are missorted to the intercellular space, indicating that AMSH3 is required not only for vacuole biogenesis but also for intracellular trafficking.
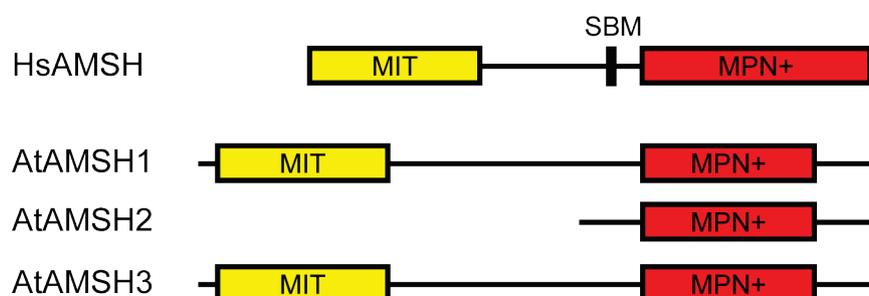
Figure 5. AMSH proteins in human and *Arabidopsis thaliana* share the N-terminal MIT and catalytic MPN+ domain.
The primary domain of the AMSH family of proteins is the enzymatically active MPN+/JAMM domain at the C-terminus. The MIT domain is located at the N-terminus. The human AMSH protein also contains a STAM-binding motif (SBM), which is missing in the *Arabidopsis* proteins. The *Arabidopsis* AMSH2 protein is missing the N-terminal MIT domain. Hs: *Homo sapiens*; At: *Arabidopsis thaliana.*
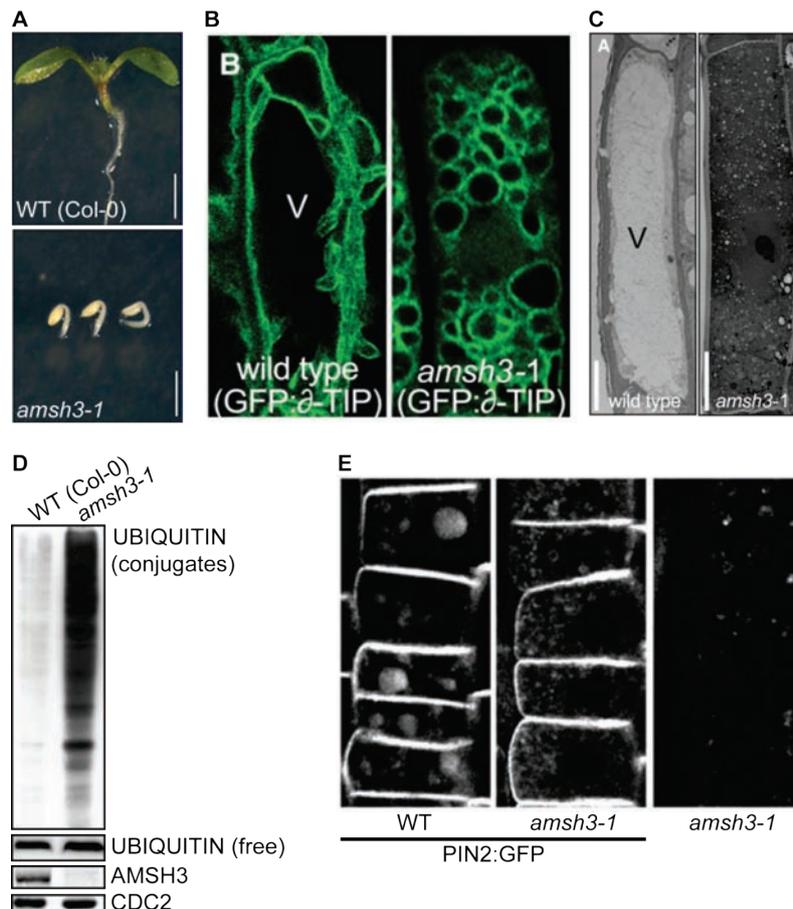
Figure 6. AMSH3 is required for intracellular trafficking and vacuole biogenesis in *Arabidopsis thaliana* (Isono et al., 2010).
(A) Phenotypes of 7-d-old seedlings of *amsh3-1* in comparison to wild-type seedlings of the same age. Bars = 1mm. **(B)** Confocal microscopy images of the vacuolar membrane marker GFP::δ-TIP in wild-type (2-d-old) and *amsh3-1* (5-d-old) mutant cells. **(C)** Transmission electron micrographs of root epidermis cells of wild-type and *amsh3-1* mutant seedlings. V, vacuole. Bars = 5 μM (wild-type) and 10 μM (*amsh3*). **(D)** Immunoblots with an anti-ubiquitin P4D1 antibody from protein extracts of 7-d-old seedlings of *amsh3-1* in comparison to wild-type seedlings of the same age. **(E)** Confocal images of PIN2:GFP in wild-type (left) and *amsh3-1* (middle) mutant cells. Vacuole-localized PIN2:GFP signals are visible in the wild-type, but not in the *amsh3* mutant. Because *amsh3* seedlings exhibit background fluorescence, a control image of an *amsh3* seedling without PIN2:GFP is shown on the right.

1.5 Factors regulating vacuole morphology

The development of diverse tonoplast marker proteins has contributed to the significant progress in cell biological characterization of the vacuolar system. Still, the difficulties in identification of vacuolar compartments lie in the complexity of the system. Compared to the function of the vacuole, there is comparably rare knowledge how the vacuole is built during cell development in plants. Vacuolar biogenesis and fusion events already take place during early embryo development. In the globular stage, many small vacuoles fuse to form larger vacuoles in the embryo, indicating the early steps of vacuole biogenesis (Rojo et al., 2001). During germination, protein storage vacuoles undergo a developmental transition, where a single vacuole can differentiate either into a storage organelle or a lytic compartment (Gattolin et al., 2010).

The molecular factors involved in homotypic membrane fusion, the fusion of two vacuoles of identical character, membrane composition or origin, were investigated in the yeast system and many of the identified factors are conserved in plants (Uemura et al., 2004).

The first observations regarding vacuole biogenesis were obtained in yeast screens that isolated a number of *vacuole protein sorting* (*vps*) mutants that showed defects in vacuolar transport (Klionsky et al., 1990). These genetic studies identified more than 40 factors that regulate vacuole morphology. Mutations in these factors led to defects in the sorting and processing of vacuolar proteins. These results indicated that the delivery of proteins to the vacuole is a complex process, which requires many different factors.

In plants, forward genetic screens for mutants with altered vacuole morphology resulted in the identification of a number of interesting mutants. One of the first vacuolar mutants described in *Arabidopsis* was the *vacuoleless1* (*vcl1*) mutant (Rojo et al., 2001). Rojo and co-workers performed a genetic screen of over 5.000 transposon lines and 150 embryo-defective lines for mutants with altered vacuolar morphology in the suspensor cells of early embryos. *vcl1* is embryo lethal, does not have visible vacuoles and shows a number of vacuolar transport defects. VCL1 is the plant homolog of the yeast Vps16p, a subunit of the tonoplast associated C-VPS/HOPS protein complex responsible for homotypic membrane fusion. This result suggested that the basic mechanism of vacuole biogenesis might be conserved in yeast and higher plants.

The results of another mutant screen were published in 2003 from the Raikhel lab (Avila et al., 2003). In this work, they analyzed progenies of an EMS-mutagenized seed population with a high-throughput confocal screening using the tonoplast marker GFP::δ-TIP. Out of 9175 M_2 seedlings, 101 mutants showed altered vacuolar morphology. Mutants were sorted into four categories due to vacuolar morphology. The *bubble-bath* (*bub*) mutants comprised the biggest group with 46 members. The *large aggregates* (*agg*) mutants contained 34 members. Eight mutants belonged to the *transvacuolar strands* (*tvs*) mutant category and 13 mutants showed more complex phenotypes. These results showed the broad spectrum of possible vacuolar mutant phenotypes and also indicated that there might be tissue-specific factors that determine vacuole morphology.

The *green fluorescent seed* (*gfs*) mutant screen performed in the Hara-Nishimura lab utilized the artificial vacuolar storage protein GFP-CT24 (Nishizawa et al., 2003; Fuji et al., 2007). Mutants defective in vacuolar trafficking secrete the artificial cargo to the intercellular lumen and therefore mutant seeds can be selected due to an increased GFP fluorescence compared to the wild-type. The screen identified over 100 *gfs* mutants, out of which 10 *gfs* mutants were analyzed in more detail.

The *vacuolar sorting receptor 1 (vsr1)* mutant was discovered in 2003 by Shimada and co-workers, who analyzed transposon mutants of possible pumpkin PV72 homologs in

Arabidopsis (Shimada et al., 2003). PV72 acts as a vacuolar sorting receptor in pumpkin seeds. Only the transposon mutant of AtVSR1/AtELP/AtBP80b showed a seed-specific phenotype, in which accumulation of storage protein precursors and missorting of storage proteins was described. Additionally, PSVs are smaller in *vsr1* seeds. *vsr1* seedlings exhibit normal growth, indicating that VSR1 acts as a sorting receptor in *Arabidopsis* and is necessary in maturing seed cells for the proper trafficking of storage proteins.

To isolate genes that mediate trafficking to the PSV, a screen was conducted using the chimeric cargo protein VAC2, a fusion of the vacuolar sorting signal (VSS) of barley lectin and the PSV specific protein CLV3 (Sanmartin et al., 2007). Mutants affected in protein transport to the vacuole, secrete and accumulate VAC2 in the extracellular space. In a reverse genetic approach two null mutants of the v-SNARE proteins VTI11 and VTI12 (Morita et al., 2002; Surpin et al., 2003) were crossed with the marker line expressing *VAC2*. Even though both mutants were viable, defects in protein trafficking to the vacuole were shown. VTI12 was shown to mediate transport to the PSV in vegetative and seed tissues, whereas VTI11 was shown to mediate transport to the LV. Moreover, the PSVs of *enhanced vti12* (*enh vti12*) mutant embryos were smaller than in wild-type. The authors concluded that deposition of storage proteins was decreased, like in the *vsr1* mutant.

The *vti11/zig/sgr4* mutant was already described in the *shoot gravitropism* (*sgr*) mutant screen, where it was isolated because of an altered shoot and gravitropism phenotype (Zheng et al., 1999; Kato et al., 2002). Due to its homology to the yeast Vti1p SNARE protein, Kato et al. suggested that vesicle transport may be involved in gravitropism. Furthermore, the authors concluded that VTI11-containing vesicles may be transported to the PVC and that VTI11 mediates traffic to lytic vacuoles.

SNARE complexes mediate membrane fusion between transport vesicles and target membranes. The plant-specific R-SNARE VAMP727 is localized to the prevacuolar compartment (MVB/PVC) (Ueda et al., 2004; Uemura et al., 2004; Ebine et al., 2008), implying a role in fusion between the PVC and the vacuole. While investigating genetic interactions between VAMP727 and other SNARE proteins, Ebine et al. discovered the *vamp727 syp22-1* double mutant (Ebine et al., 2008). SYP22/VAM3 is a Qa-SNARE protein localized to the vacuolar membrane (Ebine et al., 2008). The double mutant showed altered PSV morphology and mistargeting of storage proteins, indicating impaired protein trafficking to the PSV. Additionally, Ebine et al. isolated two more subunits of this vacuolar SNARE complex, namely VTI11 and SYP51. In conclusion, when VAMP727, SYP22/VAM3, VTI11 and SYP51 form a SNARE complex, fusion between vacuolar membranes is mediated.

The VTI12-SNARE-complex is located at the *trans*-Golgi network and consists of the subunits SYP41, SYP61 and VTI12 (Zouhar et al., 2009). AtVPS45 regulates this SNARE-complex. The *vps45* knockout mutant was gametophytic lethal, indicating the essential

function of VPS45. In RNA interference lines with reduced AtVPS45 protein levels formation of the vacuole was impaired. Furthermore, vacuolar proteins were not transported to their target destination, suggesting that AtVPS45 functions in vesicle trafficking to the vacuole.

The *Arabidopsis* homologs of VPS35 are components of the retromer complex and involved in retrograde transport in the secretory pathway. *vps35* double and triple mutants showed severe phenotypes, fragmented PSVs and missorting of vacuolar proteins (Yamazaki et al., 2008).

CHMP1A and CHMP1B (VPS46) are ESCRT-related proteins, that show redundant function. CHMP1A was shown to interact with Vps4p/AtSKD1 *in vitro*. The *chmp1a chmp1b* double mutant showed embryo development defects and mislocalization of membrane proteins (Spitzer et al., 2009). Without proper CHMP1A/B function, the recycling of auxin transporters like PINs, which are normally recycled by MVBs, was affected and the MVB cargo proteins accumulated at the vacuolar membrane.

The AAA-type (ATPase associated with various cellular activities) ATPase AtSKD1 (SUPPRESSOR OF K+ TRANSPORT GROWTH DEFECT1) was shown to be a functional homolog of the yeast Vps4p (Shahriari et al., 2010). AtSKD1 interacts with the ESCRT-III components VPS20, VPS24-1 and VPS32 at the MVB and leads to dissassembly of the ESCRT-III complex, which is necessary for proper invagination of ILVs. The dominant-negative version of AtSKD1 resulted in mistargeting of vacuolar proteins, indicating defects in vacuolar transport. Moreover, the large central vacuole in plants with the mutated version of this protein was fragmented and disappeared, indicating that without proper SKD1 function vacuole maintenance was impaired.

The myrosinase-associated protein MVP1 was isolated in an EMS screen using the marker protein GFP:δ-TIP (Avila et al., 2003; Agee et al., 2010). Myrosinases are β-glucosidases that hydrolyze the plant secondary metabolite glucosinolate. The *modified vacuole phenotype1-1* (*mvp1-1*) mutant showed perinuclear aggregation of the marker protein and various vacuole-related phenotypes. Marker proteins for the ER, the Golgi, vacuole, and plasma membrane were mislocalized to these aggregates, indicating general trafficking defects in the mutant.

Arabidopsis APOPTOSIS-LINKED GENE-2 INTERACTING PROTEIN X (ALIX) was identified as an AMSH3-interacting protein (Kalinowska et al., 2015). The *alix* knockout mutant showed a fragmented vacuolar phenotype and altered MVB formation, suggesting that ALIX is an important regulator of AMSH3 function at late endosomes.

The factors identified in the aforementioned genetic screens play an important role in the interaction of vacuolar membranes or the transport of vacuolar proteins to their target organelle.

Table 1. Known *Arabidopsis* vacuole morphology and trafficking mutants and their phenotypes.

Mutant	Type	Plant	Vacuole phenotype	Gene function	Reference
vcl1	transposon insertion	embryo lethal	no vacuole	vacuole fusion	Rojo et al. (2001)
vti11/ zig1/sgr4	fast neutron mutagenesis	viable	normal	vesicle transport, v-SNARE	Zheng et al. (1999) Kato et al. (2002)
bub, agg, tvs, unique	EMS	diverse	diverse	n.a.	Avila et al. (2003)
mag1/vps29	transposon insertion	dwarf	fragmented	retromer complex	Shimada et al. (2006)
vsr1	transposon insertion, EMS	normal	fragmented	vacuolar sorting receptor	Shimada et al. (2003) Fuji et al. (2007)
enh vti12	transposon insertion	dwarf	fragmented	vesicle transport, v-SNARE	Sanmartin et al. (2007)
vps35	transposon insertion	dwarf	fragmented	retromer complex	Yamazaki et al. (2008)
vamp727 syp22-1	transposon insertion	embryo lethal	fragmented	membrane fusion, SNAREs	Ebine et al. (2008)
vps45	RNAi	dwarf	fragmented	regulator of SNARE complex	Zouhar et al. (2009)
vps46/ chmp1a chmp1b	transposon insertion	embryo lethal, dwarf	normal	vacuolar trafficking	Spitzer et al. (2009)
mvp1	EMS	reduced growth	aggregated vacuolar marker	endomembrane trafficking	Agee et al. (2010)
AtSKD1 (AQ)	site-directed mutagenesis	normal	fragmented	AAA-type ATPase	Shahriari et al. (2010)
amsh3	transposon insertion	seedling lethal	fragmented	deubiquitinating enzyme	Isono et al. (2010) Katsiarimpa et al. (2014)
alix	transposon insertion	seedling lethal	fragmented		Kalinowska et al. (2015)

To isolate *vacuolar fusion defective* (*vfd*) mutants, a forward genetic screen had been performed with the tonoplast marker line GFP::δ-TONOPLAST INTRINSIC PROTEIN (TIP) in wild-type Columbia (Col-0) background (Cutler et al., 2000). Approximately 3,500 seeds were used for ethyl methanesulfonate (EMS) mutagenesis (Figure 7 A). EMS induces multiple random, whole-genome point mutations by nucleotide substitution from G to A. The original G:C base pair becomes an A:T pair (transition mutation). Five M_1 plants were grouped and M_2 seeds were collected (700 M_2 seed pools).
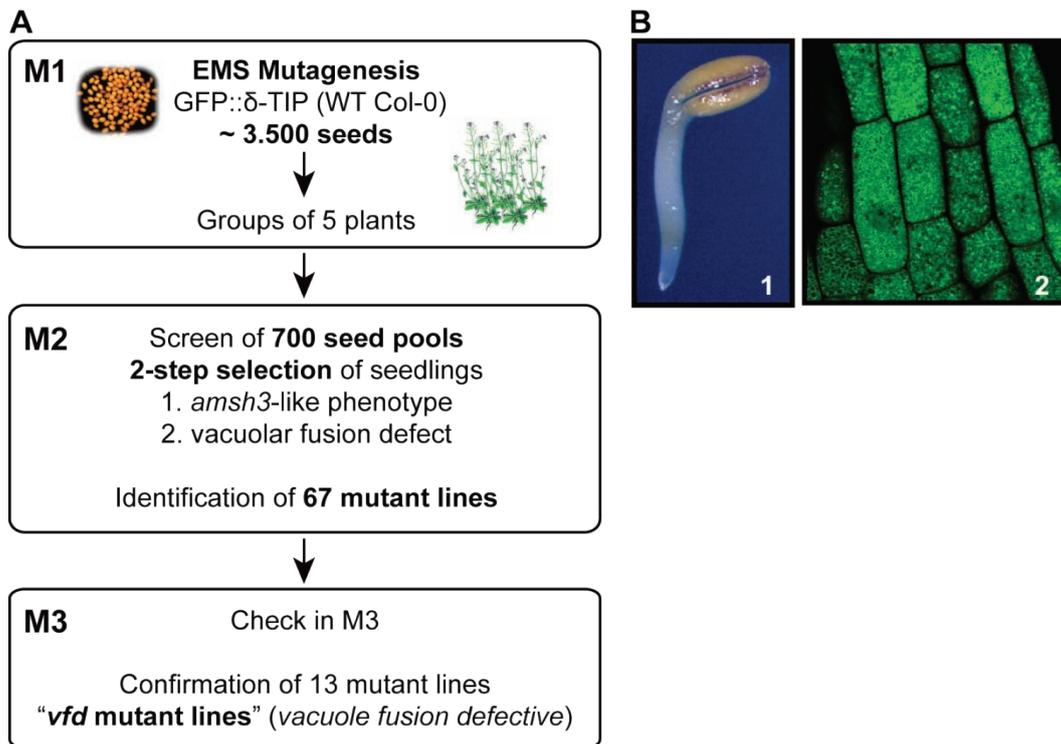
Figure 7. Forward genetic screen with two-step selection identified *vfd* mutant lines.
(A) Scheme of EMS screen set-up and screening steps in three generations (M1 to M3). EMS mutagenesis was performed on seeds of wild-type Columbia (Col-0) background carrying the tonoplast marker GFP::δ-TIP. **(B)** For selection of positive mutant lines, two screening criteria were applied: 1. *amsh3*-like phenotype. 2. vacuolar fusion defect.

The screening of the EMS generated mutant pool had been performed on 7-day-old seedlings of both the M_2 and M_3 generation that were plated on growth medium and grown under continuous light conditions. 700 M_2 pools were analyzed for two main criteria (Jeromé Morinier and Erika Isono, unpublished): First, a seedling-lethal *amsh3*-like phenotype and second, an altered vacuolar morphology (Figure 7 B). In the first step, the M_2 pools were screened for a similar seedling-lethal phenotype as the *amsh3* mutant. In the second step, vacuoles of the seedlings showing *amsh3*-like phenotypes were analyzed by confocal microscopy and those with aberrant vacuolar morphology were selected. In this primary screening 67 lines (9.6 %) were selected out of the 700 seed pools (Jeromé Morinier and Erika Isono, unpublished). Verification of these lines in the next generation identified 23 candidate mutant lines.

1.6 Aims and objectives of the project

The aim of this project was to identify novel proteins that are involved in vacuole biogenesis in *Arabidopsis thaliana* and thereby to elucidate the molecular mechanism of this yet poorly understood pathway. *Vacuolar fusion defective* (*vfd*) mutants that were seedling lethal and had fragmented vacuole phenotypes were screened from an EMS-mutated population. The obtained EMS mutants were analyzed in regard to the seedling and vacuole phenotype. For one of the mutant lines, *vfd1*, PCR-based mapping populations for further genetic analysis were established and the causative mutation was identified using whole-genome sequencing. To understand the molecular function of VFD1, cell biological and biochemical analysis was performed that provided insight as to how VFD1/FYVE1 could potentially regulate the formation of plant vacuoles.

2. Materials and Methods

2.1 Materials

2.1.1 Chemicals

All chemicals used in this study are listed in Appendix Table 15.

2.1.2 Other materials and enzymes

All other materials and enzymes used in this study are listed in Appendix Table 16.

2.1.3 Primers and plasmids

All vectors, plasmids and primers used in this study are listed in Appendix Table 17, Table 18 and Table 19, respectively.

2.1.4 Antibodies

All antibodies used in this study are listed in Appendix Table 20.

2.1.5 *Arabidopsis* plant lines and mutants

Arabidopsis lines used in this study are listed in Appendix Table 21.
Most experiments were performed with *Arabidopsis thaliana* ecotype Columbia-0 (Col-0). The mapping population was established between Col-0 and Landsberg *erecta* (L*er*-0). Analysis of the transposon insertion mutant *fyve1-1* was compared to wild-type Nossen-0 (No-0).

2.1.6 Bacterial strains

The *Escherichia coli* strains used in the present study were DH5α (Genotype: F- φ80*lac*ZΔM15 Δ(*lac*ZYA-*arg*F) U169 *rec*A1 *end*A1 *hsd*R17(rk-, mk+) *pho*A *sup*E44 *thi*-1 *gyr*A96 *rel*A1 λ-; Bethesda Research Laboratories, 1986) for cloning and propagation of plasmids and DB3.1 (Genotype: F- *gyr*A462 *end*A1 Δ(*sr1-rec*A) *mcr*B *mrr hsd*S20(rB-, mB-) *sup*E44 *ara*-14 *gal*K2 *lac*Y1 *pro*A2 *rps*L20(Smr) *xyl*-5 λ- *leu mtl*1; Hartley et al. (2000)) for propagation of Gateway vectors. The *Agrobacterium tumefaciens* strain GV3101 (pMK90) (Koncz and Schell (1986)) were used for *Arabidopsis* transformation.

2.1.7 Software used in this study

All analysis software used in this study is listed in Appendix Table 22.

2.2 Methods

2.2.1 Methods for plant analysis

2.2.1.1 Seed sterilisation and plant growth conditions

Arabidopsis seeds were sterilized for 5 (mutant lines) to 10 minutes in a saturated calcium hypochlorite solution with 0.1 % Silwet L-77 and then washed four times with sterile water with 0.05 % Silwet L-77. Seeds were plated on growth medium (GM medium: 4.3 g/l Murashige & Skoog medium [plus B5 vitamins], 10 g/l sucrose, 0.5 g/l MES, 5.5 g/l plant agar [0.55 %], pH 5.8 [adjusted with KOH]) or ½ Murashige & Skoog medium (½ MS medium: 2.15 g/l Murashige & Skoog medium [plus B5 vitamins], 0.5 g/l MES, 6.5 g/l plant agar [0.65 %], pH 5.8 [adjusted with KOH]). Seeds were stratified at 4 °C for 1 to 3 days. For the *vfd1*, *fyve1* mutant lines and respective controls, the stratification was prolonged up to 10 days. Plants were grown under continuous light (110 to 150 µmol m^{-2} s^{-1}) at 21 °C in a phytochamber.

For seed propagation and experiments with adult plants, 7-day-old seedlings were transferred to pots with standard soil and grown under continuous light, short (8 hrs light and 16 hrs dark) or long day (16 hrs light and 8 hrs dark) conditions depending on the individual experiments.

2.2.1.2 Genetic analysis

For segregation analysis, 5- to 7-day-old seedlings were counted according to phenotype. Wild-type, mutant seedlings and ungerminated seeds were scored separately.

The described *vfd* mutant lines were backcrossed at least once with the original wild-type Col-0 (GFP::δ-TIP) marker line. *Arabidopsis* plants were crossed manually with pollen of male donor plants. To avoid selfing of mother plants, stamens were removed from unfertilized florescences.

For allelism tests, the respective *vfd* lines were crossed with heterozygous *amsh3* plants or plants of other *vfd* mutant lines. Heterozygosity of the mutants was confirmed either by PCR-based genotyping or by segregation analysis in the next generation after selfing. *amsh3* heterozygous plants were identified by genotyping with gene (EI40, EI41) and transposon specific primers (p745, EI41). Seeds were sterilized and plated on GM medium agar plates. Plates were incubated for 6 days at 4 °C for stratification and grown in continuous light. After 5 days, seedlings were analyzed for phenotypes resembling *amsh3* or *vfd* homozygous mutants.

For establishment of the mapping population, heterozygous *vfd* plants of Col-0 background were crossed with wild-type L*er*. The F_1 generation was allowed to self and PCR-based mapping analysis was performed in the F_2 generation.

2.2.1.3 *Agrobacterium tumefaciens*-mediated stable transformation of *Arabidopsis thaliana*

For transformation of *Arabidopsis* plants, the floral dip method (Clough and Bent, 1998) was used. Electrocompetent *Agrobacterium tumefaciens* cells were transformed with the respective vectors via electroporation (2500 V, 4 to 6 sec). To each transformation reaction, 250 µl LB liquid medium (10 g/l tryptone, 5 g/l yeast extract, 10 g/l NaCl, pH 7.0 [adjusted with NaOH]) was added and cells were incubated for 1 hour at 30 °C. Positive transformants were selected on LB agar plates (10 g/l tryptone, 5 g/l yeast extract, 10 g/l NaCl, 15 g/l bacterial agar, pH 7.0 [adjusted with NaOH]) containing the respective antibiotics for each plant transformation vector (gentamicin [20 µg/ml], rifampicin [50 µg/ml], kanamycin [50 µg/ml]). Plates were incubated for 2 to 4 days at 30 °C.

Agrobacteria were inoculated in LB liquid culture at 30 °C over 3 days to a final volume of 500 ml. The cell culture was collected by centrifugation (5.000 rpm, 5 to 10 minutes) at room temperature and the pellet was suspended in 80 to 100 ml transformation buffer (2.2 g/l Murashige & Skoog medium [plus B5 vitamins], 50 g/l glucose, 0.5 g/l MES, 10 µl/l 6-BA [1 mg/ml], 200 µl/l Silwet L-77).

For transformation, *Arabidopsis* seeds were dispersed on soil in big pots, stratified for 3 days at 4 °C and grown under continuous light. Inflorescences of intact *Arabidopsis* plants were incubated in the transformation solution for 1 minute. After floral dip, plants were covered in a transparent plastic bag and left overnight at room temperature. The plastic bag was removed on the next day and plants were further grown in continuous light.

2.2.1.4 Selection of transgenic plant lines

Transformed T_1 seeds were selected on ½ Murashige and Skoog medium (0.65 % plant agar) with the respective antibiotics. Kanamycin and hygromycin were used in concentrations of 50 µg/ml. For selection of T_1 seeds with BASTA (Bayer) resistance, transformed T_1 seeds were dispersed on soil in big pots, stratified for 3 days at 4 °C and grown under continuous light. 7 days after germination, seedlings were sprayed with BASTA solution (1: 3000 dilution of BASTA in water). BASTA treatment was repeated after 3 days for improved selection. Plants were genotyped using construct specific primers.

2.2.1.5 Treatment with the inhibitor Brefeldin A (BFA)

For analysis of the effect of the inhibitor BFA on the Col-0 (GFP::δ-TIP) tonoplast marker line, ½ MS medium (0.65 % agar) plates containing three different concentrations of BFA (10 µM, 25 µM and 50 µM; stock concentration 50 mM, dissolved in DMSO) were used. The mock treatment consisted of ½ MS medium (0.65 % agar) without BFA. Seeds were

stratified for 3 days in dark at 4 °C. Plates were subjected to growth conditions under continuous light at 21 °C. Phenotype analysis was performed for every day for 7 days.

2.2.1.6 Transformation of *Arabidopsis* cell suspension protoplasts

For protoplast transformation, an *Arabidopsis* cell culture of cultivated root cells was used. Cells were harvested 4 to 6 days after subcultivation. 10 ml of culture were collected in a 15 ml plastic tube, spun down at 300 g for 2 minutes and washed with 10 ml WD solution (240 µl 1 M $CaCl_2$-$2H_2O$, 12 ml 1 M mannitol, 17.85 ml sterile water, sterile filtrated). Samples were spun down after washing at 300 g for 2 minutes and supernatant was discarded. Cells were resuspended in 10 ml WD solutions with enzymes (100 mg cellulase, 25 mg macerozyme, 4 ml 1 M mannitol, 6 ml sterile water, sterile filtrated) that was heated for 10 minutes at 50 °C for inactivating contaminating enzymes before the addition of 80 µl 1 M $CaCl_2$-$2H_2O$, and incubated at room temperature in the dark for 3 to 5 hours on a shaker (50 to 55 rpm). Protoplastation of the cells was monitored under the microscope.

Protoplasts were split up to five 2 ml tubes, which were centrifuged at 100 g for 2 minutes and supernatant was discarded afterwards. Cells were washed with 2 ml WD solution and centrifuged at 100 g for 2 minutes. Supernatant was removed, cells were resuspended in the remaining solution and collected in two 2 ml tubes. To each tube 2 ml of W5 solution (616 µl 5 M NaCl, 2.5 ml 1 M $CaCl_2$, 50 µl 2 M KCl, 100 µl 1 M glucose, 16.5 ml sterile water for a 20 ml solution) were added slowly, carefully mixed and centrifuged at 100 g for 2 minutes. Supernatant was removed and cells were resuspended in 2 ml of W5 solution. Protoplast samples were incubated on ice for 30 minutes. After incubation, cells were centrifuged at 100 g for 2 minutes. W5 solution was removed and cells were resuspended in 1 ml of MMM solution (75 µl 1 M $MgCl_2$, 50 µl 10 % MES, 2.5 ml 1 M mannitol, 2.375 ml sterile water for 5 ml solution) and carefully mixed. For transformation, 250 µl of protoplasts were aliquoted in a 1.5 ml tube and 20 µg of DNA were added. Additionally, 250 µl PEG solution (2 g PEG 4000, 2 ml 1 M mannitol, and 1 ml 1 M $CaCl_2$-$2H_2O$ for a 5 ml solution) were added and the sample was mixed gently by tapping and inverting the tube. Samples were incubated for 30 minutes on ice. After the second incubation step, 1 ml of W5 solution was added and tubes were inverted and gently mixed. Samples were centrifuged at 100 g for 2 minutes at 4 °C. Supernatant was removed afterwards and centrifugation steps were repeated at least two times until the cell pellet became clear and packed. Cells were suspended in 150 µl K3 solution (1 ml macro stock [1.5 g NaH_2PO_4-H_2O, 9 g $CaCl_2$-$2H_2O$, 25 g KNO_3, 2.5 g NH_4NO_3, 1.34 g $N_2H_8SO_4$, 2.5 g $MgSO_4$-$7H_2O$, filled up with H_2O to 1 liter], 10 µl micro stock [75 mg KI, 300 mg H_3BO_3, 1 g $MgSO_4$-$7H_2O$, 200 mg $ZnSO_4$-$7H_2O$, 25 mg Na_2MoO_4-$2H_2O$, 2.5 mg $CuSO_4$-$5H_2O$, 2.5 mg $CoCl_2$-$6H_2O$, filled up with H_2O to 100 ml], 10 µl vitamin stock [100 mg Nicotinamide, 100 mg

Pyridoxin/HCl, 1 g Thiamin/HCl, filled up with H_2O to 100 ml], 50 µl EDTA stock [7.46 g EDTA, 5.56 g Fe(II)SO_4-7H_2O, filled up with H_2O to 1 liter], 100 µl Ca-Phosphate stock [1.26 g CaHPO_4-2H_2O, filled up with H_2O to 200 ml, pH 3 adjusted with HCl], 1 mg Myo-Inositol, 2.5 mg D-Xylose, 1.37 g Sucrose [pH 5.6 adjusted with HCl]). Transformed protoplasts were incubated in the dark at 21 °C for 12 to 20 hours prior to analysis with microscope.

For western blot analysis, the solution containing transformed protoplasts was diluted with 1 ml of 1x PBS buffer and centrifuged for 2 minutes at 0.2 g. This step was repeated twice to remove the K3 solution completely. 40 µl of 1x SDS sample buffer were added to the cell pellet and sample was incubated at 98 °C for 5 minutes for protein denaturation.

2.2.2 Molecular biology techniques

2.2.2.1 Transformation of *Escherichia coli*

For propagation of plasmids, chemically competent *E. coli* DH5α cells were transformed with 1 µl of DNA. Samples were incubated on ice for 30 minutes. Heat-shock of cells was performed by incubation at 42 °C for 30 seconds. Then 300 µl of LB medium were added and samples were incubated at 37 °C for 1 hour with shaking. Cells were subsequently plated onto the correct selective LB agar plates.

2.2.2.2 Plasmid DNA isolation from *Escherichia coli*

For extraction of plasmid DNA, a 3 ml LB liquid culture was inoculated with a single bacterial colony and grown overnight at 37 °C. The pellet was gained by centrifugation at 13,000 rpm (maximum speed) for 1 minute. The liquid medium of the supernatant was discarded and the pellet was suspended with 150 µl of P1 buffer (50 mM glucose, 25 mM Tris-HCl [pH 8.0], 10 mM EDTA [pH 8.0]), 250 µl of P2 buffer (0.2 N NaOH, 1 % SDS) were added and sample was inverted. For neutralization, 150 µl of P3 buffer (3 M sodium acetate [pH 4.8]) were added and sample was inverted. Next, 100 µl of a 1:1 phenol:chloroform solution were added and sample was inverted. Samples were centrifuged at 13,000 rpm for 10 minutes at room temperature. The supernatant was transferred to a new reaction tube supplied with 450 µl isopropanol and sample was mixed. For precipitation of DNA, the sample was incubated for 5 minutes at room temperature and centrifuged at 13,000 rpm for 15 minutes at 4 °C. The supernatant was discarded and the pellet was washed with 150 µl of 70 % ethanol and centrifuged for 1 minute at maximum speed. After removal of residual ethanol, the pellet was dried for 20 to 30 minutes. DNA was resuspended in 50 µl of RNAse A solution (1:100 dilution of RNAse A stock in water) and incubated for 20 minutes at 37 °C.

Alternatively, the Plasmid Miniprep Kit I (Peqlab) was used for extraction of DNA plasmids. For medium sized plasmid purifications of liquid cultures of a volume of up to 200

ml, the JetStar 2.0 Plasmid Midiprep Kit (Genomed) was used. The kits and protocols were used according to the manufacturer's instructions.

2.2.2.3 DNA extraction from *Arabidopsis* plants

For extraction of genomic DNA (gDNA), plant materials were frozen in liquid nitrogen and crushed manually with a plastic pistil or with 3 to 7 glass beads (0.45 mm) and a shredder (Tissuelyzer II, speed: 30, 1 minute). Next, 200 µl of DNA extraction buffer (250 mM NaCl, 200 mM Tris-HCl [pH 7.5], 25 mM EDTA [pH 8.0] and 0.5 % SDS) were added and samples were incubated for 20 to 30 minutes in a water bath at 65 °C. 200 µl of a 1:1 phenol:chloroform solution were added, samples were mixed and centrifuged for 15 minutes at maximum speed at room temperature. The supernatant was transferred to a new reaction tube supplied with 450 µl isopropanol and sample was mixed. For precipitation of gDNA, the sample was incubated for 5 minutes at room temperature and centrifuged for 15 minutes at 4 °C. The supernatant was discarded, pellet was washed with 350 µl of 70 % ethanol and centrifuged for 1 minute at maximum speed. After removal of residual ethanol, the pellet was dried for 20 to 30 minutes and gDNA was resuspended with 100 µl of sterile water. For DNA extraction of homozygous *amsh3-1, fyve1- and vfd1-1* mutants and embryos the volumes were decreased to 100 µl and the final suspension volume was decreased to 30 or 50 µl.

2.2.2.4 Cloning of overexpression constructs

All primers used for cloning are listed in Appendix Table 19.
For complementation and expression analysis, three different overexpression constructs of *FYVE1* were cloned using the Gateway Technology (Invitrogen).

The p35S::FYVE1 construct (pCK35) combined the p35S promoter with 835 bp length, the *FYVE1* full length CDS with 1806 bp length and the CaMV 35S terminator with 410 bp length. *Arabidopsis* cDNA was used to amplify *FYVE1* with primers CK40 and CK41. *FYVE1* was then cloned into pDONR207 (Invitrogen) and recombined with the destination vector pGWB414 (Nakagawa et al., 2007).

The N-terminal fusion construct pUBQ10::GFP-FYVE1 (pCK51) combined the pUBQ10 promoter with 639 bp length, *GFP* with 717 bp length and the *FYVE1* full length CDS with 1805 bp length. *Arabidopsis* cDNA was amplified using the primers CK40 and CK132 (altered stop codon) and *FYVE1* was introduced into pDONR207. The new ENTRY vector was named pENTRY-N-FYVE (pCK47). As destination vector pUBN-GFP-DEST was used (Grefen et al., 2010).

The C-terminal fusion construct pUBQ10::FYVE1-GFP (pCK52) combined the pUBQ10 promoter with 639 bp length, the *FYVE1* full length CDS with 1806 bp length and *GFP* with 717 bp length. *Arabidopsis* cDNA was amplified using the primers CK131 (altered

start codon) and CK41 and *FYVE1* was introduced into pDONR207. The new ENTRY vector was named pENTRY-FYVE-C (pCK48). As destination vector pUBC-GFP-DEST was used (Grefen et al., 2010).

All constructs were confirmed by restriction digestion tests and DNA sequencing.

In general, PCR products and plasmids were digested with appropriate restriction enzymes and buffers for 2 to 4 hours at recommended reaction temperature in a reaction volume of 10 µl (analytical) or 50 µl (preparative). Digested DNA was analyzed with a 0.7 % agarose gel.

For ligation, DNA concentration was estimated by comparing the DNA band with the marker in an agarose gel. The molar ratio of insert to vector was chosen as 3:1 or 2:1. A 10 µl reaction volume for ligation contained insert, vector DNA, T4 DNA ligase buffer and 2.5 u of T4 DNA ligase. Ligation reaction was incubated over night at room temperature and transformed in *E. coli* on the next day.

For construction of binary plasmids, the Gateway® cloning system (Invitrogen) was used. The coding region was amplified from cDNA with primers that attached attB1 and attB2 sites to the gene ORF (open reading frame) of interest. The resulting PCR products with attB sites were then inserted into the Gateway® donor vector pDONR207 (gentamycin resistance). After selection and plasmid isolation of the entry clone, a LR reaction was conducted and the DNA fragment was inserted into the respective destination vectors. For BP and LR reactions, the reaction mix was set up according to the protocol of the manufacturer (Gateway BP/LR Clonase II enzyme mix, Invitrogen), except that all reactions were scaled to 4 µl of total volume. Reactions were incubated at room temperature over night, terminated by protease K treatment followed by heat-inactivation of protease K and transformed to *E. coli*.

2.2.2.5 Polymerase chain reaction (PCR)

For genotyping of *Arabidopsis* plants, analytical amplification of DNA fragments was conducted using 10x PCR reaction buffer (20 mM Tris/HCl [pH 8.4], 50 mM KCl and 2.5 mM MgCl$_2$) and lab-made *Taq* DNA polymerase. Each reaction had a final volume of 30 µl (5 µl gDNA, 17.1 µl water, 3 µl 10x PCR reaction buffer, 3 µl dNTPs [20 mM each], 0.3 µl of each primer [50 µM] and 0.3 µl *Taq* DNA polymerase). For cloning of complex DNA constructs, *Phusion High-Fidelity* DNA polymerase (New England BioLabs) and *Phusion* HF buffer were used.

The PCR program varied for desired product length and amplification cycles. In general, a genotyping PCR program with *Taq* DNA Polymerase consisted of an initial denaturation step at 95 °C for 2 minutes, step 1 at 95 °C for 30 sec, step 2 at 58 °C for 1 min, step 3 for 72 °C for 1 min. Step 1 to 3 were repeated 25 to 30 times. The final elongation step was set to 72 °C for 5 minutes and the reaction was then cooled to 10 °C. The primer

annealing temperature was calculated as primer melting temperature minus 2 °C. The elongation time per cycle was calculated due to the used polymerase (*Taq* polymerase 30 s/kb, *Phusion* polymerase 1 min/kb). For analysis of PCR products 0.7 % agarose gels with 0.1 % ethidium bromide were cast and checked under an UV light illuminator. For extraction of DNA fragments from agarose gels, the QIAEX II Gel Extraction kit and protocol (QIAGEN) were used.

2.2.2.6 DNA purification

For general purification of DNA (PCR products and restriction digest fragments), the Wizard SV Gel and PCR Clean-Up System (Promega) was used. The protocol was used according to the manufacturer's instructions. DNA concentration and purity was measured with the Nanodrop 2000c (Thermo Scientific).

2.2.2.7 Sanger DNA sequencing

For DNA sequencing, samples were purified with the Wizard SV Gel and PCR Clean-Up System (Promega). DNA sequencing was performed by Eurofins MWG Operon.

2.2.2.8 SSLP markers for molecular mapping of EMS induced mutations

For rough and fine mapping purposes, simple sequence length polymorphism (SSLP) markers were used. SSLP markers, also called insertion-deletion markers, are tandemly repeated di- to tetranucleotides flanked by unique sequences and differ in each ecotype of *Arabidopsis*.

Back-crossed, homozygous *vfd1* mutants of hybrid Col-0/L*er* background from the F_2 generation of the established mapping population were used as samples. Pure Col-0 and L*er* wild-type samples were used as controls. Samples were pooled for bulk segregant analysis. Standard PCR was performed with primer pairs specific for each SSLP marker. The PCR products were analyzed using gel electrophoresis. For higher resolution of small PCR products high percentage (3 to 4 %) agarose gels were run. The first 5 minutes 50 V were applied, after this time 100 V were applied for 40 minutes.

Using bulk segregant analysis, the obtained PCR products included a mixture of Col-0 and L*er* DNA fragments. By analyzing the ratio between Col-0 and L*er* product bands, linkage between a possible mutation site and the marker product was obtained. Because the *vfd1* mutation was linked to Col-0 background, a thicker Col-0 band indicated linkage to a specific marker site.

2.2.2.9 Next generation sequencing (NGS)

To define the *vfd1* mutation and exact location of the SNP mutation, a DNA sample of the *vfd1* mutant line (Col-0, GFP::δ -TIP) was prepared for next generation sequencing (NGS).

42 specimen of 7-day-old homozygous *vfd1* mutants were collected and genomic DNA was extracted following standard protocol for mutant samples and eluted with 40 µl of double distilled water. As control sample, ten 7-day-old seedlings of wild-type Col (GFP::δ-TIP) marker line were used. DNA samples were sent for library preparation and sequencing to the Genome Center of the MPI in Tübingen. Whole-genome sequencing was performed with a HiSeq 2000 (Illumina) and 150 bp paired-end reads. Bioinformatical data analysis was performed by Jörg Hagmann (MPI, Tübingen). The sample sequence was compared to the reference sequence from wild-type Columbia (TAIR 10).

2.2.2.10 CAPS marker for *vfd1* specific SNP mutation

For genotyping of the EMS generated *vfd1* mutant, the SNP mutation itself was used as a cleaved amplified polymorphic sequence (CAPS) marker. By using the primers CK92 and CK93, a fragment of genomic DNA including the *vfd1* specific SNP was amplified by standard PCR reaction. The PCR product was digested at 55°C for 1 to 2 hours with the restriction enzyme *Mae*III (Roche Life Science) and analyzed on an standard agarose gel. The *Mae*III restriction site sequence included the *vfd1* specific SNP. Reaction volume was 20 µl or 50 µl.

If plants were homozygous for the *vfd1* specific SNP, the PCR product was homogenously cleaved into two shorter fragments and bands characteristic for the *vfd1* allele were observed. If plants were wild-type (without the SNP), the PCR fragment was not cleaved and bands specific for the wild-type allele were observed. If plants were heterozygous, one fraction of the PCR product reflecting the wild-type allele was not cleaved, the other fraction was cleaved, resulting in two bands.

2.2.2.11 RNA extraction from plants

For extraction of total RNA of 7-day-old *Arabidopsis* seedlings, the NucleoSpin® RNA Kit and protocol (Macherey-Nagel) were used to manufacturer's instructions. RNA was eluted with 40 to 60 µl of RNase-free water. RNA concentration and quality was measured with the Nanodrop 2000c.

2.2.2.12 First strand cDNA synthesis

cDNA was synthesized with M-MuLV Reverse Transcriptase (Thermo Scientific) following the manufacturer's protocol. 2 µg of template (total RNA) were used per reaction

and 1 µl of a Oligo(dT)$_{18}$ primer (20 µM) were added to a total volume of 10 µl reaction mix. After incubation for 5 minutes at 65 °C, samples were cooled on ice. Next, the 5x reaction buffer, 10 mM of each dNTPs and 40 units of M-MuLV reverse transcriptase were added. Reaction was incubated for 1 hour at 37 °C and terminated by incubation at 70 °C for 10 minutes. The cDNA was further diluted with 20 µl of water after termination of the reaction.

2.2.2.13 Quantitative real-time PCR (qRT-PCR)

For quantitative real-time PCR (qRT-PCR), a cDNA equivalent of 25 ng total RNA and the *iTaq Universal SYBR Green Supermix* (Bio-Rad) were used in a 10 µl PCR reaction volume. A two-step-program (10 s at 95 °C, 30 s at 60 °C) with 40 cycles was run on the *CFX96 Real-Time System C1000 Thermal Cycler* (Bio-Rad). For each experiment, at least two biological replicates and four technical replicates were examined. The expression data of single genes were normalized against the expression of the gene *ACTIN8* (*ACT8*). The mean value and the standard deviation were analyzed.

2.2.3 Biochemical methods

2.2.3.1 Protein extraction from plants

For preparation of total protein extracts of *Arabidopsis*, plant material was frozen in liquid nitrogen and homogenized with addition of protein extraction buffer (50 mM Tris-HCl [pH 7.5], 150 mM NaCl, 0.5 % Triton X-100, 10 µM MG132, 0.1 µM PMSF and 0.1 µM Complete EDTA free inhibitor cocktail). For 100 mg of plant material, 200 µl protein extraction buffer was added. For removal of cell debris, the samples were centrifuged at 4 °C maximum speed for 10 minutes and the soluble supernatant was transferred to a new reaction tube.

Protein concentration was determined by Bradford assay (Bio-Rad) (Bradford, 1976). For soluble proteins, 5x Laemmli buffer (310 mM Tris-HCl [pH 6.8], 50 % glycerine, 10 % SDS, 0.5 % bromophenolblue and 3.5 % β-mercaptoethanol) was added to the protein extracts and samples were heated at 95 °C for 5 minutes. For membrane proteins, like PIN and FYVE1, samples were incubated at 42 °C for 10 minutes.

2.2.3.2 Subcellular fractionation by ultracentrifugation

For detection of PIN proteins and differentiation of membrane and soluble proteins, subcellular fractionation was performed with an ultracentrifuge. For ultracentrifugation, protein extraction buffer A without Triton X-100 was prepared (PEB A: 75 µl 1 M Tris-HCl [pH 7.5], 45 µl 5 M NaCl, 15 µl PMSF, 15 µl Complete EDTA free inhibitor cocktail, 7.5 µl MG132, 1.3425 ml H$_2$O). After protein extraction, samples were centrifuged for 10 minutes at 13,000 g at 4 °C. The supernatant (S13 fraction) was transferred into an ultracentrifugation tube.

Samples were centrifuged at 100,000 g at 4 °C in the Sorvall MTX 500 benchtop centrifuge (Thermo Scientific) used with a S55-A2 rotor (Thermo Scientific). The resulting supernatant was termed S100 and the pellet fraction P100. For PIN protein blots, only the P100 fraction was used, dissolved in 1x Laemmli buffer (diluted with PEB A) and incubated at 42 °C for 10 minutes while rotating at 1400 rpm to solve the pellet.

2.2.3.3 Sodiumdodecylsulfate-polyacrylamid-gel electrophoresis (SDS-PAGE)

Total protein extracts and membrane fractions were separated by SDS-PAGE (Laemmli, 1970). The 4x stacking gel buffer contained 0.5 M Tris and 0.4 % SDS, adjusted with 32 % HCl to pH 6.8 and filled up with water. The 4x separating gel buffer contained 1.5 M Tris and 0.4 % SDS, adjusted with 32 % HCl to pH 8.8 and filled up with water.

4.5 % stacking gels (4x stacking gel buffer, 30 % polyacrylamide solution, 10 % APS, Temed, filled up with water) and 8 to 12 % separating gels (4x separating gel buffer, 30 % polyacrylamide solution, 10 % APS, Temed, filled up with water) were used. For gel preparation a 30 % polyacrylamide solution (acrylamid/bisacrylamid 29:1) was used. Gels were run in *Mini Protean III* cells (Bio-Rad) for approximately 1 hour with 20 mA constant current per gel.

2.2.3.4 Western blot

For immuno-detection, proteins were transferred from SDS-PAGE gels to blotting membranes (PVDF or nitrocellulose for PIN blots) with a semi-dry blotter (Bio-Rad) and the semi-dry (SD) transfer buffer (25 mM Tris, 192 mM glycine, 20 % methanol, 1.3 mM SDS, pH 8.3 adjusted with NaOH). The general blotting program was set to 1 hour at 50 V, 2-3 mA per cm² gel. For ubiquitination profiles, a condition of 2 hours at 25 V and 3 mA per cm² gel was used. After transfer, the membrane was incubated for 10 minutes in 5 % milk powder blocking solution with 1x PBST (10x PBS [1.39 M NaCl, 27 mM KCl, 125 mM NA_2HPO_4, 18 mM KH_2PO_4] and 0.5 % Tween 20) or 1x TBST (10x TBS buffer [50 mM Tris-HCl, 150 mM NaCl, 1 mM $MgCl_2*6H_2O$, pH 7.8 adjusted with HCl] and 0.05 % Triton X-100), respectively. Incubation with the primary antibody (diluted in blocking solution) was performed for 1 hour at room temperature or at 4 °C over night. Next, the membrane was washed three times for 10 minutes with PBST or TBST and incubated for 1 hour with the secondary antibody that was diluted in PBST or TBST at room temperature. After the incubation period, the membrane was washed again three times for 10 minutes with PBST or TBST. TBST was used for western blots in general. For PIN blots, PBST was used. Chemiluminescence was detected with the *Super Signal West Femto Maximum Sensitivity Substrate* (Thermo Fisher Scientific) and *Luminescent Image Analyzer LAS-4000 mini* (Fujifilm).

2.2.4 Microscopy

2.2.4.1 Confocal microscopy

Microscopy was performed with a fluorescence microscope (Olympus BX61 with black-white digital camera XM10, Olympus) and with a confocal laser scanning microscope (FV1000/IX81 with objectives UPLFL 10x, UPLFLN 20x, PLAPO 40xW and UPLSAPA 60xW, Olympus). GFP signals were visualized using the 488 nm laser line and RFP signals with the 559 nm laser line. For image acquisition, cellSens Dimension and FluoView FV1000 Software (Olympus) were used. Images were processed using Adobe Photoshop CS3 Extended (version 10.0) and Adobe Illustrator CS3 (version 13.0.0).

2.2.4.2 FM4-64 staining and BFA treatment

Arabidopsis wild-type and mutant seedlings were grown on GM plates at continuous light for 2 or 5 days, respectively, to obtain wild-type seedlings of similar phenotype and developmental stage like the mutants. Seedlings were incubated for at least 10 minutes in FM4-64 solution (2 mM stock solution in water, 1:1000 dilution for use, Invitrogen) prior to observation with the confocal microscope. For BFA treatment, seedlings were incubated for one hour in a FM4-64/BFA solution (50 mM stock solution in DMSO, 1:1000 dilution for use). For dilution prior to incubation, liquid MS medium was used.

2.2.5 Database and sequence analysis

For *Arabidopsis* DNA and protein sequence acquisition, the "The Arabidopsis Information Resource 10" (TAIR10; www.arabidopsis.org) database was used. For other sequences, the National Center for Biotechnology Information (NCBI) database (www.ncbi.nlm.nih.gov), the UniProtKB database (www.uniprot.org) or the JGI Phytozome database (www.phytozome.net) for sequences of other plant species were used.

Primer, DNA, RNA and protein sequences were analyzed and aligned using the Geneious Pro software (version 5.3.6, Biomatters Ltd.) using the pairwise alignment and score matrix Blosum62. For phylogenetic analysis, the Geneious Pro software was also used.

3. Results

3.1 EMS mutagenesis screen for *vfd* mutants

At the beginning of this study, 13 mutant lines that showed the *vacuolar fusion defective* (*vfd)* phenotype reproducibly were chosen for analysis. Due to the altered vacuole morphology and the assumption that the candidate mutants had a defect in vacuolar membrane fusion, they were named *vfd*1 to *vfd*13. Table 2 offers an overview over all obtained mutant lines, which are part of the new *vfd* mutant collection.

The *vfd* mutants combined two major characteristics of the *amsh3* mutant: firstly, *vfd* mutants were seedling lethal. Mutants stopped seedling growth at a developmental stage comparable to 2-day-old wild-type seedlings. Moreover, *vfd* mutants displayed whitish color, suggesting that also chlorophyll biosynthesis was affected during seedling development. After 7 days in light, mutants only developed cotyledons and roots were shorter and mostly without any root hairs. Secondly, mutants showed the *amsh3*-like vacuole phenotype (Figure 8). The *vfd* mutants did not develop large central vacuoles, but instead had fragmented, small vacuoles that showed a bubble-like structure.

Table 2. Overview of the 13 identified *vfd* mutant lines.
The respective M_2 lines were given a *vfd* number. Segregation analysis is shown in mutant number vs. total seedling number (percentage of mutants in comparison to percentage of mutants plus ungerminated seeds). Allele test crosses with *amsh3* mutants were performed (n.a.: not available/not conducted).

vfd #	Original *vfd* line #	Segregation (mut %; mut + ungerminated %)	Allele test to *amsh3*
1	#343.36	37/251 (14.7 %; 21.9 %)	non-allelic
2	#505.9	2/495 (0.4 %; 9.9 %)	non-allelic
3	#621.30	2/326 (0.6 %; 5.2 %)	non-allelic
4	#230.13	2/227 (0.9 %; 12.8 %)	non-allelic
5	#327.1	3/444 (0.7 %; 19.4 %)	non-allelic
6	#124.15	5/128 (3.9 %; 9.4 %)	n.a.
7	#202.2	7/272 (2.6 %; 4.8 %)	n.a.
8	#229.13	2/230 (0.9 %; 21.3 %)	n.a.
9	#251.8	2/297 (0.7 %; 9.8 %)	non-allelic
10	#379.13	3/109 (2.8 %; 2.8 %)	n.a.
11	#399.4	3/324 (0.9 %; 21.6 %)	non-allelic
12	#444.7	1/159 (0.6 %; 11.9 %)	n.a.
13	#491.2	1/287 (0.3 %; 9.8 %)	n.a.

GFP::δ-TIP
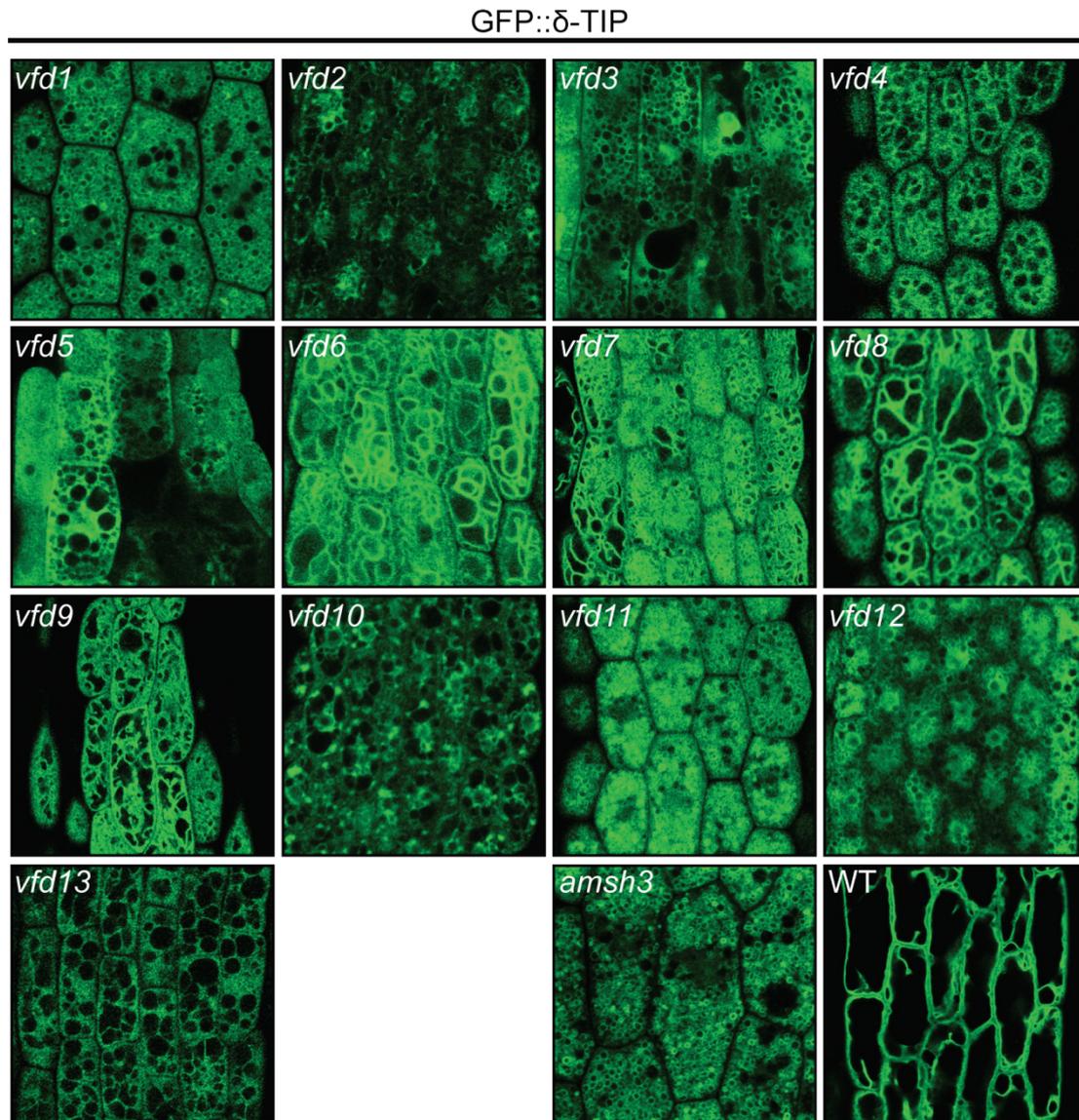
Figure 8. The EMS Screen resulted in a collection of 13 *vfd* mutants, which all show an aberrant vacuole morphology. The vacuolar membrane is outlined by the tonoplast marker protein GFP:: δ-TIP. Hypocotyl cells of 7-d-old *vfd* mutant seedlings are shown.

It was not possible to categorize the *vfd* mutants in respect to the vacuolar phenotype, because the severeness of the vacuolar morphology defect was variable even among mutant seedlings of the same *vfd* line.

To analyze whether *vfd* mutations are monogenous and whether the mutation is recessive or dominant, the segregation ratio in each mutant was examined (Table 2). For a typical monogenous recessive mutant, a 25 % appearance of the mutant phenotype was to be expected. In analyzed lines, the proportion of *vfd* mutants was less than the expected percentage for a recessive phenotype. Instead, depending on the *vfd* mutant line, a very small number of mutants ranging from 0.3 to 14.7 % was observed. The segregation analysis revealed that the *vfd* mutants had a higher number of ungerminated seeds in comparison to the wild-type or *amsh3* mutant, suggesting that the *vfd* mutation causes embryo lethality. By

prolonging the time of stratification up to 10 days, the germination rate of *vfd1* mutants could be improved. However, even with prolonged stratification, the proportion of mutants within the analyzed population reached in the highest case 14.7 %, but never the expected 25 %, suggesting that *vfd1* is probably monogenous and that *VFD1* is required for proper embryo development and germination.

Because of the similarity between *vfd* and *amsh3* mutants, possible allelism between *vfd* and *amsh3* was tested. For this purpose, heterozygous *vfd* plants were crossed with heterozygous *amsh3* plants. Heterozygosity of *vfd* plants was determined by segregation analysis in the next generation after selfing. Crosses were analyzed in the F_1 generation for the segregation ratio of wild-type-looking seedlings and *vfd* mutants (Table 2). If the *vfd* mutation would be another *amsh3* allele, the F_1 progeny should show a segregation pattern of 25 % *amsh3*-like phenotype and 75 % of wild-type-looking seedlings. If an independent gene locus was affected, then no *amsh3*-like phenotypes would be observed. The result of this analysis showed that all tested *vfd* lines were indeed independent of the *AMSH3* gene locus (Table 2). To verify that the allele-test crosses were successful, eight seedlings of each cross were genotyped for the *amsh3* transposon insertion. Due to segregation of the independent *amsh3* allele, 50 % of F_1 seedlings were heterozygous for the *amsh3* transposon.

To examine whether *vfd1* and *vfd3* were allelic, heterozygous parents were crossed and F_1 progeny was analyzed. Heterozygosity of *vfd* plants was determined by segregation analysis in the next generation after selfing. No mutants or ungerminated seeds were observed in the F_1 progeny for two independent crosses ($n_1=28$, $n_2=34$; n: number of F_1 progeny), indicating that *vfd1* and *vfd3* are independent mutant alleles.

To confirm that *vfd1* is a monogenetic mutation, heterozygous *vfd1* plants were backcrossed with the wild-type GFP::δ-TIP (Col-0) marker line (Table 2). Heterozygosity of *vfd* plants was determined by segregation analysis in the next generation after selfing. Crosses were analyzed in the F_1 generation for the respective segregation ratio. For all analyzed *vfd* lines, the F_1 progeny looked 100 % like the wild-type, indicating a recessive inherited mutation. Segregation analysis of R_1F_2 progeny from four *vfd1* backcrosses showed the expected segregation of 50 % heterozygous and 50 % wild-type R_1F_1 plants (n= 10 R_1F_2 lines; 5 lines heterozygous, 5 lines wild-type; > 200 seedlings for each line) confirming the monogenous nature of the *vfd1* mutation.

To investigate whether the *vfd* mutants shared further characteristics with the phenotypically similar *amsh3* mutants, the ubiquitination profile and AMSH protein levels were analyzed by western blot (Figure 9). Ubiquitination profiling of the mutant lines *vfd1*, *vfd2*, *vfd3, vfd11* and *vfd12* was carried out (Figure 9 A and B). Like in the *amsh3* mutant, ubiquitin conjugates accumulated in the *vfd* mutants, indicating that VFD proteins may
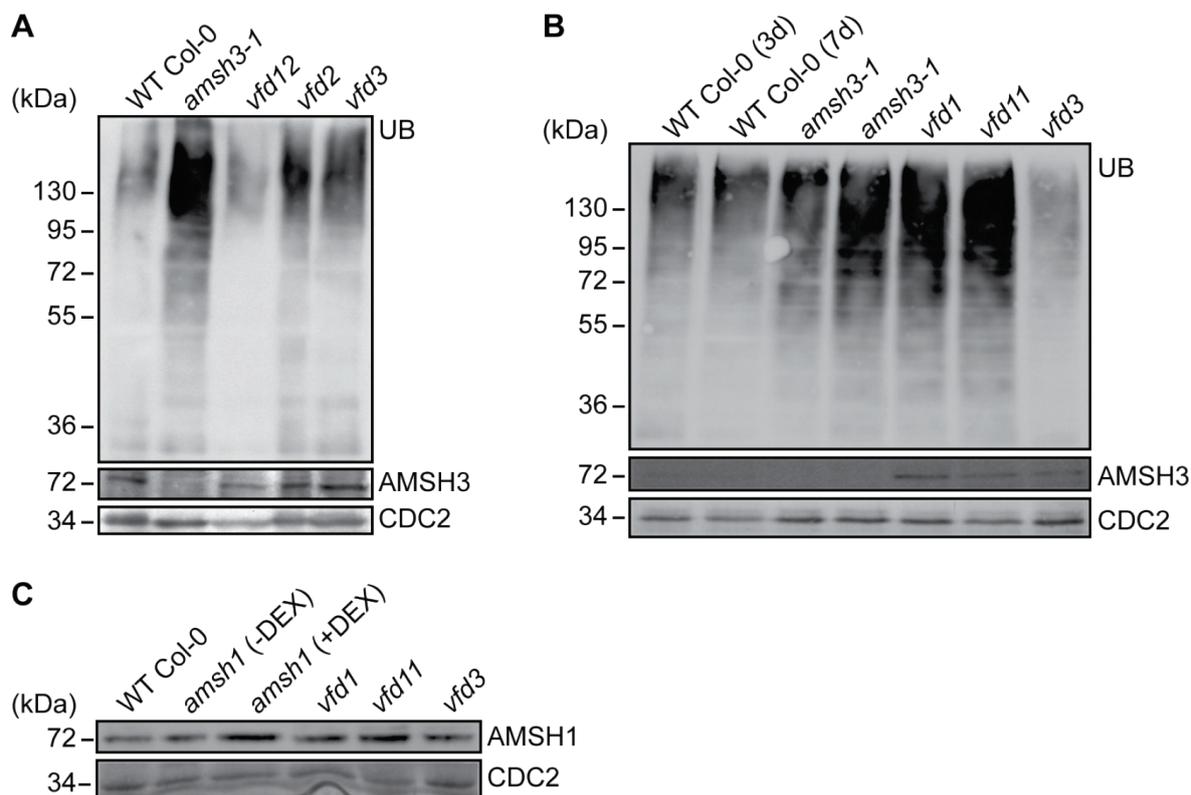
Figure 9. *vfd* mutants show accumulation of ubiquitin conjugates and express AMSH proteins.
(A) and **(B)** Ubiquitination profile of selected *vfd* mutant lines. anti-AMSH3 western blot showed that AMSH3 was not affected in mutants. WT Col-0 and *amsh3* homozygous mutants as control. Loading control: CDC2. **(C)** AMSH1 is present in selected *vfd* mutant lines. WT Col-0 and Dex-inducible *amsh1* mutants as control. Loading control: CDC2.

function in the same cellular process of AMSH3. On the other hand, the *vfd* mutants did not show alteration in the abundance of AMSH1 (Figure 9 C) and AMSH3 (Figure 9 A and B), indicating that they are not regulating AMSH protein stability.

3.2 Characterization of the *vfd1* (*fyve1-2*) mutant as a new *amsh3*-like mutant

For further characterization, the *vfd1* mutant line was selected in this study. This line showed a wild-type to mutant ratio that was closest to the expected Mendelian segregation, indicating that *vfd1* is monogenic and recessive (Table 3).

Table 3. *vfd1* is a homozygous recessive mutant.

Line	wild-type	ungerminated	mutants	total
GFP::δ-TIP (Col-0)	270 (100 %)	0	0	270
amsh3	206 (79.2 %)	9 (3.5 %)	45 (17.3 %)	260
		54 (20.8 %)		
vfd1	196 (78.1 %)	18 (7.2 %)	37 (14.7 %)	251
		55 (21.9 %)		
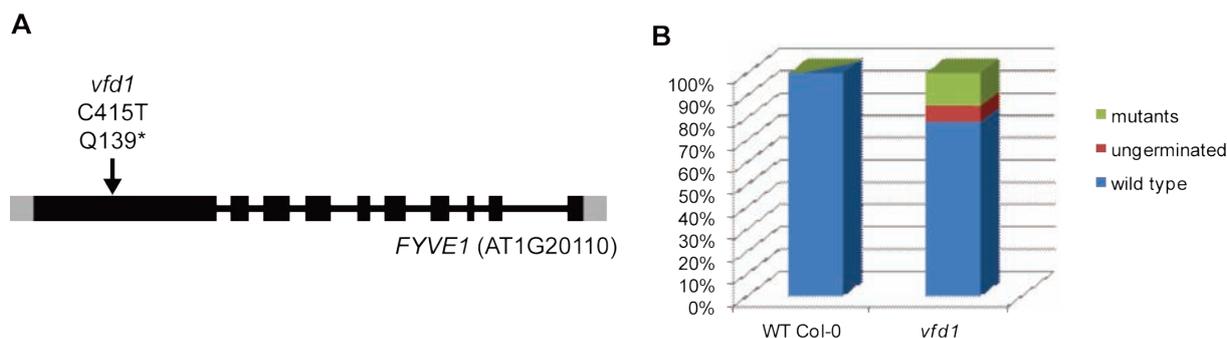
Figure 10. The SNP mutation in gene AT1G20110 leads to the recessive inheritance of the *vfd1* mutation.
(A) Localization of the EMS SNP mutation site of the *vfd1* mutant in the *FYVE1* gene. The nucleotide exchange of C to T at position 415 leads to the change of amino acid 139 from glutamine (Q) to a stop codon. Thick black bars symbolize exons, thin black lines represent introns. Grey bars represent UTR regions. **(B)** Schematic of segregation ratio of wild-type, ungerminated seeds and homozygous mutants between wild-type Col-0 (GFP::δ-TIP) and *vfd1* mutant (numbers are shown in Table 3).

The *vfd1* mutant showed the two characteristic *vfd* phenotypes: *vfd1* showed seedling lethality, lacking development of proper roots, secondary leaves or greening of cotyledons (Figure 11 A). *vfd1* mutants also showed defects in central vacuole formation and seemed to accumulate many smaller vacuoles (Figure 11 B). In addition, the *vfd1* mutant accumulated higher amounts of ubiquitinated proteins compared to the wild-type, like the *amsh3* mutant (Figure 9 B).

The genetic allele test with the *amsh3* mutant has already shown, that the *vfd1* mutation is independent of the *AMSH3* gene locus and therefore *vfd1* is not another *amsh3* mutant allele. In addition to the allele test with the *amsh3* mutant and western blots with α-AMSH1 and α-AMSH3 antibodies (Figure 9), the gene loci of *AMSH2* and *AMSH3* in *vfd1* were examined by classical Sanger sequencing. This should exclude at the DNA sequence level that the *vfd1* mutant was another mutant allele of *amsh3*.
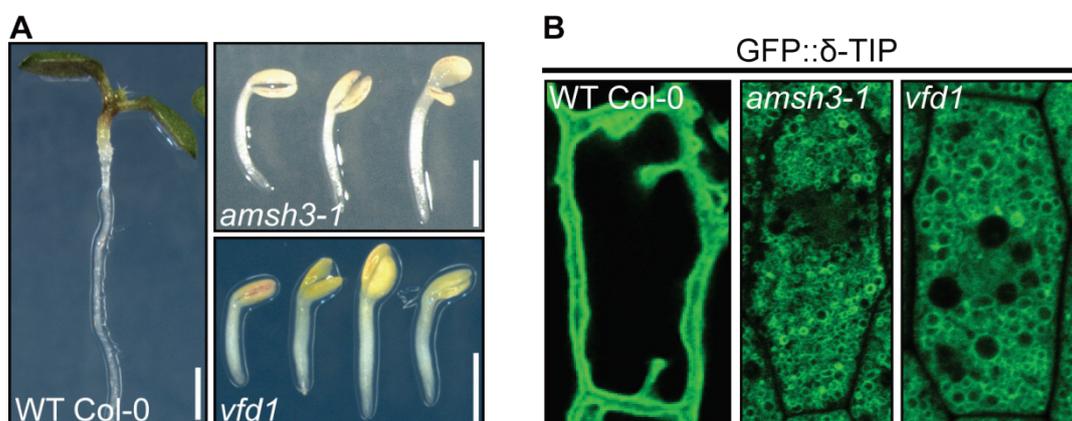
Figure 11. The *vfd1* EMS mutant shows the same phenotypes as the *amsh3* mutant.
(A) Phenotypes of 7-day-old seedlings of wild-type Col-0 (GFP::δ-TIP), homozygous *amsh3-1* mutants and homozygous *vfd1* mutants. Scale bars: 1 mm. **(B)** Vacuolar phenotype of 7-day-old seedlings of wild-type Col-0 (GFP::δ-TIP), homozygous *amsh3-1* mutant and homozygous *vfd1* mutant. Hypocotyl cells are shown. GFP::δ-TIP tonoplast marker is outlining the vacuolar membranes.

The *AMSH2* gene locus was investigated, because the genetic mapping of *vfd1* indicated the EMS SNP was located to the same region of chromosome 1. The *AMSH2* (AT1G10600) gene is located to *Arabidopsis* chromosome 1 and consists of 7 exons and a total length of 1,426 bp from the start codon ATG to the stop codon TAA. The *AMSH3* (AT4G16144) gene is located to *Arabidopsis* chromosome 4 and consists of 13 exons (3,370 bp ATG-TAA gDNA). Both loci were fully sequenced and analyzed for classical EMS generated C to T SNP mutations. No SNPs or mutations were found for the *AMSH2* gene. For the *AMSH3* gene, only slight sequence variations were detected (Figure 12). Four of the nucleotide variations were silent mutations. The amino acid change from glutamic acid (E) to lysine (K) is an already known polymorphism between different *Arabidopsis* ecotypes and is probably not leading to dramatic differences in protein function. Together, these results indicated that the *vfd1* mutant is not allelic to *amsh3*.

The *vfd1* SNP mutation (C415T) was localized to Exon1 (Figure 10 A) and leads to an exchange of the amino acid glutamine (CAA) to a stop codon (TAA). This amino acid change results in a truncated protein of 138 amino acids without the characteristic domains of the FYVE1 protein, suggesting that the truncated protein is probably non-functional.

Since there was no antibody available for detection of the endogenous FYVE1 protein, qRT-PCR analysis was carried out to investigate the gene expression of *FYVE1*. qRT-PCR was performed with cDNA derived from 7-day-old *vfd1* homozygous mutants and wild-type GFP::δ-TIP (Col-0). Two primer combinations were used. One primer combination detected transcript levels of the truncated version of *FYVE1*, detecting 60 bp at the start of the first exon (Figure 13 A). The other primer combination detected the full length gene product, spanning the intronic region between second and third exon. Both RNA products are present in the EMS mutant *vfd1*. qRT-PCR analysis revealed that both gene products are expressed in *vfd1*, but to a higher extent compared to the wild-type (Figure 13 B). This could hint to a higher expression ratio, because the *vfd1* mutant lacks a functional FYVE1 protein, directing the protein biosynthesis machinery of the cell to produce more FYVE1 protein.
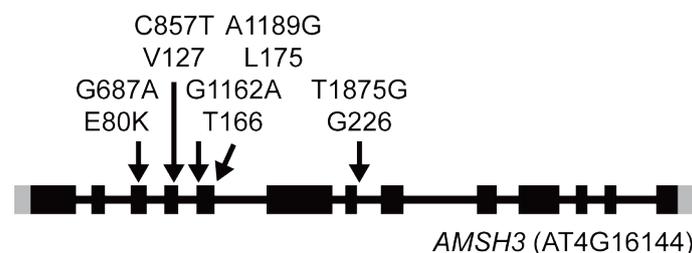
Figure 12. Sequencing of the *AMSH3* gene locus of *vfd1* reveals several point mutations.
Five nucleotide alterations are shown with sequence position and resulting amino acid change. Only one observed mutation leads to an amino acid change. Thick black bars symbolize exons, thin black lines represent introns. Grey bars represent UTR regions.
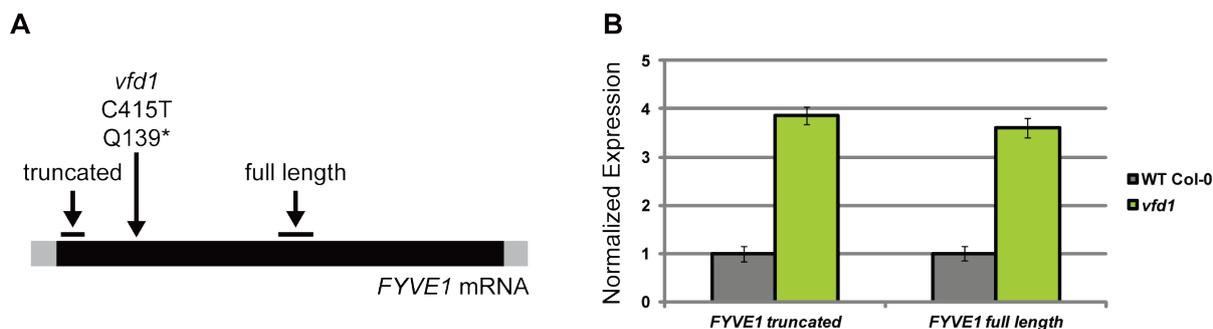
Figure 13. The *vfd1* EMS mutant has increased *FYVE1* RNA transcript levels.
(A) Primer target sites of qRT-PCR analysis for a *FYVE1* truncated transcript and for a *FYVE1* full length transcript. SNP mutation site for *vfd1* is shown. **(B)** Expression levels of *FYVE1* mRNA in WT Col-0 (GFP::δ-TIP) and *vfd1* mutant. 7-d-old seedlings were used for qRT-PCR analysis.

3.3 Identification of *VFD1*

3.3.1 Classical mapping of the *VFD1* candidate region

For identifying *VFD1*, a mapping population was established for the *vfd1* line by crossing multiple heterozygous *vfd1* plants with wild-type *Landsberg erecta* (L*er*). F$_1$ plants were allowed to self and F$_2$ seeds were collected for further analysis.

Map-based cloning was performed in two steps. First, a rough mapping was conducted to identify the chromosome to which the *vfd1* mutation is located. Secondly, the target chromosome was fine-mapped in a smaller genetic interval to narrow down the region of the *vfd1* mutation. Most *Arabidopsis* ecotypes exhibit specific nucleic acid sequence polymorphisms relative to other ecotypes. By crossing two different ecotypes, the genetic differences specific for each ecotype are segregating and are used as genetic markers. The *vfd1* mutation locus was determined by measuring the recombination frequencies between this locus and genetic markers with defined positions in the genome. In the F$_2$ generation homozygous *vfd1* mutant seedlings were scored and collected based on the seedling lethal phenotype (Table 4).

Five of ten F$_2$ lines were heterozygous for the mutant allele, indicating that the F$_1$ cleanly divided in 50 % wild-type hybrids and 50 % heterozygous plants. Homozygous *vfd1* mutants occurred in a percentage of 2.3 to 14.0 %, still indicating a high variability in germination efficiency. If mutants and ungerminated seeds were taken together, 15.1 to 24.3 % of the expected 25 % of a recessive inherited mutation were observed.

Table 4. Segregation analysis of the F$_2$ generation of the *vfd1* mapping population.

F$_2$ Line #	wild-type	ungerminated	mutant	total
#3	219 (78.2 %)	52 (18.6 %)	9 (3.2 %)	280
#5	233 (80.0 %)	36 (12.4 %)	22 (7.6 %)	291
#8	243 (75.7 %)	33 (10.3 %)	45 (14.0 %)	321
#9	294 (84.2 %)	33 (9.5 %)	22 (6.3 %)	349
#10	298 (84.9 %)	45 (12.8 %)	8 (2.3 %)	351

For bulk segregant analysis, 106 *vfd1* mutant seedlings were collected from five F$_2$ lines. Genomic DNA of the bulk sample was extracted and analyzed by PCR. Specific SSLP marker primers (Table 19) were used for mapping and the *vfd1* mutant pool genotype was determined. 10 primer pairs, two for each chromosome of *Arabidopsis*, were used for rough mapping PCRs (Figure 14).

Linkage and frequency of occurrence of the allele were determined by comparing the migration pattern of the PCR (Figure 15). Marker NGA63 showed a higher intensity of the Col-0 allele band, indicating a linkage of the *vfd1* mutation to this marker position. All other markers resulted in heterozygous distribution of both alleles, revealing that the *vfd1* mutation is located on chromosome 1.

To further define the position of the *vfd1* mutation on chromosome1, fine mapping was carried out with ten additional SSLP markers to cover the distance in smaller intervals. Markers CIW12, NF7G19, F16J7-TRB, T16N11 and NGA392 showed a higher intensity band and tendency for the Col-0 allele. Fine mapping resulted in a 7 Mbp candidate region from 3 Mbp to 10 Mbp on the upper arm of chromosome 1. Given that approximately 20 to 30 gene loci are present in a 100 kbp region (Weigel and Glazebrook, 2002), a genetic distance of 7 Mbp contains around 2.100 candidate genes.
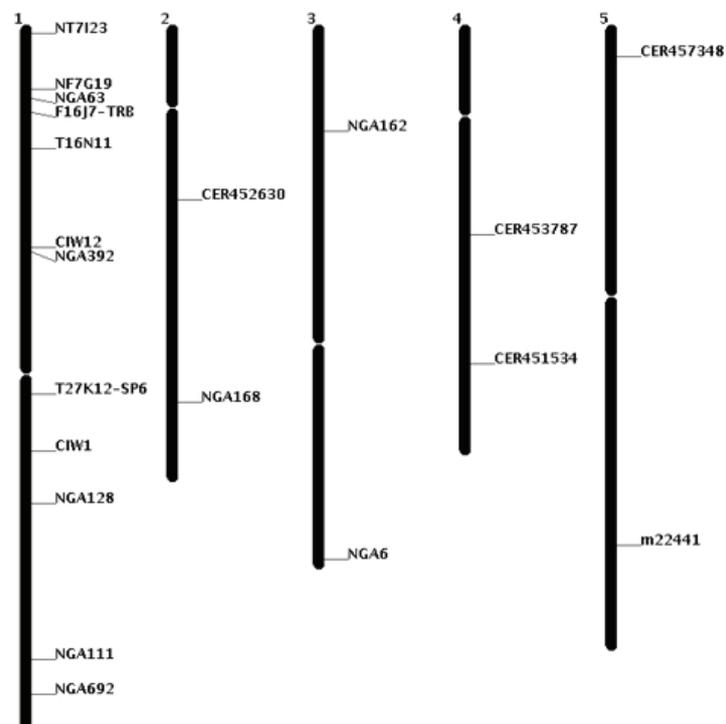
Figure 14. SSLP markers were used for classic genetic mapping of the EMS mutation site. This chromosome map shows the positions of used SSLP markers for rough and fine mapping of all five *Arabidopsis* chromosomes (Chromosome Map Tool, TAIR).
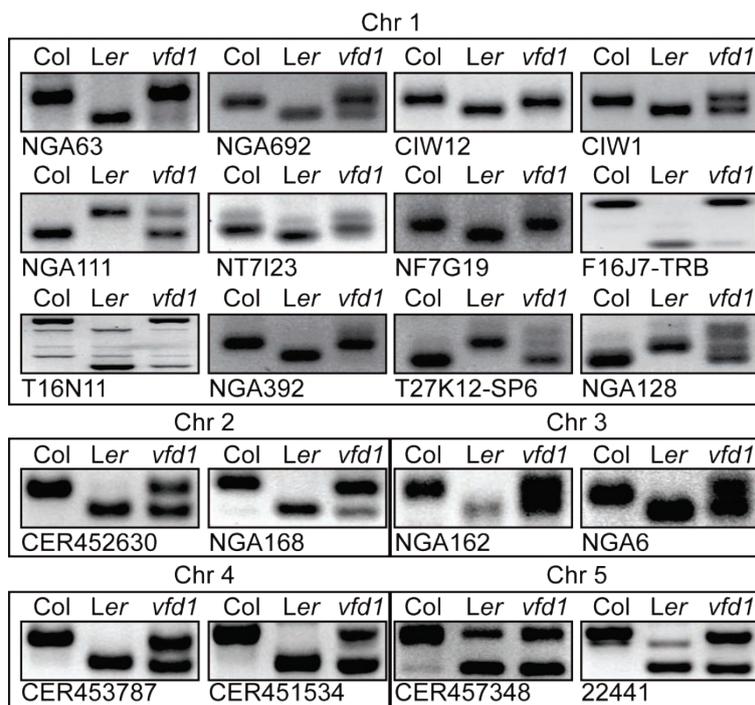
Figure 15. Positional mapping of *vfd1* mutation indicates SNP position on 7 Mbp candidate region on the upper arm of chromosome 1. PCR analysis with respective SSLP markers of *vfd1* mutant pool, wild-type Col-0 (Col) and wild-type L*er* controls.

3.3.2 Next generation sequencing (NGS)

To identify polymorphisms within the candidate region, whole genome sequencing was performed. For NGS, gDNA was extracted from 42 homozygous *vfd1* mutants that were backcrossed once. Library preparation, NGS and data analysis were conducted in collaboration with Jörg Hagmann of the MPI Tübingen. For data analysis and plot imaging only high-scoring (SHORE-specific score (Schneeberger et al., 2009): support above 5, concordance above 70 %, non-repetitive) EMS-like SNPs were selected. As a result 344 SNPs were found on all five chromosomes and most of the hits cluster on chromosome 1. When plotted in a 1.000.000 bp window, the smooth curve indicated a candidate region between 6 and 7 Mbp on chromosome 1 (Figure 16).

In total, 35 SNPs were localized to the candidate region between 5 and 9 Mbp on chromosome 1, that contained 12 non-synonymous SNPs. The list of candidate mutations and the gene identity are shown in Table 5 and Table 6, respectively. Candidate SNPs were verified by Sanger sequencing and all tested SNPs were present in the *vfd1* mutant genome. Among the 12 non-synonymous mutations, candidate 4 in AT1G20110 was the only non-sense mutation, where a change of C to T resulted in the exchange of the amino acid glutamine (Q) to a stop codon, leading to the production of a truncated and maybe non-functional protein.
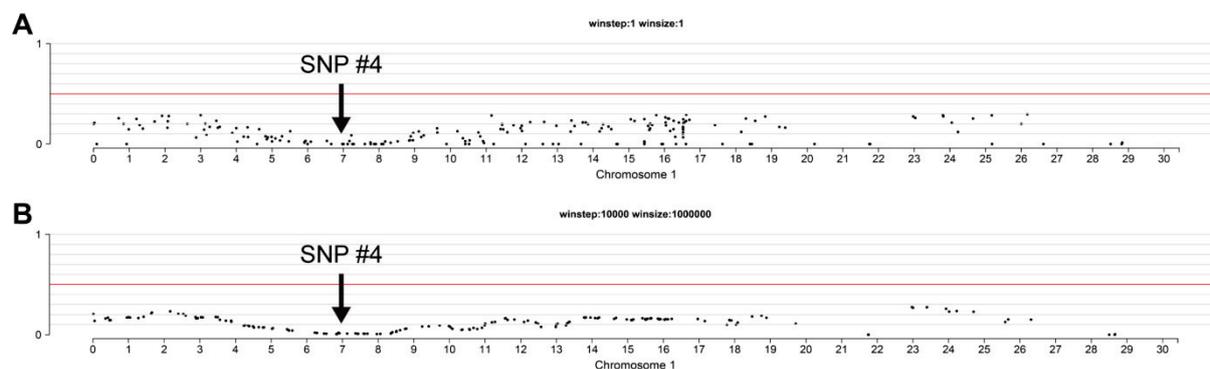
Figure 16. Next generation sequencing data analysis pinpointed *vfd1* mutation to a candidate region between 6 and 7 Mbp on chromosome 1.
(A) Allele frequency analysis of NGS data of chromosome 1 with a winsize of 1 bp. **(B)** Allele frequency analysis of NGS data of chromosome 1 with a winsize of 1.000.000 bp. Arrow marks the position of candidate SNP No. 4 at 6971968 bp. Data by Jörg Hagmann, MPI Tübingen.

Table 5. List of candidate SNPs and respective gene ID.

No.	Chromosome	Position	Reference sequence base	Alternative sequence base	Percentage of reads supporting the base change	Annotation feature	Gene ID	Putative change	Reference amino acid	Alternative amino acid	Codon sequence
1	1	5097496	C	T	68	CDS	**AT1G14790**	Nonsyn	V	I	Gtc
2	1	5225120	C	T	54	CDS	**AT1G15180**	Nonsyn	L	F	Ctc
3	1	5917255	C	T	44	CDS	**AT1G17280**	Nonsyn	G	D	gGc
4	1	6971968	C	T	72	CDS	**AT1G20110**	Nonsyn	Q	*	Caa
5	1	7120923	C	T	64	CDS	**AT1G20560**	Nonsyn	M	I	atG
6	1	7253521	C	T	75	CDS	**AT1G20850**	Nonsyn	P	L	cCc
7	1	7603018	C	T	80	CDS	**AT1G21651**	Nonsyn	V	M	Gtg
8	1	7760069	C	T	65	CDS	**AT1G22030**	Nonsyn	R	H	cGt
9	1	7865659	C	T	64	CDS	**AT1G22270**	Nonsyn	P	S	Ccc
10	1	8118034	C	T	101	CDS	**AT1G22930**	Nonsyn	L	F	Ctt
11	1	8845721	C	T	57	CDS	**AT1G25240**	Nonsyn	S	L	tCg
12	1	8959556	C	T	57	CDS	**AT1G25510**	Nonsyn	G	E	gGg

Table 6. List of candidate genes.

No.	Gene ID	Annotation
1	**AT1G14790**	ATRDRP1, RDR1, RNA-DEPENDENT RNA POLYMERASE 1
2	**AT1G15180**	MATE efflux family protein
3	**AT1G17280**	UBC34, UBIQUITIN-CONJUGATING ENZYME 34
4	**AT1G20110**	RING/FYVE/PHD zinc finger superfamily protein
5	**AT1G20560**	AAE1, ACYL ACTIVATING ENZYME 1
6	**AT1G20850**	XCP2, XYLEM CYSTEINE PEPTIDASE 2
7	**AT1G21651**	zinc ion binding
8	**AT1G22030**	unknown protein, Protein BYPASS related
9	**AT1G22270**	SMO2 (Small Organ 2)
10	**AT1G22930**	T-complex protein 11
11	**AT1G25240**	ENTH/VHS/GAT family protein
12	**AT1G25510**	Eukaryotic aspartyl protease family protein

3.4 AT1G20110 encodes a FYVE domain-containing protein

The *Arabidopsis* gene *VFD1* (AT1G20110) encodes a FYVE domain-containing protein. It was annotated FYVE1 by van Leeuwen et al., who reviewed all proteins with a predicted FYVE domain in the *Arabidopsis* genome in 2004 (van Leeuwen et al., 2004).

AtFYVE1 is a protein of 601 amino acids and has a molecular weight of 65,4 kDa (TAIR10; Figure 17). The N-terminal part consists of a proline-rich (aa 20 - 201) and a serine-rich (aa 156 - 293) region. The FYVE domain (aa 447 - 516) is the main characteristic of the protein. The domain contains all three motifs: a N-terminal WxxD motif (aa 452 - 455), the basic R+HHC+XCG (or R(R/K)HHCR) patch (aa 473 - 481) and the C-terminal RVC motif (aa 505 - 507). The C-terminal part of the protein contains a coiled-coil region of 26 aa (aa 530 - 555).

Figure 17. FYVE1 is a FYVE domain-containing protein of *Arabidopsis thaliana*.
The FYVE domain and coiled-coil domain (CC) are localized at the C-terminus. The arrow marks the SNP mutation site at amino acid position 139 of the *vfd1* (*fyve1-2*) mutant. Domains were defined by SMART.

3.5 Complementation of the *vfd1* mutant with p35S::FYVE1

To find out whether AT1G20110 is *VFD1*, complementation analysis was performed. The overexpression construct pCK35 used for complementation testing contained *FYVE1* CDS and the CaMV 35S terminator region. After transformation, positive T_1 transformants were selected for their kanamycin resistance and the presence of the transgene was verified by PCR-based genotyping using transgene specific primers. Next, positive transformants were analyzed for their SNP in AT1G20110 by Sanger sequencing (Figure 18 D). Wild-type plant material showed a clear cytosine (C) nucleotide peak at the respective SNP position (position δ 415 of gDNA), while the mutated allele showed a thymine (T). Eleven adult T_1 plants were harboring the *35S-FYVE1* transgene and were heterozygous for the SNP in AT1G20110. All plants showed a wild-type phenotype. The *vfd1* mutant (GFP::δ-TIP in Col-0 background) was complemented with a construct overexpressing the wild-type FYVE1 protein under control of the cauliflower mosaic virus (CaMV) 35S promoter (Figure 18 C).

The T_2 generation was checked for homozygous *vfd1* plants and segregation analysis was performed on 7-day-old seedlings (Table 7). The *vfd1* heterozygous line used as a control showed 2.9 % seedlings with mutant phenotype and 23.5 % ungerminated seeds. For the selected T_2 lines #1 and #9, 4.9 % and 2.6 % seedlings with mutant phenotypes were observed, respectively. When ungerminated seeds were included, numbers added up to 11.3 and 12.4 %, respectively. Approximately 60 % of ungerminated seeds showed the mutant vacuole phenotype (#1: 60 % *vfd1* type, 23/39) and could be counted as mutants, suggesting that approximately 8.7 % (4.9 + 6.4 x 0.6 %) of the progeny were homozygous mutants. This number was significantly lower than that of the *vfd1* heterozygous plant, indicating that the transgene is complementing the mutant phenotype.

Whereas viable homozygous *vfd1* plants containing the transgene were found in line #1 and #2, there was no complete complementation of the plant phenotype. However, in lines #3 and #9, *vfd1* homozygous plants that contain the transgene were indistinguishable from the wild-type (Figure 18 A and B). Out of 40 T_2 plants, at least four plants (#3-8, #3-15, #3-32 and #3-34) were identified as lines in which the mutant phenotype was complemented.

Table 7. Segregation ratio of *vfd1* complemented lines in T_2.

Line	wild-type	ungerminated	mutants	total
GFP::δ-TIP (Col-0)	211 (99.5 %)	1 (0.5 %)	0	212
vfd1	307 (73.6 %)	98 (23.5 %)	12 (2.9 %)	417
		110 (26.4 %)		
vfd1/pCK35 #1	539 (88.7 %)	39 (6.4 %)	30 (4.9 %)	608
		69 (11.3 %)		
vfd1/pCK35 #9	552 (87.6 %)	62 (9.8 %)	16 (2.6 %)	630
		78 (12.4 %)		
vfd1/pCK35 #2	448 (88.7 %)	44 (8.7 %)	13 (2.6 %)	505
		57 (11.3 %)		
vfd1/pCK35 #3	529 (93.0 %)	29 (5.1 %)	11 (1.9 %)	569
		40 (7.0 %)		
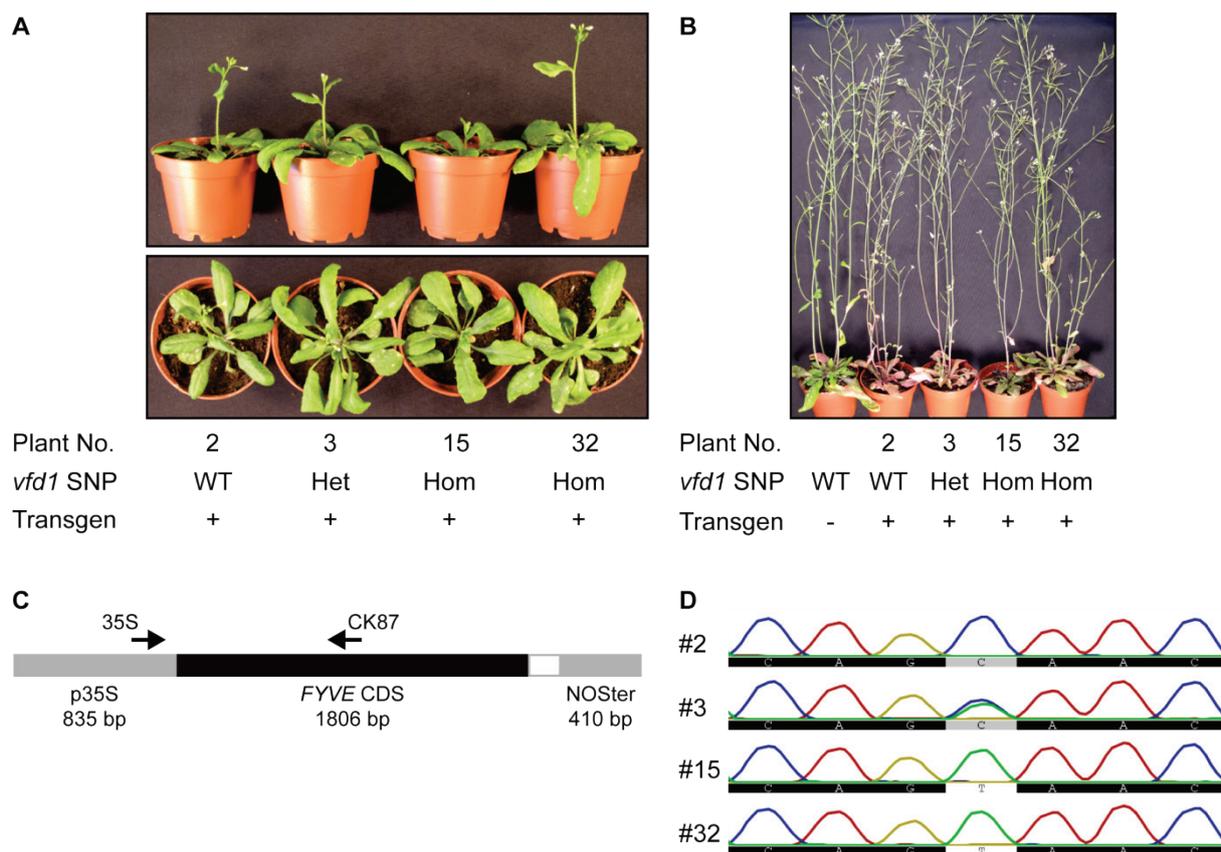
Figure 18. Complementation testing verified the candidate gene to be AT1G20110 (*FYVE1*).
(A) T_2 plant phenotype of complemented line #3. Shown plants are 25 days old. **(B)** T_2 plant phenotype of complemented line #3 shown with age of 40 days. **(C)** Scheme of the complementation construct p35S::FYVE1 (pCK35) and sites of transgene specific genotyping primers. **(D)** SNP sequencing analysis of *vfd1* gene locus of complemented plants. #2 is a homozygous wild-type plant. #3 is a heterozygous plant, combining peaks of C and T nucleotides. #15 and #32 are plants homozygous for the mutated *vfd1* SNP.

The complemented lines were examined for expression of the transgene using RT-PCR (Figure 19). Expression of the complementation construct was shown for all positive transformants with a transgene specific primer combination (F). To distinguish between cDNA and genomic DNA contamination, a CDS specific primer combination (G) was used. Since *FYVE1* does not contain an intron, *SH3P3* was used as control for gDNA contamination and showed that all cDNA samples were gDNA free. The complementation construct pCK35 (*p35S::FYVE1*) was expressed in all complemented plants.
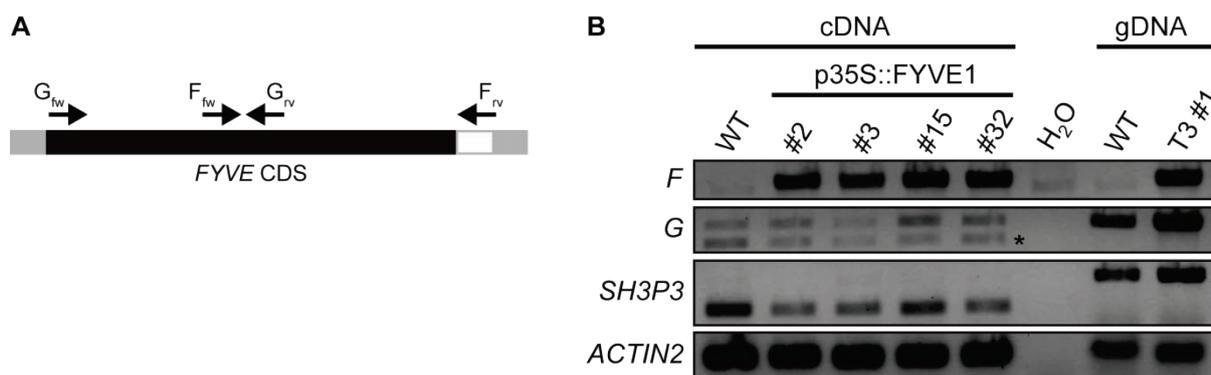
Figure 19. Semi-quantitive RT-PCR analysis of complemented plants verifies transgene expression. **(A)** Primer sites for sqRT-PCR analysis: Primer combination F is transgene specific. Primer combination G is CDS specific. **(B)** Semi-quantitative RT-PCR analysis of complemented plants for transgene expression. Genomic DNA samples are used for primer controls. F shows construct specific transgene expression. G shows CDS/cDNA specific *FYVE1* expression levels. Asterisk indicates unspecific product bands. *SH3P3* was used as control for gDNA contamination. *ACTIN2* was used as loading control (primers were not CDS specific and also amplified gDNA product).

Segregation analysis was also performed in the T_3 generation for complementing line #3 (Table 8). By sequencing for the *vfd1* SNP, the *vfd1* genotype was verified. Two lines, #3-8 and #3-34, were 100 % homozygous for the *vfd1* SNP (*vfd1* -/-, TG +). Presence of *vfd1* mutants of seedling lethal phenotype and a higher number of ungerminated seeds indicated that the transgene segregated.

Scored seedling lethal *vfd1* mutants in T_3 were genotyped via SNP-PCR and restriction digestion with *MaeIII* was used to determine the genotype and if the transgene was present. All scored *vfd1* mutants did not contain the transgene and were homozygous for the *vfd1* SNP (Figure 20). These results conclude that the transgene was properly expressed in complemented plants, but a minimal fraction of uncomplemented progeny remained. By counting mutants and ungerminated seeds together, the recessive ratio of 25 % was approached. *vfd1* mutants were also verified by confocal microscopy for the *vfd1* specific vacuolar phenotype.

Table 8. Segregation ratio of *vfd1* complemented lines in T_3.

Line	Genot.	wild-type	ungerminated	mutants	total	Phenotype
GFP::δ-TIP (Col-0)	WT TG -	124 (96.9 %)	4 (3.1 %)	0	128	wild-type
vfd1/pCK35 #3-1 control	Het +/- TG +/+	355 (99.7 %)	1 (0.3 %) 1 (0.3 %)	0	356	wild-type (compl.)
vfd1/pCK35 #3-4 control	Het +/- TG -	76 (73.1 %)	26 (25.0 %) 28 (26.9 %)	2 (1.9 %)	104	25 % *vfd1* mut
vfd1/pCK35 #3-8	Hom -/- TG +/-	198 (77.3 %)	54 (21.1 %) 58 (22.7 %)	4 (1.6 %)	256	wild-type (compl.)
vfd1/pCK35 #3-34	Hom -/- TG +/-	235 (78.1 %)	64 (21.3 %) 66 (21.9 %)	2 (0.6 %)	301	wild-type (compl.)
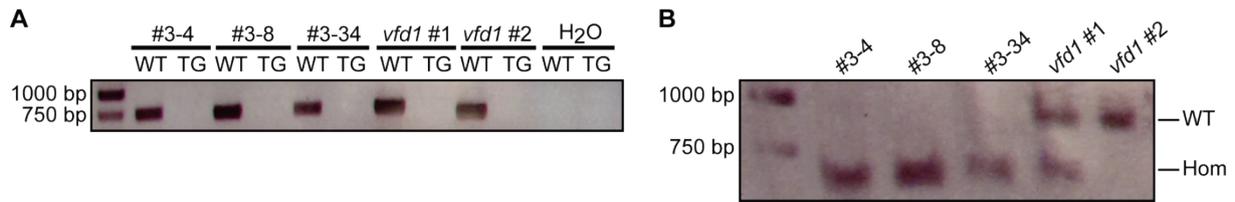
Figure 20. T$_3$ genotype analysis of seedling-lethal *vfd1*/pCK35 mutants affirms homozygosity and lack of transgene.
(A) Genotyping agarose gels of mutant pools for transgene. *vfd1* #1 and #2 served as wild-type controls. WT: PCR control, TG: transgene. **(B)** Agarose gel of *MaeIII*-digest with SNP specific band pattern. Lower bands (603 bp) are specific for the *vfd1* SNP mutation, higher bands (844 bp) are specific for wild-type SNP. T$_3$ mutant pools all showed homozygous *vfd1* SNP mutation. *vfd1* #1 and #2 served as heterozygous and wild-type control, respectively.

15 seedlings of each line (#3-1, #3-4, #3-8 and #3-34) were genotyped according to the transgene and *vfd1* genotype. In complementing lines #3-8 and #3-34, the transgene was present in all seedlings tested. After adding the scored *vfd1* mutants without transgene, this concludes that the transgene is present in a heterozygous state. Via SNP sequencing the *vfd1* genotype was verified. #3-1 seedlings were 100 % heterozygous, #3-8 and #3-34 seedlings were 100 % homozygous for the *vfd1* SNP.

8-day-old homozygous *vfd1* seedlings, which contained the transgene, looked like wild-type in respect to seedling and vacuolar phenotype (Figure 21). The plant phenotype of lines #3-8 and #3-34 was wild-type, showing that overexpression of FYVE1 rescues seedling lethality and also the vacuole formation defect of *vfd1*.
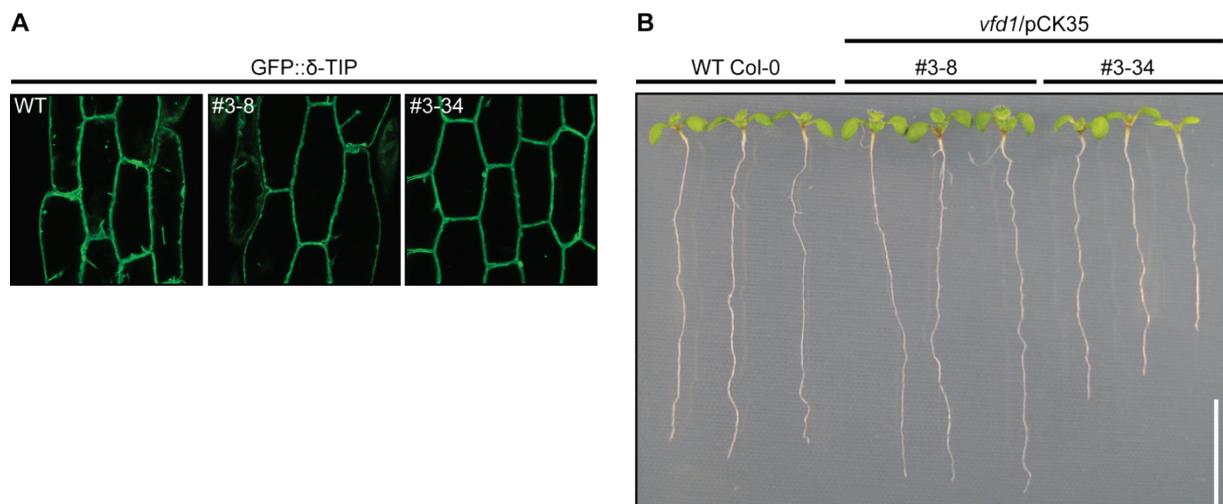
Figure 21. T$_3$ phenotype analysis of complementing line *vfd1*/pCK35 confirms full rescue of the *vfd1* mutant.
(A) Vacuolar phenotype of complemented seedlings in hypocotyl cells (7 DAG). Tonoplast is stained by GFP::δ-TIP marker. **(B)** Seedling phenotype of complemented lines #3-8 and #3-34 in comparison to wild-type Col-0 seedlings of the same age (8 DAG).
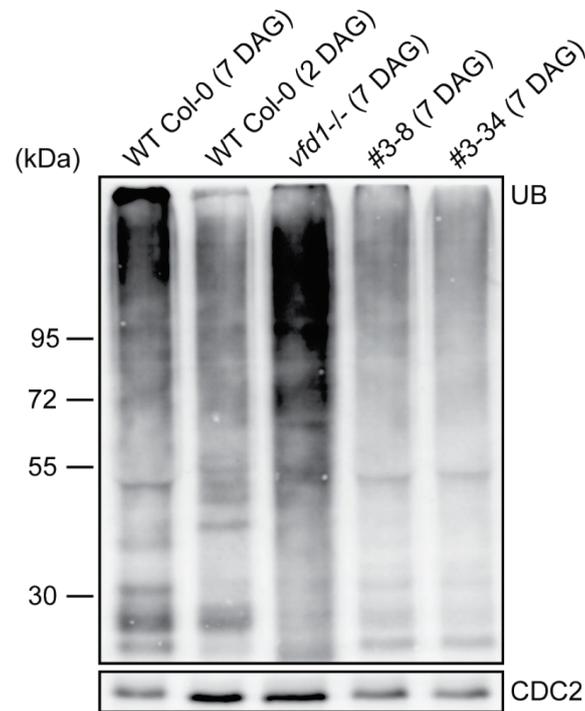
Figure 22. Ubiquitination profile of complemented lines *vfd1*/pCK35 in T$_3$ shows rescue of ubiquitin accumulation back to wild-type levels.
Ubiquitination profile of complemented lines #3-8 and #3-34 in comparison to wild-type and *vfd1*-/-mutant. UB: ubiquitin-conjugates, CDC2: loading control.

The complementation with *p35S::FYVE1* also resulted in an alteration of the ubiquitination profile. The amount of ubiquitin conjugates was decreased to wild-type levels in the complemented lines (Figure 22), indicating the defect in FYVE1 is indeed responsible for this phenotype.

A second complementation approach of the *vfd1* mutant was undertaken with a construct containing the endogenous *FYVE1* promoter, genomic *FYVE1* sequence and the *FYVE1* terminator region. Unfortunately, the transgene product could not be detected via immunoblot nor could the ECFP-tag be detected by confocal microscopy, therefore it had to be assumed, that expression of this construct failed in plants.

3.6 Characterization of the *fyve1-1* transposon mutant as a mutant allele of *VFD1*

In parallel to the complementation analysis, a transposon insertion mutant of *fyve1* was analyzed. The line 15-1960-1 (resource number: RIKEN pst18264, Nossen (No-0) background) was named *fyve1-1* in this study. Sequencing analysis revealed that the transposon insertion site was localized to exon 1 in *FYVE1* (Figure 23 A). The insertion of the transposon disrupts the original gene sequence and most likely disables the gene. The truncated protein would be of a size of 155 amino acids and would only be a part of the N-terminal sequence of the full length protein, excluding the functionally important FYVE domain.

Phenotypic and standard segregation analysis was performed with the *fyve1-1* transposon line to analyze the similarities of both mutants. The number of wild-type seedlings, ungerminated seeds and *amsh3*-like mutants was counted (Figure 23 B; Table 9). Seven days after germination, a minor fraction (8.1 %) of the seedlings showed seedling lethality (Figure 24 A). Genotyping of these mutant seedlings by PCR revealed that they are homozygous for the transposon insertion. A majority of the seedlings (80.4 %) had a wild-type Nossen phenotype. Genotyping of plants with wild-type phenotype revealed a segregating population of wild-type plants and plants heterozygous for the transposon insertion in a ratio of 1:2 wild-type to heterozygous plants. Intermediate phenotypes were not detected. This 1:2:1 wild-type:heterozygous:mutant segregation ratio indicated that the phenotype is caused by a single, recessive nuclear mutation.

As was the case for *vfd1*, the ratio of homozygous mutants was below the expected 25 % of a recessive inherited mutation, suggesting that mutations in *FYVE1* also cause gametophyte defects.
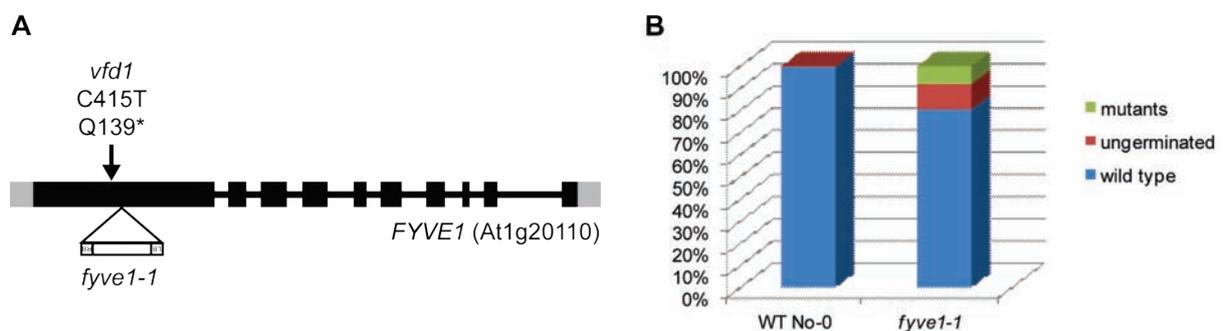
Figure 23. The *fyve1-1* transposon mutation site is also localized to exon 1 of gene AT1G20110 and segregation ratio of *fyve1-1* is comparable to *vfd1* mutant.
(A) Localization of SNP mutation site and transposon insertion site of both mutants in the *FYVE1* gene.
(B) Schematic of segregation ratio of wild-type, ungerminated seeds and homozygous mutants between wild-type No-0 and *fyve1-1* mutant.

47

Table 9. *fyve1-1* is a recessive inherited mutant allele.

Line	wild-type	ungerminated	mutants	total
WT No-0	304 (99.7 %)	1 (0.3 %)	0 (0.0 %)	305 (100 %)
fyve1-1	287 (80.4 %)	41 (11.5 %)	29 (8.1 %)	357 (100 %)
		70 (19.6 %)		

In comparison to wild-type No-0 that had 0.3 % ungerminated progeny, the heterozygous *fyve1-1* progeny showed 11.5 % ungerminated seeds. This high number of ungerminated seeds indicated a similar germination defect as is the case for the *vfd1* mutant.

To determine the genotype of ungerminated seeds, embryos were dissected from the seed coat and analyzed by genotyping PCR. 79.2 % (19/24) of ungerminated embryos were homozygous for the transposon insertion. Five embryos could not be analyzed due to low DNA quality.

For analysis of vacuolar morphology of homozygous mutant seedlings, the line was crossed with the GFP::δ-TIP (Col-0) tonoplast marker line. Mutant seedlings also showed a vacuolar fusion defect (Figure 24 B), indicating FYVE1 is indeed important for vacuole formation.

To check if the expression levels of *FYVE1* are altered in the *fyve1-1* mutant qRT-PCR analysis was performed on pools of 7-day-old wild-type No-0 and homozygous *fyve1-1* mutant seedlings (Figure 25). In comparison to the wild-type, the transposon insertion mutant showed a down regulation of *FYVE1* gene transcript levels. Gene expression was down regulated for the full length product (4 % of the wild-type) as well as for the putative truncated product (15 % of the wild-type).
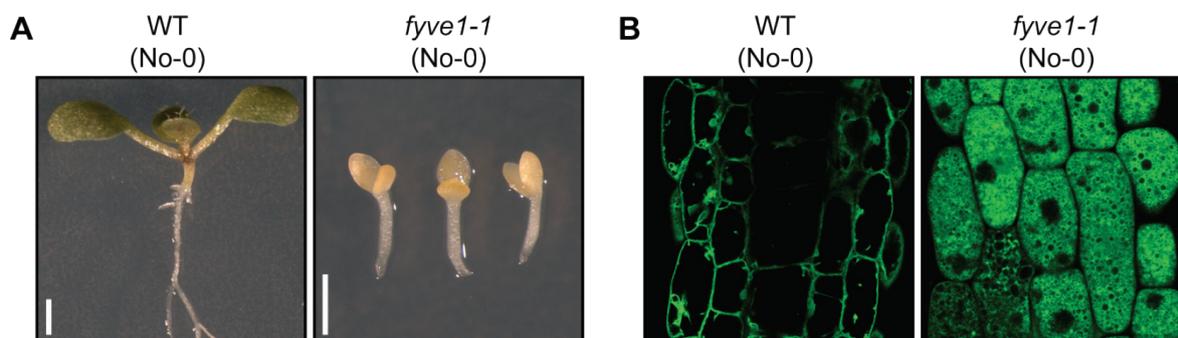
Figure 24. Phenotype of the transposon insertion mutant *fyve1-1* is identical to the *vfd1* phenotype in regard to seedling and vacuole phenotype.
(A) Phenotype of 7-day-old seedlings of wild-type (No-0) and *fyve1-1* mutant line. Scale bars: 1 mm.
(B) Vacuolar phenotype of 7-day-old seedlings of wild-type (No-0) and *fyve1-1* mutant line. GFP::δ-TIP tonoplast marker is outlining the vacuolar membranes (partially cytosolic).

A

truncated   full length

FYVE1 (At1g20110)

fyve1-1

B

Gene expression level

1,5

1,0

0,5

0,0

FYVE1 full length   FYVE1 truncated

■ WT No-0
■ *fyve1-1*
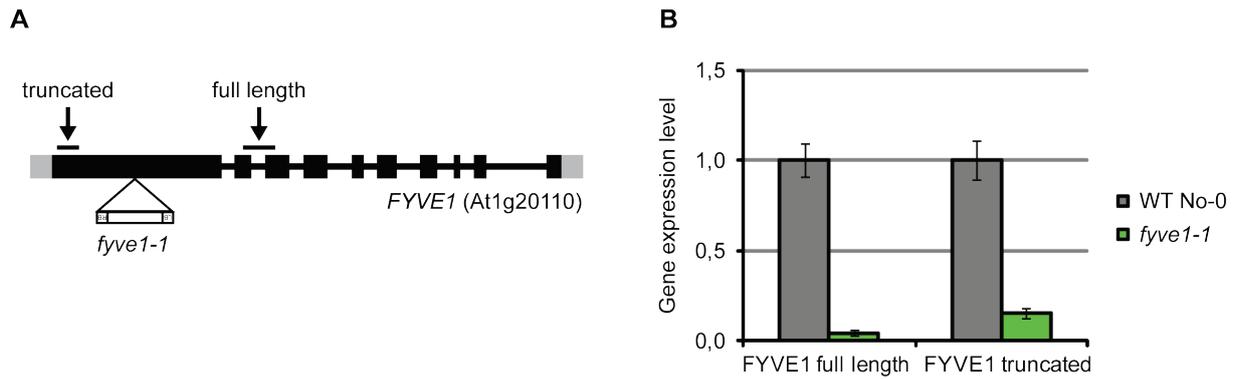
Figure 25. The *fyve1-1* mutant is a knockdown mutant and *FYVE1* gene expression is decreased. **(A)** Primer target sites of qRT-PCR analysis for a *FYVE1* truncated transcript and for a *FYVE1* full length transcript. Transposon insertion site for *fyve1-1* is shown. **(B)** Expression levels of *FYVE1* in WT No-0 and *fyve1-1* mutant. Primer combinations were chosen for a *FYVE1* full length transcript as well as for a *FYVE1* truncated transcript. *FYVE1* RNA levels are downregulated in *fyve1-1* mutant.

In addition to the two primary *amsh3*-like attributes, the *fyve1-1* mutant is also accumulating ubiquitinated proteins (Figure 26 A). More ubiquitinated cargo proteins were detected in the *fyve1-1* mutant compared to the wild-type. Dividing membrane-bound and soluble ubiquitinated proteins by ultracentrifugation showed that most ubiquitinated cargo proteins are in the membrane bound fraction (Figure 26 B), suggesting that ubiquitinated proteins are associated to membranes and not in the cytosol.

A

B
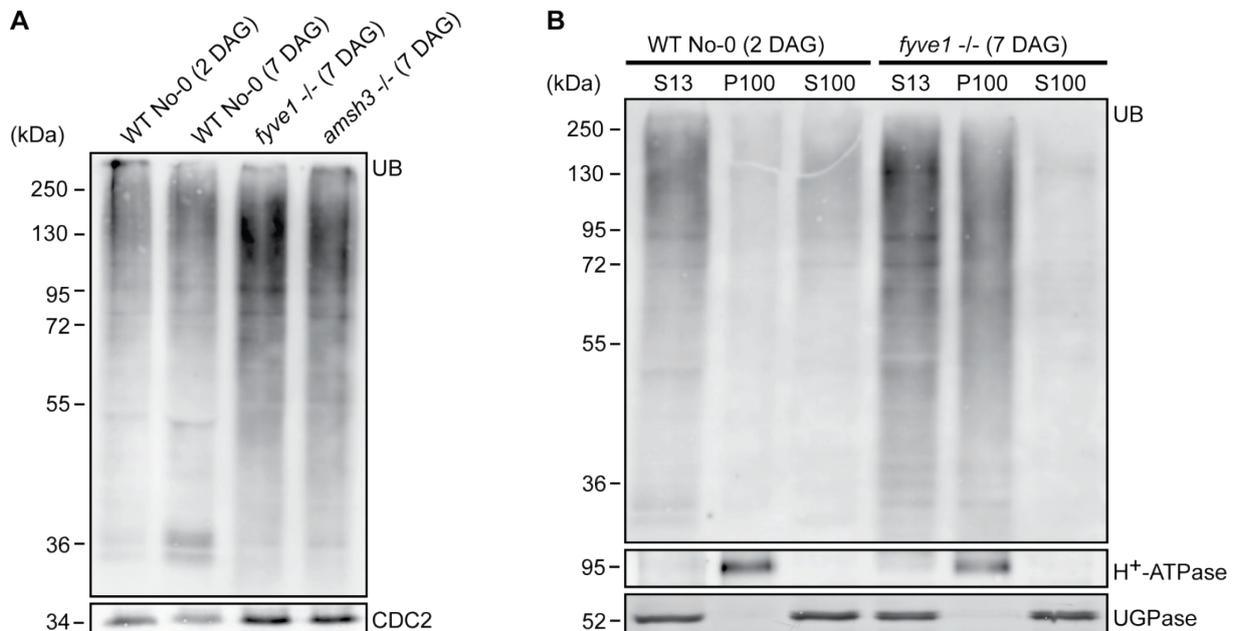
Figure 26. Ubiquitination profile of the *fyve1-1* mutant shows accumulation of ubiquitinated proteins. **(A)** Western blot of ubiquitination profile of *fyve1-1* mutant. Loading control: CDC2. **(B)** Western blot of ubiquitination profile with supernatant (S13), membrane (P100) and soluble (S100) fractions. Loading controls: H$^+$-ATPase for P100 fraction, UGPase for S13 and S100 fraction.

3.7 Complementation with pUBQ10::sGFP-FYVE1 (pCK51) rescues *fyve1-1* mutant

To make sure that the transposon insertion in gene AT1G20110 is the cause of the mutant phenotype, the wild-type gene was introduced as a transgene and tested for complementation. For complementation and phenotypic rescue of the *fyve1-1* transposon mutant, two constructs were used. Synthetic green fluorescent protein sGFP was fused N- and C-terminally to the *FYVE1* CDS under the control of the Ubiquitin-10 constitutive overexpression promoter pUBQ10, which is driving expression in nearly all tissues of *Arabidopsis* (Figure 27 A). In the protoplast system, both complementation constructs were expressed and showed localization to the cytosol and to foci (Figure 27 B).

Both constructs were used to transform the *fyve1-1* transposon mutant line to test for complementation. After selection of T_1 seedlings with Basta, positive transformants were genotyped for the transposon insertion and the transgene to exclude false positives. Progeny of the selfed T_2 generation was analyzed.

For the N-terminal complementation construct pCK51, two independent lines were used for analysis. Lines #3 and #34 showed 14.9 % and 6.1 % of mutants and ungerminated seeds, respectively (Table 10).
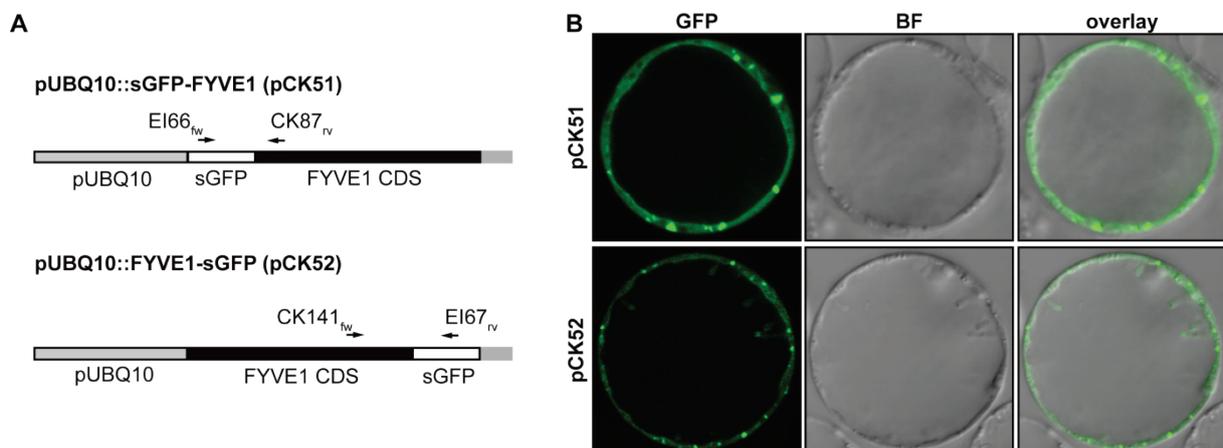
Figure 27. FYVE1 complementation constructs are functional in the protoplast expression system. **(A)** Schematic overview of GFP-fusion constructs and primer combinations for genotyping of transgene. **(B)** Expression of constructs after transformation of root protoplasts.

Table 10. T_2 segregation analysis of the complementation of the *fyve1-1* mutant.

Line	wild-type	ungerminated	mutants	total
WT No-0	304 (99.7 %)	1 (0.3 %)	0 (0.0 %)	305 (100 %)
fyve1-1	287 (80.4 %)	41 (11.5 %) 70 (19.6 %)	29 (8.1 %)	357 (100 %)
fyve1-1/pCK51 #3	126 (85.1 %)	21 (14.2 %) 22 (14.9 %)	1 (0.7 %)	148 (100 %)
fyve1-1/pCK51 #34	336 (93.9 %)	21 (5.9 %) 22 (6.1 %)	1 (0.3 %)	358 (100 %)

The expression of sGFP-FYVE1 was confirmed by western blot analysis using anti-GFP and anti-FYVE1 antibodies (Figure 28). Lines #3, #29 and #34 showed expression of sGFP-FYVE1. Line #3 was selected for further analysis.

From each positive complementing line, 16 seedlings were genotyped. For the line *fyve1-1*/pCK51 #3 four wild-type, eight heterozygous seedlings and three seedlings homozygous for the transposon insertion were found, which was in accordance with the Mendelian segregation of 1:2:1. T_2 plants were grown on soil to analyze the correlation of genotype and phenotype. Genotyping revealed a segregation ratio of 6:10:4 between wild-type, heterozygous and homozygous plants. All four plants that were homozygous for the transposon insertion showed a phenotype indistinguishable from the wild-type (Figure 29), indicating that the observed *fyve1-1* phenotype was indeed a result of the dysfunction of the *FYVE1* gene and that sGFP-FYVE1 is a functional fusion protein.
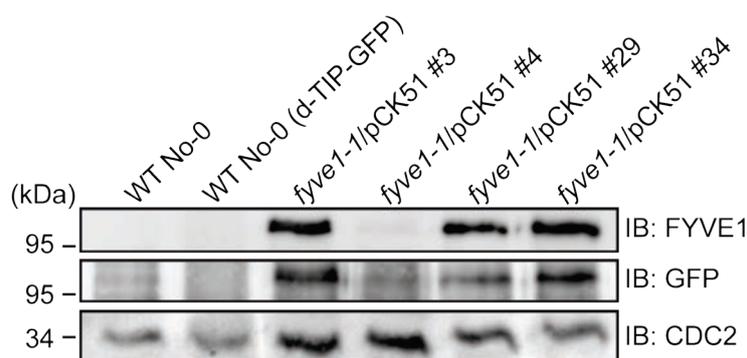
Figure 28. Western blot confirms expression of FYVE1 in complemented line of *fyve1-1*/pCK51. Samples represent a pool of 7-day-old seedlings of each line. Overexpression of sGFP-FYVE1 was detected with anti-FYVE1 and anti-GFP antibodies. Loading control: CDC2.
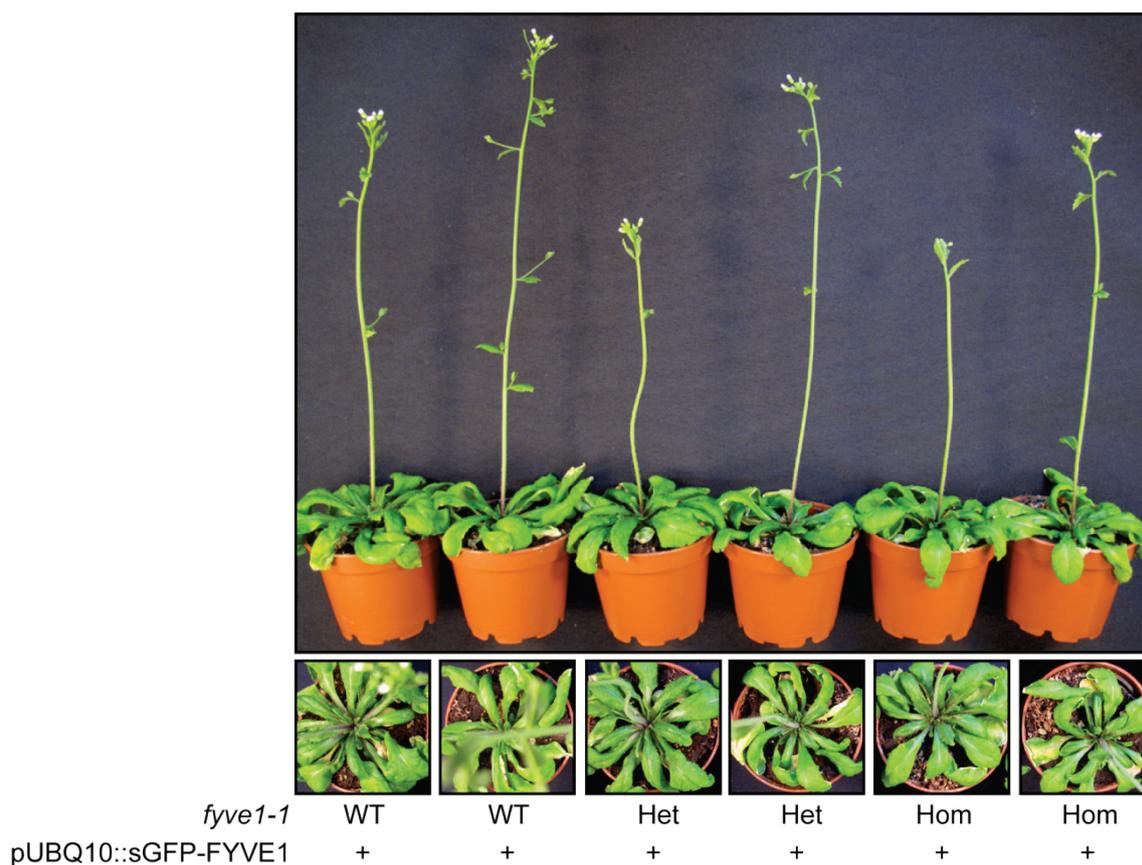
Figure 29. pUBQ10::sGFP-FYVE1 construct complements *fyve1-1* mutant phenotype.
5-week-old plants of complementing line *fyve1-1*/pCK51 #3 showed only wild-type phenotype. Plants were genotyped for *fyve1-1* transposon insertion and presence of transgene (+). Scale bar: 1 cm.

T$_3$ seedlings homozygous for *fyve1-1* that contained the transgene all showed wild-type phenotype. Expression of the sGFP-FYVE1 was verified by confocal microscopy and western blot of protein extracts of 7-day-old seedlings (Figure 30 A). The complementation with the *pUBQ10::sGFP-FYVE1* construct also resulted in the rescue of the ubiquitin accumulation phenotype (Figure 30 B). The amount of ubiquitin conjugates decreased to wild-type levels in the complemented lines. This could also be shown after fractionation via ultracentrifugation (Figure 30 C), indicating that the defect in *FYVE1* was the cause of this phenotype.

Table 11. T$_3$ segregation analysis of the complementation of the *fyve1-1* mutant.

Line	Genotype	wild-type	ungerminated	mutants	total
fyve1-1/pCK51 #3-8	WT TG -/-	248 (98 %)	5 (2 %)	0 (0 %)	253 (100 %)
fyve1-1/pCK51 #3-16	WT TG +/+	309 (100 %)	0 (0 %)	0 (0 %)	309 (100 %)
fyve1-1/pCK51 #3-18	Hom -/- TG +/+	170 (85 %)	50 (15 %)	0 (0 %)	220 (100 %)
fyve1-1/pCK51 #3-30	Hom -/- TG +/+	124 (70 %)	107 (30 %)	0 (0 %)	231 (100 %)

For the C-terminal GFP-fused construct pCK52, progeny of five independent T_2 lines were analyzed. When analyzed under a confocal microscope, no GFP signals could be observed, indicating that FYVE1-sGFP was not properly expressed in plants, although the expression was verified in protoplasts. The C-terminal fusion of GFP to FYVE1 may interrupt the function of the C-terminal FYVE or coiled-coil domain and therefore be non-functional *in vivo*.
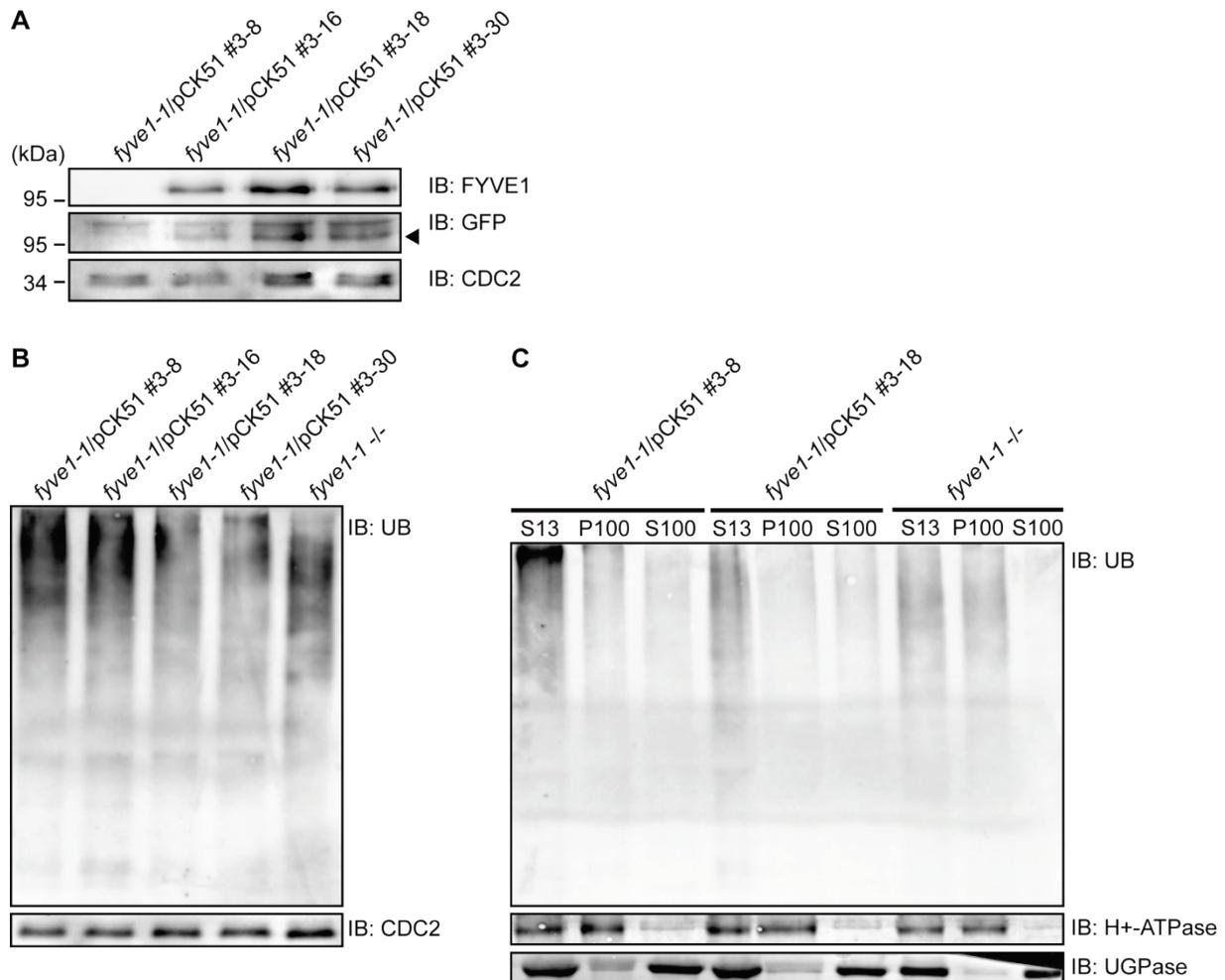
Figure 30. sGFP-FYVE1 is expressed in complemented lines and rescues the ubiquitination profile.
(A) Expression of sGFP-FYVE1 was confirmed by western blot with antibodies against FYVE1 and GFP. Arrowhead marks sGFP-FYVE1 specific band. Loading control: CDC2. **(B)** Ubiquitination profile of complementing lines in comparison to *fyve1-1* mutant. Lines #3-18 and #3-30, homozygous for *fyve1-1*, showed rescue of ubiquitination phenotype. Loading control: CDC2. **(C)** Ubiquitination profile of S100/P100 fractions. P100 ubiquitin conjugates decreased in comparison to *fyve1-1*.

3.8 Characterization of sGFP-FYVE1 fusion protein

The functional fusion protein sGFP-FYVE1 localizes to the cytosol, the nucleus and also accumulates in foci, that may represent endosomal vesicles (Figure 31).

To analyze whether the fusion protein sGFP-FYVE1 was soluble or membrane-bound, protein extracts were fractionated by ultracentrifugation. Endogenous levels of FYVE1 could not be detected with the anti-FYVE1 antibody. The fusion protein sGFP-FYVE1 mainly appeared in the S100 soluble fraction, indicating that the fusion protein was mostly soluble and therefore localized to the cytosol (Figure 32). The membrane-bound sGFP-FYVE1 can be seen as a very weak band in the P100 fraction, representing the amount of fusion protein targeted to membrane domains (Kolb et al., 2015).

To analyze the localization of sGFP-FYVE1, the *sGFP-FYVE1* line was crossed with three different marker lines expressing RFP- or monomeric Kusabira-Orange (mKO)-tagged marker proteins for different organelles (Figure 33). Colocalization was defined as a complete overlap of two fluorescence signals and therefore of vesicles. Association of vesicles was defined as a partial overlap of the fluorescence signal. Independent vesicles did neither show colocalization, nor association.
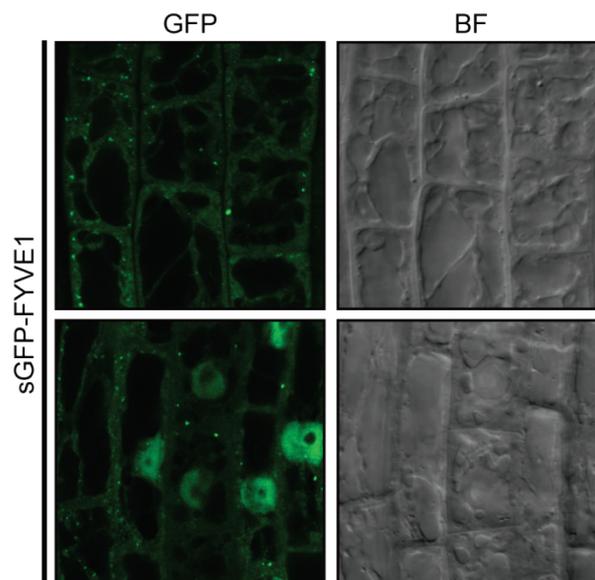
Figure 31. sGFP-FYVE1 is localized to cytosol, nucleus and endosomal vesicles.
Subcellular localization of complementation construct sGFP-FYVE1 (pCK51). Confocal analysis of 7-day-old seedlings of complementing line *fyve1-1*/pCK51 #3 showed expression of sGFP-FYVE1 in cytosol, nucleus and endosomal compartments (dots). BF: bright field.
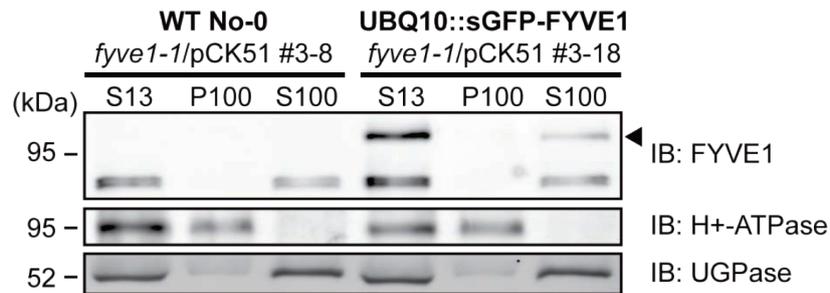
Figure 32. Fusion protein sGFP-FYVE1 appeared in the S100 soluble fraction.
Ultracentrifugation of wild-type (#3-8) and complementing line (#3-18) protein extracts. sGFP-FYVE1 was mainly detected in the S100 fraction. Arrowhead marks sGFP-FYVE1 specific band. Membrane bound H^+-ATPase is P100 control, soluble UGPase is S100 control.

SYNTAXIN OF PLANTS 61 (SYP61) is a Q-SNARE and marker protein for the *trans*-Golgi network (TGN). 33.3 % of sGFP-FYVE1 vesicles were associated with SYP61-positive organelles, but the major portion (66.7%) of FYVE1 protein localized on independent vesicles (Figure 34, n= 81).

The CLATHRIN LIGHT CHAIN (CLC) protein is part of the clathrin cage that forms the coat of newly endocytosed vesicles (clathrin-coated vesicles, CCVs) and fuses with early endosomes and the TGN. CLC-mKO (Karasawa et al., 2004) was used as a marker for clathrin-positive vesicles.
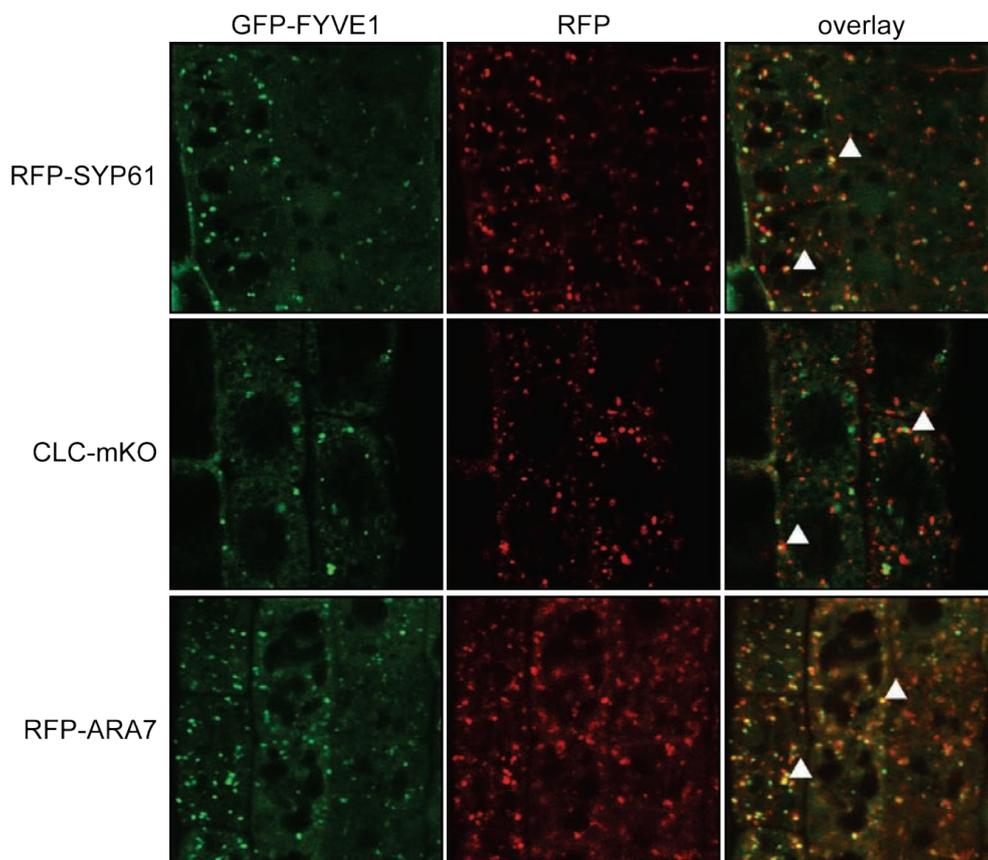
Figure 33. sGFP-FYVE1 colocalizes with different endosomal marker proteins. SYP61 is a TGN marker, CLC is a TGN/EE marker and ARA7 is a LE marker.
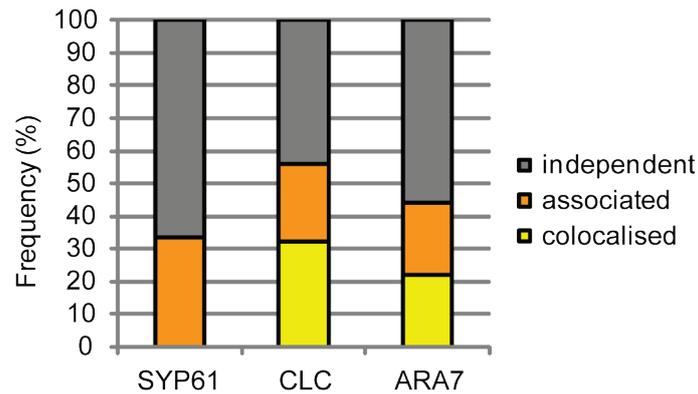
Figure 34. FYVE1 colocalized with CLC and ARA7 positive endosomes.
Quantification of colocalization between GFP-FYVE1 and three organelle marker proteins: SYP61 (n=81), CLC (n=100) and ARA7 (n=100).

32 % of GFP-FYVE1 marked vesicles colocalized with the CLC-mKO marker and 24 % showed association (n=100).

RFP-ARA7 was used as a marker protein for endosomal vesicles of the later steps of endocytosis (late endosomes, LE). ARA7 (AtRABF2b) is an *Arabidopsis* Rab5 GTPase-like protein (Ueda et al., 2001; Vernoud et al., 2003). sGFP-FYVE1 colocalized with ARA7 only partially (22 %) and showed 22 % association (n=100).

These results indicate that FYVE1 is a protein that is localized to a different type of endosomes, including CCVs and late endosomes.

3.9 GFP-CT24 is missorted in *fyve1-1* mutant embryos

As the *fyve1-1* mutant displayed severely altered vacuole morphology, it was interesting to know, to what degree the vacuolar sorting and trafficking was impaired in the mutant. To investigate how seed protein storage vacuoles (PSVs) were affected in *fyve1-1,* mutants were transformed with the model vacuolar cargo GFP-CT24 (Nishizawa et al., 2003). This construct expresses an artificial vacuolar cargo protein derived from the α' subunit of soybean β-conglycinin, a seed storage protein of the 7S globulin class. The fusion protein contains a signal peptide (SP), GFP and the C-terminal 24 amino acids (CT24) of the α' subunit that is necessary for vacuolar sorting (Figure 35 A). It was shown by Nishizawa et al. that this artificial cargo is directed to the matrix of PSVs in wild-type *Arabidopsis* seeds (Nishizawa et al., 2003). Transformed seeds expressing SP-GFP-CT24 can be detected with a fluorescence binocular due to strong GFP signals. If GFP-CT24 is missorted in a vacuolar sorting mutant, as was shown for example for *vsr1-1* (Fuji et al., 2007), the fusion protein is secreted to the intercellular space as the default pathway of non-targeted proteins.

3. Results
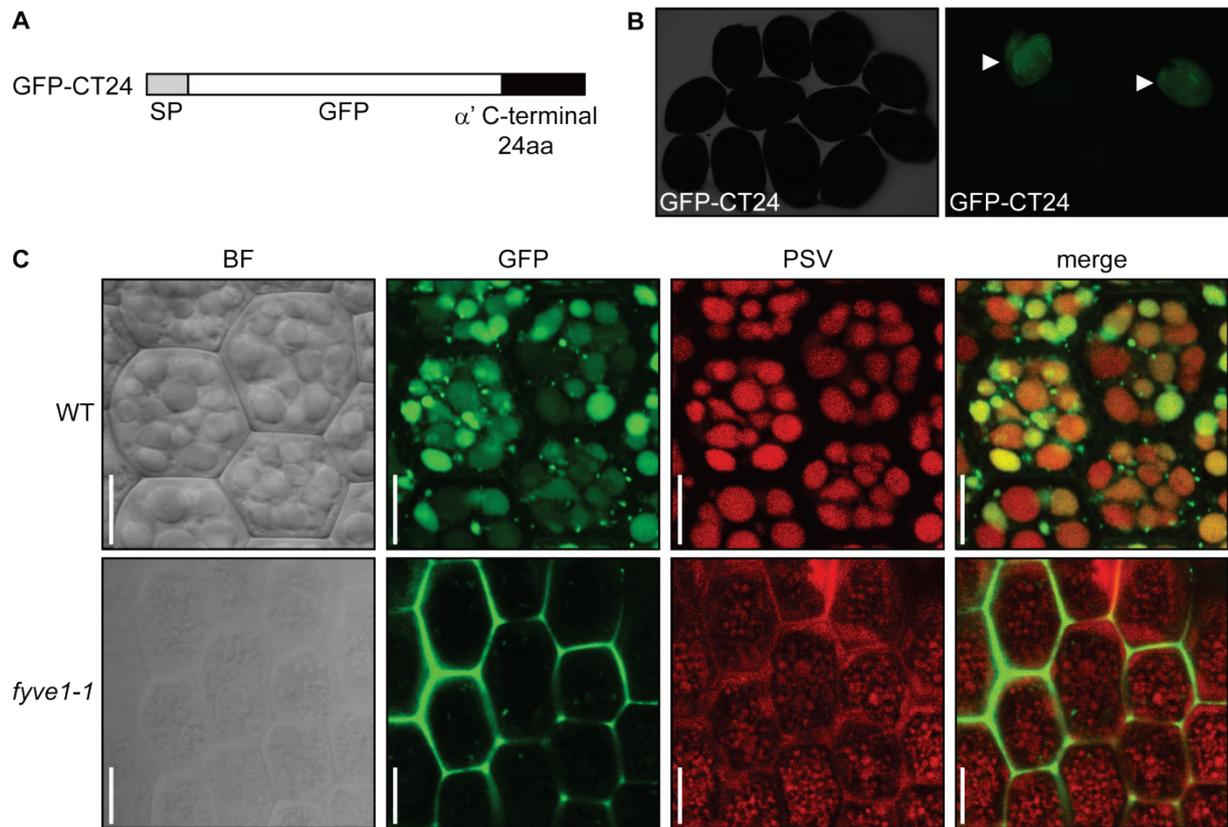
Figure 35. Secretion of GFP-CT24 in the *fyve1-1* mutant showed defects in targeting of proteins to the PSVs.
(A) Scheme of the GFP-CT24 construct. The fusion protein contains a signal peptide (SP), green fluorescent protein (GFP) and the C-terminal 24 amino acids of the α' subunit of β-conglycinin (CT24).
(B) T_2 seeds segregate for the transgene GFP-CT24. Arrowheads indicate *fyve1-1* mutant seeds.
(C) Cells of dissected embryos of wild-type and mutant *fyve1-1* T_2 seeds. Wild-type embryo cells showed GFP-CT24 expression in PSVs and smaller vesicles. PSV autofluorescence completely overlaps with GFP signal. In the *fyve1-1* mutant GFP-CT24 is secreted in the intercellular space. PSVs in the mutant are of much smaller size. Scale bars: 10 μm.

For analysis in the T_2 generation, GFP-CT24 lines in wild-type (No-0) and heterozygous *fyve1-1* were further analyzed. For embryo dissection and subsequent confocal microscopy, green fluorescent seeds were selected (Figure 35 B). In wild-type GFP-CT24 seeds, GFP fluorescence was detected in the PSVs that merged with the autofluorescence of vacuoles. Signals of GFP-CT24 in homozygous *fyve1-1* embryos showed much higher intensity of GFP fluorescence in the intercellular space than in wild-type, indicating that most of the GFP-CT24 fusion protein was missorted in *fyve1-1* (Figure 35 C). In addition to this finding, the PSVs of *fyve1-1* embryos appeared much smaller and more numerous compared to the wild-type.

3.10 Influence of Brefeldin A on vacuole morphology and trafficking

To examine the effect of the potent inhibitor Brefeldin A (BFA) on vesicle transport, *Arabidopsis* seedlings were grown on ½ MS agar medium (0.65 %) with different concentrations of BFA. Addition of BFA blocks the function of ADP ribosylation factor guanine nucleotide exchange factors (ARF-GEFs) and thus the recycling of membrane proteins to the plasma membrane and the progress of endosomal vesicles to multivesicular bodies (MVBs) (Nebenführ et al., 2002). It was already shown that BFA leads to disrupted auxin (indole-3-acetic acid, IAA) transport in seedlings as well as disruption of root gravitropism (Nishimura et al., 2012). At high concentrations of BFA seedling growth is strongly inhibited, which leads to seedling lethality.

With 10 µM of BFA, root gravitropism was strongly affected and increasing concentrations of BFA lead to enhanced effects on root gravitropism and seedling growth (Figure 36 A). With 50 µM of BFA, seedling growth was strongly inhibited, although seedlings were still greening. After five days, seedlings turned yellowish and resembled the *vfd1/fyve1* phenotype. Nine days after germination, seedlings growing on 25 µM as well as 50 µM BFA were severely affected, turning yellowish.

To further investigate the similarity between the effect of BFA and the *vfd1/fyve1* phenotype, morphology of vacuoles was analyzed with confocal microscopy. No effects on vacuolar morphology were detected with 10 µM of BFA (Figure 36 B). At higher concentrations of BFA, the vacuolar membrane was slightly affected, building more transvacuolar strands and bulbs (Figure 36 B). In comparison to the vacuole morphology in *vfd1/fyve1*, the observed structures were larger and central vacuoles could be observed.

Next, the effect of BFA on endocytic trafficking in *fyve1-1* was examined. 5-day-old *fyve1-1* mutant seedlings were pre-treated for 10 minutes with the lipophilic endocytosis marker dye FM4-64 (2 µM). The endocytic tracer dye is known to be taken up from the plasma membrane over clathrin coated vesicles (CCVs) to the *trans*-Golgi network (TGN) and furthermore stained endosomal vesicles (Bolte et al., 2004) (Figure 37 C). Seedlings were incubated for one hour in liquid GM medium with 50 µM BFA. 2-day-old wild-type No-0 seedlings of a comparable size served as control. Seedlings were analyzed after one hour of incubation. FM4-64 was rapidly taken up by cells and staining of the plasma membrane was already visible after five minutes of incubation. Positive FM4-64 vesicles of endosomal origin accumulate in the cytosol and aggregate to so-called BFA compartments or bodies.
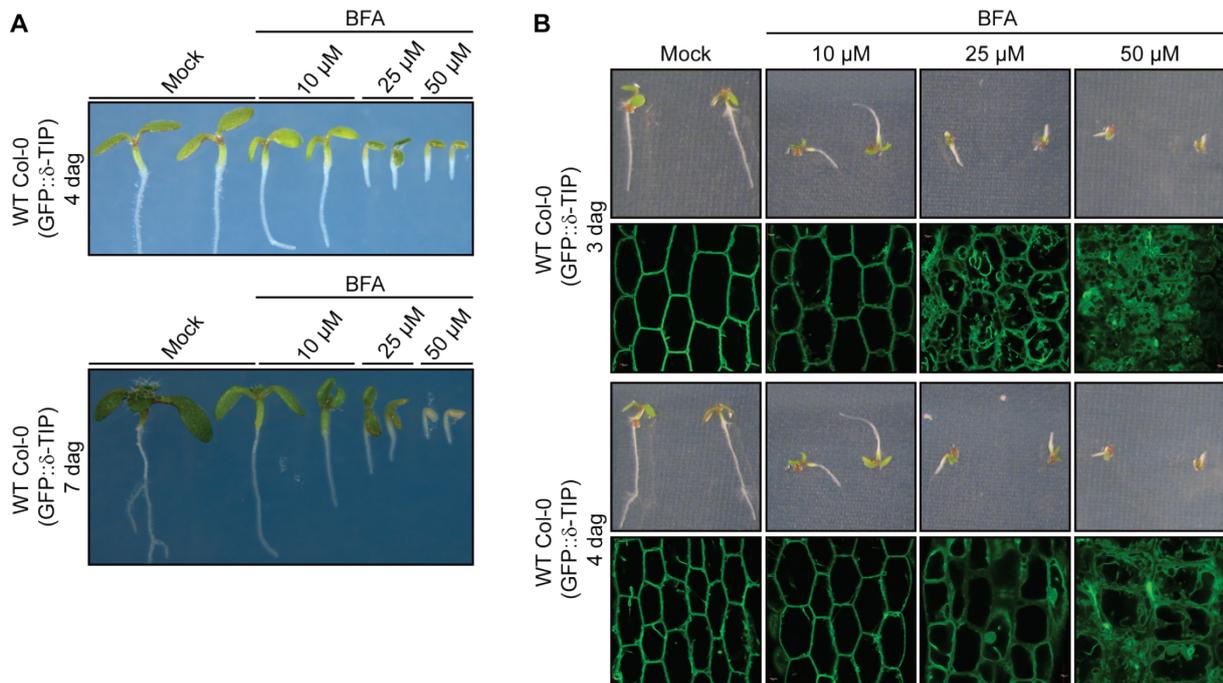
Figure 36. High concentrations of BFA led to an *amsh3*-like phenotype, but did not alter vacuole morphology.
(A) Phenotype comparison of wild-type Col-0 seedlings grown on increasing BFA concentrations at 4 dag and 7 dag. **(B)** Phenotype of 3- and 4-day-old wild-type Col-0 seedlings grown vertical on a ½ MS agar plate supplemented with the indicated concentrations of BFA. Upper row: seedling development with increasing concentrations of the inhibitor BFA, lower row: corresponding vacuole morphology with tonoplast marker GFP::δ-TIP.

After one hour of incubation with BFA, large BFA bodies appeared in wild-type cells, whereas FM4-64-stained intracellular structures in *fyve1-1* were visibly smaller (Figure 37 A). The size of BFA compartments in 2-day-old wild-type seedlings had a mean area of 15.7 µm² (n= 47 cells), whereas those in *fyve1-1* had a clearly reduced size of 2.7 µm² (n= 54 cells). Furthermore, the number of BFA compartments, although smaller in size, increased for the *fyve1-1* mutant (Figure 37 B). *fyve1-1* showed in average two compartments per cell, whereas in wild-type cells one aggregate of larger size was overrepresented (Figure 37 B). Cells with three or more BFA bodies occurred in higher numbers in the mutant compared to the wild-type (Figure 37 B). These results indicate that the intracellular trafficking of endosomal vesicles was altered in the *fyve1-1* mutant.
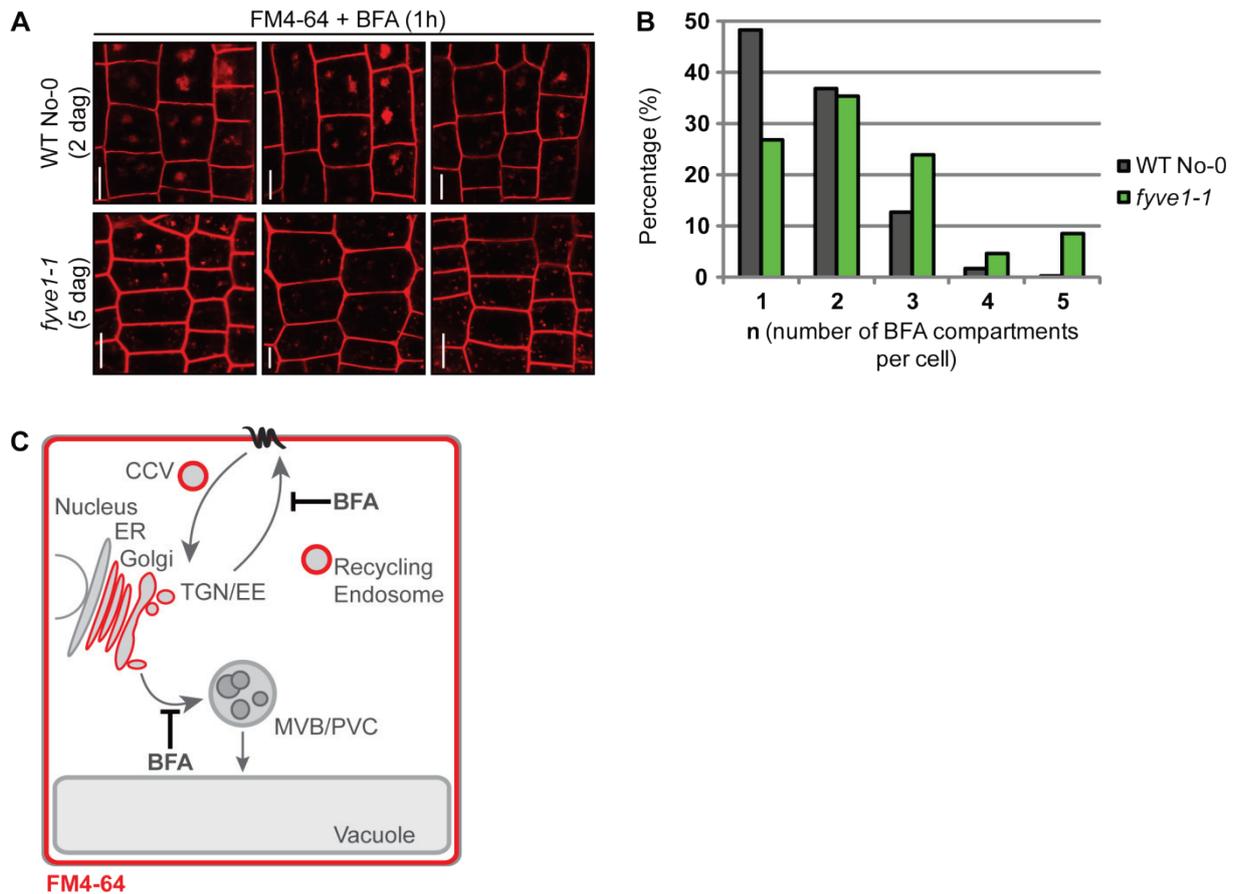
Figure 37. Inhibition of endocytosis with BFA leads to smaller BFA compartments with increased number of vesicles in the *fyve1-1* mutant.
(A) Treatment of 2-day-old wild-type seedlings and 5-day-old *fyve1-1* mutants with BFA for one hour. Pretreatment with the endocytic lipophilic marker dye FM4-64 stained the plasma membrane, all endosomal membranes and BFA compartments. Scale bar: 10 μm. **(B)** Quantification of number of BFA compartments in cells in percentage comparing wild-type and *fyve1-1* mutant. n: number of BFA compartments per cell. **(C)** Modell of BFA function in the cell. BFA inhibits recycling to the plasma membrane and vesicle maturation and fusion to MVBs. FM4-64 stains the plasma membrane and endocytotic vesicles and membranes. MVB/PVC and vacuole are not stained, because BFA treatment inhibits trafficking of the endocytic dye. CCV: clathrin-coated vesicle, ER: endoplasmic reticulum, TGN: *trans*-Golgi network, EE: early endosome, MVB: multivesicular body, PVC: prevacuolar compartment.

3.11 Endocytic degradation of PIN1 in *fyve1-1*

To expand the understanding of the endosomal trafficking defects of the *fyve1-1* mutant, the behavior of two plasma membrane proteins, PIN1 (AT1G73590) and PIN2/EIR1/AGR (AT5G57090), were investigated. PIN (PIN-FORMED) proteins are integral membrane proteins and efflux transporters of the phytohormone auxin (Dhonukshe et al., 2007). As such, PIN proteins facilitate the polar auxin transport in plant cells and their expression is tightly regulated by auxin, other hormonal pathways and plant growth regulators. Protein stability and localization at the plasma membrane is controlled by subcellular trafficking and endocytic recycling. PIN proteins are constitutively recycled, endocytosed by clathrin-coated vesicles (CCVs) and transported via the endosomal system

to the vacuole for degradation (Dhonukshe et al., 2007). PIN1 is expressed in the whole plant and in the vascular tissue of the root. PIN1 function is essential for flower development. PIN2 is only expressed in the three outer cell tissues of roots: epidermis, cortex and endodermis. PIN2 function is essential for the gravitropic response of the root. As plasma membrane proteins that are transported to the vacuole for degradation, PIN proteins are the ideal cargo proteins to investigate the specific defects of endosomal trafficking mutants.

The P100 fractions of protein extracts of 7-day-old *fyve1-1* and 2-day-old wild-type (No-0), phenotypically identical to the *fyve1-1* mutant, were compared. The *amsh3-1* mutant and the *pin1*/PIN1-RFP complemented knockout mutant were used as controls. For PIN detection, ultracentrifugation was performed on the total protein extract to isolate the membrane-bound proteins. PIN1 protein levels in both mutants were higher compared to the wild-type (Figure 38 B). Endogenous PIN2 could not be detected with the used method. For better detection of PINs only root tips of seedlings could be taken for protein extraction, but this method was not applicable for 2-day-old wild-type or *fyve1-1* mutant seedlings, where the root is not yet fully elongated and the number of mutants is limiting.

To exclude the possibility that accumulation of PIN1 in the mutants is a result of higher transcript levels, the gene expression of *PIN1* and *PIN2* in wild-type and *fyve1-1* mutant were analyzed by qRT-PCR. The expression of *PIN1* was not altered significantly in the *fyve1-1* mutant, suggesting that PIN1 accumulates due to post-transcriptional mis-regulation (Figure 38 A).

To analyze how endocytosed PIN proteins are transported to the vacuole and how the loss of FYVE1 may interfere with this specific recycling and degradation pathway, the pPIN2::PIN2-GFP marker line (Laxmi et al., 2008) was crossed with the *fyve1-1* mutant. Under normal growth conditions, PIN2-GFP showed polar localization in root tips of the *fyve1-1* mutant like the wild-type (Figure 38 C). Targeting of PIN proteins to the plasma membrane and proper recycling at the early steps of endocytosis were not affected. In darkness, PIN2 proteins are endocytosed and transported to the vacuole for degradation (Laxmi et al., 2008; Leitner et al., 2012). The fusion protein PIN2-GFP accumulates in the wild-type in the vacuole after 10 hours of incubation in the dark. In the *fyve1-1* mutant this accumulation took place much later than in the wild-type. PIN2-GFP reached the vacuole in 24 hours of dark incubation (Figure 38 D). This indicates that the vacuolar transport of membrane proteins, like the PIN proteins, is delayed in the *fyve1-1* mutant.
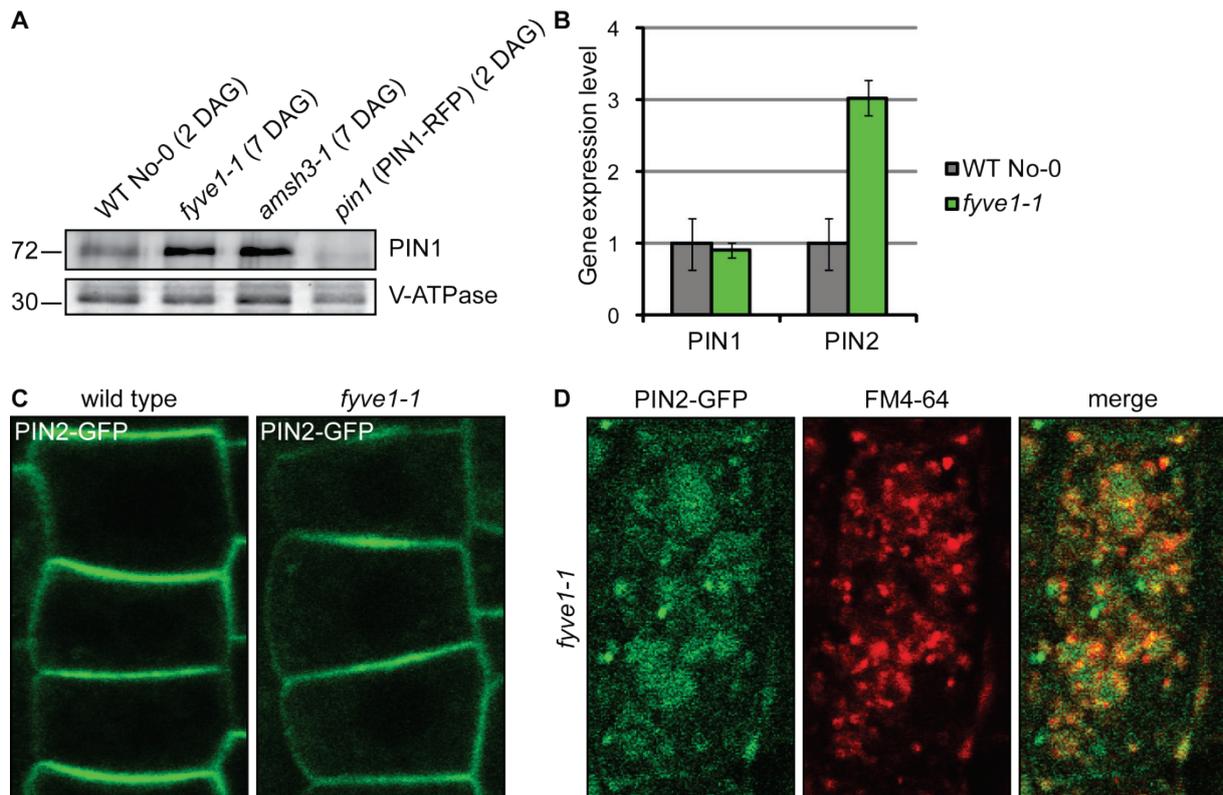
Figure 38. *PIN2* expression levels are increased, but PIN2 localization is not altered in *fyve1-1*.
(A) *PIN*1 and *PIN2* gene expression analysis via qRT-PCR showed no variations in *PIN1* gene expression, but higher expression levels of PIN2. *ACTIN8* was used for normalization. **(B)** Western blot expression profile of PIN1 in *fyve1-1* and *amsh3-1* mutant in comparison to wild-type and knockout mutant *pin1* of comparable phenotype. *fyve1-1* and *amsh3-1* accumulate PIN1 protein. Vacuolar ATP-ase (V-ATPase) was used as P100 loading control. **(C)** Polar localization of plasma membrane protein PIN2-GFP was not altered in the *fyve1-1* mutant. **(D)** Endocytosis of PIN2-GFP was impaired in the *fyve1-1* mutant, but endocytosed PIN2-GFP reached the vacuole after 24 hours of dark incubation. *fyve1-1* mutant was pre-incubated with endosomal tracer dye FM4-64 for 10 minutes and incubated in 1 µM Concanamycin A (ConcA) solution for 24 hours in the dark. ConcA, a vacuolar ATPase inhibitor, was added for increased stability of vacuolar PIN2-GFP.

3.12 Model for FYVE1 function

Taken together, the FYVE1 protein is involved in intracellular trafficking and contributes to directing vacuolar proteins to their target destination, the vacuole. Therefore, FYVE1 is a novel factor in plant intracellular trafficking and vacuolar protein transport.

FYVE1 contains one major characteristic domain: its phospholipid-binding FYVE domain. Moreover, N-terminal and C-terminal regions suggest multiple protein-protein interacting domains, even though FYVE1 lacks any domains for enzymatic function. FYVE1 binds interaction partners and guides those to the target organelle, the PI(3)P-branded MVB. Due to the localization studies of the here presented work and in taking in the additional findings of the works of Barberon et al. and Gao et al., FYVE1 fulfills multiple functions in a plant cell. Because of its cytosolic and late endosomal (MVB) localization, FYVE1 can be assumed to possess a broad interaction field, where interacting proteins can attach. By directly binding to the endocytosis tagging protein ubiquitin, FYVE1 can interact with

endocytosed cargo proteins from the plasma membrane and can direct those proteins to their destination.

The same can probably be achieved through direct interaction with specific interactors of FYVE1. FYVE1 interacts directly with the plasma membrane transporter IRT1 and plays a role in the membrane targeting. FYVE1 may be the protein guiding AMSH3 to the MVB. Furthermore, FYVE1 interacts with the ESCRT-I subunits VPS23A and VPS23B. Gao et al. suggest that FYVE1-ESCRT-I interaction may be important for ILV formation (Gao et al., 2014). This could indicate a general targeting role of FYVE1 for the ESCRT-complexes and related proteins at the MVB. By interacting with autophagosome-localized SH3P proteins, FYVE1 also connects endocytosis and the autophagy pathway. FYVE1 may grab the SH3P interacting protein and pull it towards the MVB, thereby it could be promoting membrane attachment of autophagosome and vacuole and induce membrane fusion of both organelles.

In summary, FYVE1 is a unique and plant-specific protein and plays an essential role in endocytosis as well as vacuolar protein transport. It is essential for plant development and vacuole biogenesis. In addition, the recent finding in the FYVE1 story by Gao et al. proposed a dual function for FYVE1 in *Arabidopsis* (Gao et al., 2015). First, the regulation of MVB and vacuole biogenesis via its interaction with the ESCRT-I complex via its N-terminal proline rich region and second, its regulatory function in autophagy via its interaction with SH3P2 with its C-terminal coiled-coil domain.
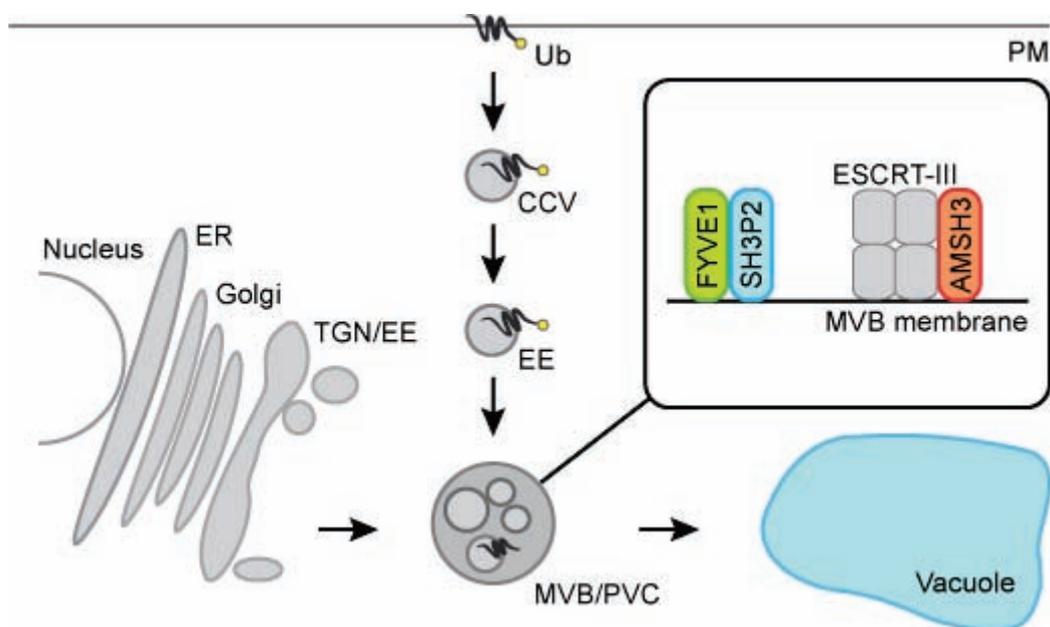
Figure 39. FYVE1 localizes to late endosomes and regulates intracellular trafficking and vacuole biogenesis.
Due to its FYVE lipid-binding domain, FYVE1 binds to specific phospholipids at the membrane of late endosomes. It acts as an effector protein for other proteins, targeting interacting proteins to the endosomal membrane. The ESCRT-machinery necessary for endocytosis is located at the MVB, where AMSH3 binds to two subunits of the ESCRT-III complex and deubiquitinates endocytosed cargo proteins prior to invagination into ILVs of the MVB. The FYVE1 interacting protein SH3P2 is an important regulator in autophagy and membrane fusion of autophagosomes with vacuolar compartments.

4. Discussion

4.1 *VFD* genes play a role in vacuole biogenesis

The *vacuolar fusion defective* (*vfd*) mutants identified and characterized in this study expand the spectrum of vacuole mutants in plants. Due to the fact that the plant vacuole is a central and essential organelle of plant cells, loss-of-function mutants either show severe defects in early stages of plant development or have less severe phenotypes without prominent mutant characteristics. The *amsh3* mutant is one of the rare vacuole mutants that can develop to the seedling stage and that is identified and characterized until know (Isono et al., 2010). The EMS screen presented in this study aimed to identify additional mutants, that showed similar characteristics like the *amsh3* mutant, to broaden our understanding of the interplay between vacuole biogenesis and endocytosis and to further define the pathway in which AMSH3 is playing an essential role.

This work provides a selection of 13 *vfd* mutants, which all showed the *amsh3*-like attributes: a seedling lethal and vacuolar fusion defective phenotype. Causes for altered vacuolar morphology may be that either precursor vacuoles (or prevacuoles) in the mutants cannot fuse to form the central vacuole during seedling development or the biosynthetic pathway for vacuole biogenesis is defective or blocked and vacuolar cargo is not correctly transported to the vacuole. This could mean that the process of homotypic membrane fusion is perturbed in the *vfd* mutants.

As secondary phenotype, the *vfd* mutants *vfd1*, *vfd2*, *vfd3*, and *vfd11* accumulated ubiquitinated proteins like the *amsh3* mutant. The protein levels of AMSH1, AMSH2 and AMSH3 did not change. This indicates a connection between the deubiquitinating function of AMSH proteins and the newly identified VFD proteins. The affected *VFD* genes are playing a role either upstream or downstream as enzyme substrates of the AMSH proteins. Seven of the identified *vfd* mutants are genetically distinct from the *amsh3* mutant and point toward new and unknown genes and proteins playing a role in the AMSH3-related pathway of vacuole biogenesis and membrane fusion events.

The remaining *vfd* mutant lines are required for testing, if they are allelic to the *amsh3* mutant or to one another to ensure independent mutant lines. Further characterization of the *vfd* mutants and their defective genes will broaden our perspective of this not yet fully understood and complex mechanism of vacuolar fusion. The remaining, not yet investigated *vfd* mutant lines may include other interesting genes, that have not been described before and may be linked to endocytosis and vacuolar trafficking.

All *vfd* mutants showed severe germination defects, which might be linked to water deficiency, reduced water uptake or impaired swelling of the seed coat. For proper seed germination, a functional vacuole is needed for cell elongation and stability, so that the

seedling radicle can break through the seed coat. Water is a prerequisite for germination. The seeds need to take up water (imbibition), which leads to swelling and breaking of the seed coat. For emerging of the radicle, embryo root cells need to elongate and push through the micropyle. This process may need a fully functional vacuole, which can express a defined turgor pressure. In *vfd* mutants, this turgor pressure may be critical for germination.

Seed development seemed to be normal in *vfd* mutants, neither embryo development nor seed maturation were affected. This would exclude a defect in water uptake during germination in the process of imbibition and may hint to impaired cell elongation and a defect in elongation of the embryonic axis, which inhibits radicle protrusion and completion of germination. During this step of germination, the vacuole is playing an important role in cell growth and stability.

Several phytohormones are known to play a role in regulating seed dormancy and germination (Koornneef et al., 2002). The phytohormone abscisic acid (ABA) promotes seed dormancy and inhibits germination. In addition, ABA is important for water uptake in plant cells. The phytohormone gibberellin (GA) is working antagonistically to ABA. GA promotes seed germination and induces loss of dormancy. GA-deficient mutants are unable to germinate without exogenous GA. The germination deficiency in *vfd1/fyve1* mutants could indicate a hypersensitivity to ABA, which can be regulated by ABA-inhibitors like norfluorazon (Debeaujon and Koornneef, 2000), or an insensitivity to endogenous GA, which could be overcome by addition of exogenous GA. It would be interesting to further investigate the influence of ABA and GA on *vfd* mutant germination and mutant seedling development. Reciprocal crosses would be necessary to determine if the *vfd* mutation leads to partial embryo lethality, gametophytic or pollen viability defects.

4.2 FYVE1 is an essential protein in *Arabidopsis*

To understand the role of FYVE1 in the cellular network, the molecular function of its FYVE domain is of importance. FYVE domains are known as lipid-binding domains and therefore FYVE domain-containing proteins are important factors in the lipid signaling system of plant cells.

4.2.1 Phospholipid signaling in plants

All cell membranes consist of a phospholipid bilayer and additional attached membrane proteins (fluid mosaic model of Singer and Nicolson (1972)). Phospholipids are a class of lipids and the main structural component of all biological membranes. They consist of two long hydrophobic fatty acid tails and a hydrophilic head group, a phosphate group and glycerol, and therefore are of amphipathic character. In addition to their function in membrane structure, phospholipids are also signaling molecules and act as precursors for

second messengers (Munnik and Testerink, 2009). Glycolipids, storage lipids and structural phospholipids compose around 90 % of all plant lipids (Munnik and Testerink, 2009).

Phosphatidylinositol is the basic component of the phosphatidylinositol phosphates (PIPs) or polyphosphoinositides (PPIs). The phospholipid head group consists of a phosphate group and a hexameric inositol (sugar alcohol) ring. The inositol ring can be modified by phosphor groups at the D-3, D-4 and D-5 position, leading to a set of different phosphoinositides. Phosphatidylinositol 3-kinases (PI3K) produce phosphoinositides phosphorylated at the D-3 position of the inositol ring to form PI(3)P. All mono- and bisphosphorylated combinations have been found in plants, which represent less than 1 % of the total membrane phospholipids of the cell (van Leeuwen et al., 2004; Munnik and Nielsen, 2011).

The lipid signaling system was first investigated in animal cells, which is nowadays the basis for the plant phospholipid signaling pathway. Although there are differences between animal and plant cells in regard to phospholipid composition and existing proteins functioning in lipid signaling.

In animal cells, the phosphoinositol/phospholipase C (PI/PLC) system was discovered as the principal pathway for lipid signaling (Oude Weernink et al., 2007; Munnik and Testerink, 2009). After activation of a membrane receptor, the phospholipase C (PLC) is activated and hydrolyses the signal precursor phosphatidylinositol-4,5-bisphosphate $(PI(4,5)P_2)$ into the two second messengers inositol tri-phosphate (IP_3) and diacylglycerol (DG). IP_3 diffuses into the cytosol, binds to specific receptors at the ER membrane and leads to calcium (Ca^{2+}) release out of internal stores. Diacylglycerol remains in the membrane and recruits protein kinase C (PKC), which phosphorylates other downstream signaling proteins, leading to activation or inactivation of these. Phosphatidylinositol-4-phosphate (PI(4)P) and $PI(4,5)P_2$ are the common signaling molecules in animal cells. The second important lipid signaling protein is the phosphatidylinositol 3-kinase (PI3K). PI3K phosphorylates the phospholipid $PI(4,5)P_2$ to phosphatidylinositol-3,4,5-trisphosphate $(PI(3,4,5)P_3)$ - another important signaling molecule in animal cells. $PI(3,4,5)P_3$ triggers Ca^{2+} release from intracellular stores via ligand-gated Ca^{2+} channels. This PI/PLC reaction cascade sets of the cellular response to environmental stimuli.

In plants, several of the animal factors are missing. There is no evidence that plants have a receptor for IP_3, which is thought to have been lost during evolution in higher plants (Wheeler and Brownlee, 2008). In plants, the sugar alcohol inositol hexakisphosphate or phytic acid (IP_6), called phytate in salt form, is playing a more important role than IP_3. IP_3 is immediately converted into IP_6 by the enzymes PLC and inositol polyphosphate multikinases (IPKs). IP_6 is stored in seeds, because phosphate and inositol are required for germination. Phytate is the main storage form of phosphorus in many plant cells. IP_6 induces Ca^{2+} release

in guard cells (Munnik and Vermeer, 2010). Interestingly, IP_6 was shown to bind to the auxin receptor TIR1 (Tan et al., 2007), indicating that IP_6 is the second messenger alternative for IP_3 in plants.

Plant cells lack protein kinase C (PKC), which is the target protein of the DG signaling pathway. Plants do have a row of other protein kinases, which are playing a role in lipid signaling: the calcium-responsive CBL-interacting protein kinase (CIPK), phosphoinositide-regulated AGC kinases and calcium/calmodulin-dependent protein kinase (CDPK) (Munnik and Testerink, 2009).

In contrast to the animal PI/PLC signaling system, plants only contain one class of phospholipase C (PLC) isoform, instead of the six existent isoforms in animals (Oude Weernink et al., 2007; Munnik and Testerink, 2009). PLC hydrolyses phosphatidylinositol-4-phosphate (PI(4)P) and phosphatidylinositol-4,5-bisphosphate (PI(4,5)P_2) and is regulated by calcium.

Instead of DG, the main lipid second messenger in plants is phosphatidic acid (PA), which is the phosphorylated derivative of DG. PA can be synthesized via two enzyme pathways: from PI(4,5)P_2 by the PLC/DGK-enzyme cascade and directly by the enzyme phospholipase D (PLD) via hydrolysis of structural lipids like phosphatidylcholine (PC) and phosphatidylethanolamine (PE). Therefore, DG exists only in low concentrations in plant cells and is immediately phosphorylated by the DG kinase (DGK) to gain PA. Because plants lack the protein PKC, they have to circumvent the DG pathway. The enzyme PLD is activated by biotic and abiotic stresses and PA is synthesized very rapidly in response (Munnik and Testerink, 2009). The *Arabidopsis* genome encodes 12 PLD genes, humans only have two PLD genes, indicating a higher importance of PA in signal transduction in plants (Munnik and Testerink, 2009).

The lipid composition of membranes in plant cells is also different from those in animal cells. The phosphatidylinositol monophosphate (PIP) PI(4)P is the main phospholipid in plant cells and occurs in the plasma membrane and the membrane of the Golgi apparatus. In plant cells, 80 % of the PIP pool is made up of PI(4)P, with 5 to 15 % PI(3)P and a small fraction of PI(5)P (Meijer et al., 2001; Munnik and Vermeer, 2010).

Similar to animal cells, PI(4)P and PI(4,5)P_2 are the main signaling precursors and signaling molecules in plants. The PI(4)P content is similar to animal cells, but plant cells have very low concentrations of PI(4,5)P_2. PI(4,5)P_2 was shown to be predominantly cytosolic, but in response to salt stress it is recruited to the plasma membrane and clathrin-coated vesicles (van Leeuwen et al., 2007). Plants have also small amounts of PI(3,5)P_2, another phosphatidylinositol bisphosphate (PIP$_2$), but increase concentrations of PIP$_2$s in response to osmotic stress (Meijer et al., 1999). PIP$_2$s are important for intracellular trafficking and the endocytic system. PI(3,5)P_2 is synthesized by the Fab1/PIKfyve family of

PI(3)P 5-kinases in yeast and animal cells and is important for membrane trafficking and vacuole/lysosome homeostasis (Dove et al., 2009). In contrast to the animal system, plants lack phosphatidylinositol trisphosphates (PIP$_3$) (Meijer and Munnik, 2003; van Leeuwen et al., 2004; Munnik and Testerink, 2009).

Several protein domains are known to exhibit lipid-binding character and also exist in plants (van Leeuwen et al., 2004). The pleckstrin homology (PH) domain binds specifically to the phospholipids PI(4)P and PIP$_2$ and also shows nonspecific binding capacities. The FYVE domain binds specifically only to PI(3)P (Gaullier et al., 1998). The Phox homology (PX) domain binds PI(3)P, P(3,4)P$_2$ and PA. The epsin N-terminal homology (ENTH) domain binds to the signaling lipid PI(4,5)P$_2$. *Arabidopsis* contains around 70 proteins with a predicted lipid-binding domain (van Leeuwen et al., 2004).

The plant lipid signaling pathways use phospholipids as docking sites on membranes, which are targeted by signaling proteins. The lipid interacting proteins activate downstream signaling events like (de-)phosphorylation, thereby activating or deactivating other enzymes. Moreover, these target proteins can act as molecular scaffolds for the assembly of multiprotein complexes (van Leeuwen et al., 2004). Proteins with lipid-binding domains act as effectors of lipid signaling by being recruited to a specific membrane site marked by phospholipids. These effector proteins can either be directly (de-)activated upon interaction with phospholipids or they interact with other proteins.

4.2.2 The phospholipid-binding FYVE domain is involved in membrane fusion

The FYVE domain belongs to the superfamily of zinc finger (Znf) domains. The two other main zinc finger domains are the RING (Really Interesting New Gene) and PHD (Plant Homeo Domain) domains, which are structurally different from the FYVE zinc finger. The FYVE domain is named after the four proteins in which the domain was first discovered and described: Fab1p, YOTB, Vac1p and EEA1 (van Leeuwen et al., 2004). In general, FYVE domains consist of 60 to 80 amino acids (Figure 40). Due to eight conserved, zinc-coordinating cysteine residues, the secondary structure of the domain is build up of two small β-hairpins (zinc knuckles) and one small C-terminal α-helix, which form two Zn^{2+}-binding clusters (Misra and Hurley, 1999). FYVE domains are known lipid-binding domains and play a role in lipid signaling. They function as effectors of lipid signaling by recruiting proteins to membranes with specific phospholipid composition. The basic motif R(R/K)HHCR of the FYVE domain acts as a highly specific binding pocket for one phosphatidylinositol 3-phosphate (PI(3)P) molecule (Dumas et al., 2001). The C-terminal coiled-coil region of FYVE1 may function as a protein-protein-interaction domain. FYVE domain proteins are known to form homodimers.
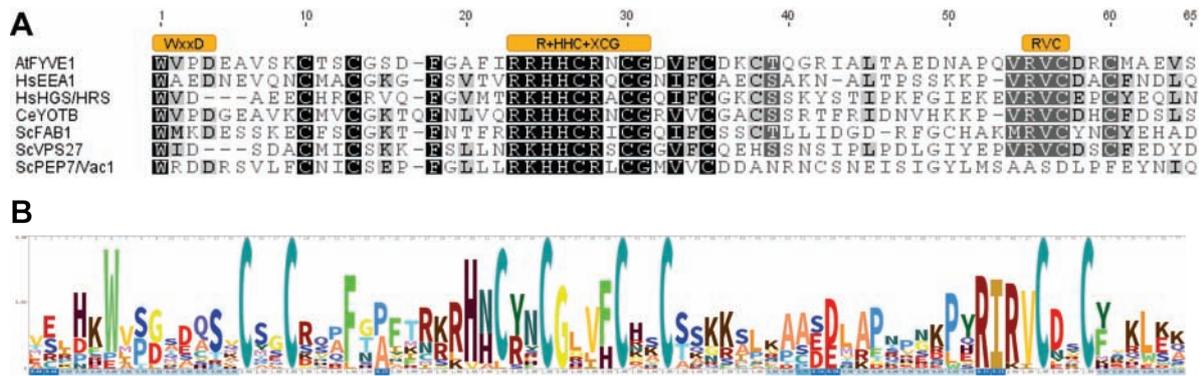
Figure 40. The FYVE domain and its major motifs are conserved across kingdoms.
(A) FYVE domain alignment of the major FYVE domain proteins of different species. At: *Arabidopsis thaliana*, Hs: *Homo sapiens*, Ce: *Caenorhabditis elegans,* Sc: *Saccharomyced cerevisiae*.
(B) Hidden Markov Model (HMM) logo of the FYVE domain highlighting conserved amino acid sites. The FYVE logo is based on the alignment of the seven sequences shown in (A). Big letters show the conserved motifs.

The FYVE (Fab1p, YOTB, Vac1p, EEA1) domain was first characterized in proteins of mammalian and yeast model organisms. The first reference for the FYVE domain was given in 1996 for the autoantigen EARLY ENDOSOME ANTIGEN 1 (EEA1) in human cells (Stenmark et al., 1996). In this publication, the FYVE domain was distinguished from other zinc finger-like domains, like the RING or PHD finger, due to its capability to bind two Zn^{2+} ions and the characteristic central R+HHC+*X*CG motif. On the basis of sequence similarity of the FYVE domain between EEA1 and the yeast proteins Vps27p, Fab1p and Vac1p, Stenmark et al. proposed to call the conserved zinc finger-like domain the FYVE finger. EEA1 carries the FYVE domain at its C-terminal end, following long patches of coiled-coil domains. EEA1 was shown to bind specifically to PI(3)P via its FYVE domain and to localize to early endosomes. In this context, it is also noteworthy that the Rab5 GTPase is interacting and colocalizing with the EEA1 protein on early endosomes, playing a role in membrane fusion of endocytic vesicles (Stenmark et al., 1996; Simonsen et al., 1998). Loss of EEA1 inhibits homotypic endosome fusion *in vitro*, which also requires Rab5-GTP and PI3-kinase activity, leading to the proposition that EEA1 functions as an effector of Rab5 and PI(3)P by tethering Rab5-positive membranes (Stenmark and Aasland, 1999). Another mammalian FYVE-finger protein is HRS/HGS (hepatocyte growth-factor-regulated tyrosine-kinase substrate), which is also localizing to early endosomes and forms together with STAM (signal transducing adaptor molecule) the ESCRT-0 complex (Stenmark and Aasland, 1999). ESCRT-0 is necessary for MVB formation.

The yeast Fab1p protein contains a N-terminal FYVE domain and functions as a phosphoinositol-4-phosphate 5-kinase (PI(4)P 5-kinase), which converts PI(4)P to PI(4,5)P_2 (Yamamoto et al., 1995). The yeast *fab1* mutant shows formation of aploid and binucleate (fab) cells and leads to defects in vacuole function and morphology. *fab1* accumulates very large, swollen vacuoles. The product of the Fab1p reaction is PIP$_2$, which may play a role in

Table 12. FYVE domain-containing proteins in human, yeast and plant (modified after Stenmark and Aasland, 1999).

Human	Yeast	Plant	Domains	Putative function
EEA1	Vac1p		C2H2 finger, coiled-coil regions, Rab5 binding domain	Tethering of Rab5-positive vesicles and endosomes
PIKfyve	Fab1p	FAB1A/B	DEP-domain, chaperonin-domain, PI 5-kinase domain	PI 5-kinase, formation of MVB
Hrs/Hgs	Vps27p		VHS domain, coiled-coil region, STAM-binding domain	Formation of MVB, ESCRT-0

membrane fusion events of the vacuole or as a regulator in membrane trafficking. The mammalian ortholog of Fab1p is PIKfyve (Efe et al., 2005).

Another interesting PI 3-kinase in yeast is Vps34p. Knockout mutants of Vps34p show severe defects in protein sorting to the vacuole/lysosome (Herman and Emr, 1990). PI(3)P seems to be exclusively needed in vacuolar protein sorting, because it is the only pathway affected in the *vps34p* mutant (Stenmark and Aasland, 1999). Subsequently, Fab1p/PIKfyve catalyzes the reaction from PI(3)P to PI(3,5)P_2.

Vac1p/Vps19p/Pep7p is involved in vacuole inheritance and vacuolar protein sorting (Weisman and Wickner, 1992). Yeast *vac1* mutants accumulate endocytic vesicles, indicating that Vac1p is involved in homotypic vacuole fusion (Stenmark and Aasland, 1999). The yeast Vac1p protein is the closest homolog to the human EEA1 FYVE domain. Both proteins bind to the SNARE-associated protein Vps45p, emphasizing their role in membrane fusion events (Piper et al., 1995; Stenmark and Aasland, 1999).

In contrast, the yeast FYVE protein Vps27p is implicated in the late stages of endocytosis. *vps27p* mutants in yeast show defects in vacuolar protein sorting of vacuolar hydrolases, accumulation of endocytic vesicles and formation of 'class E' compartments (Stenmark and Aasland, 1999). Vps27p is homologous to mammalian Hrs, functioning in MVB body formation via the ESCRT-0 complex.

When mammalian and yeast FYVE proteins are compared, the protein structure can be very diverse with combinations of various domains in addition to the FYVE domain. The position of the FYVE zinc finger varies strongly and only the FYVE phospholipid-binding domain acts as the connecting feature.

4.2.3 *Arabidopsis* FYVE1 is a unique FYVE domain protein

The *Arabidopsis* genome encodes 15 FYVE domain-containing proteins (van Leeuwen et al., 2004; Wywial and Singh, 2010). Wywial and Singh categorize the *Arabidopsis* FYVE proteins into five classes on basis of their domain composition (Table 13). Van Leeuwen and Munnik group into three categories (group number indicated in brackets) (van Leeuwen et al., 2004).

Class I consists of the FAB family of phosphatidylinositol phosphate 5-kinases with the two members FAB1A and FAB1B (category 1). *Class II* includes the two close homologs FYVE2 and FYVE3. *Class III* consists of FYVE4 with a N-terminal localized FYVE domain. FYVE1 is categorized in *class IV* as the only protein with a C-terminal FYVE domain. *Class V* comprises the PRAF protein family (P̲H domain, R̲egulator of Chromosome Condensation (RCC) and F̲YVE), whose nine members contain a PH, a RCC and a FYVE domain and are plant specific (category 2).

Most *Arabidopsis* FYVE proteins are characterized in reference to a protein domain with enzymatic function. The primary function of the FYVE domain is targeting the protein to a specific membrane domain containing a distinct membrane lipid composition.

The *Arabidopsis* Fab1/PIKfyve homologs, FAB1A and FAB1B, localize to endosomes in root epidermal cells and function in vacuolar acidification, vacuole formation and endocytosis (Hirano et al., 2011). Besides the N-terminal phospholipid-binding FYVE domain, both proteins contain the catalytic phosphoinositol proteinkinase domain, which catalyses the reaction from PI(3)P to PI(3,5)P$_2$. Knockdown mutants showed pleiotropic phenotypes, including root growth inhibition and hyposensitivity to exogenous auxin, which links FAB1A/B function in *Arabidopsis* to auxin signaling. The *fab1a/fab1b* double knockout mutant shows defects in pollen development, including abnormally large vacuoles (Whitley et al., 2009). The pollen development and vacuole defects were also observed in the *Arabidopsis vps34* mutant and were proposed to be caused by a lack of PI(3)P production (Lee et al., 2008).

Table 13. *Arabidopsis* FYVE domain proteins. Modified, van Leeuwen et. al, 2004. Names in brackets are outdated.

Name	AGI no.	Domains	Class	References
FYVE1	AT1G20110	FYVE	IV	Barberon, 2014; Kolb, 2015; Gao, 2014; Gao, 2015
FYVE2	AT3G43230	FYVE	II	
FYVE3	AT1G29800	FYVE	II	
FYVE4	AT1G61690	FYVE	III	
FAB1A	AT4G33240	FYVE + Chaperonin + PIP5K	I	Whitley and Doughty, 2009; Hirano, 2011
FAB1B	AT3G14270	FYVE + Chaperonin + PIP5K	I	Whitley and Doughty, 2009; Hirano, 2011
PRAF1	AT1G76950	PH + RCC1 + FYVE	V	
PRAF2	AT3G47660	PH + RCC1 + FYVE	V	
PRAF3	AT1G69710	PH + RCC1 + FYVE	V	
PRAF4	AT1G65920	PH + RCC1 + FYVE	V	
PRAF5	AT5G42140	PH + RCC1 + FYVE	V	
PRAF6	AT3G23270	PH + RCC1 + FYVE	V	
PRAF7	AT4G14368	PH + RCC1 + FYVE	V	
PRAF8 (UVR8)	AT5G12350	PH + RCC1 + FYVE	V	Kliebenstein, 2002
PRAF9	AT5G19420	PH + RCC1 + FYVE	V	
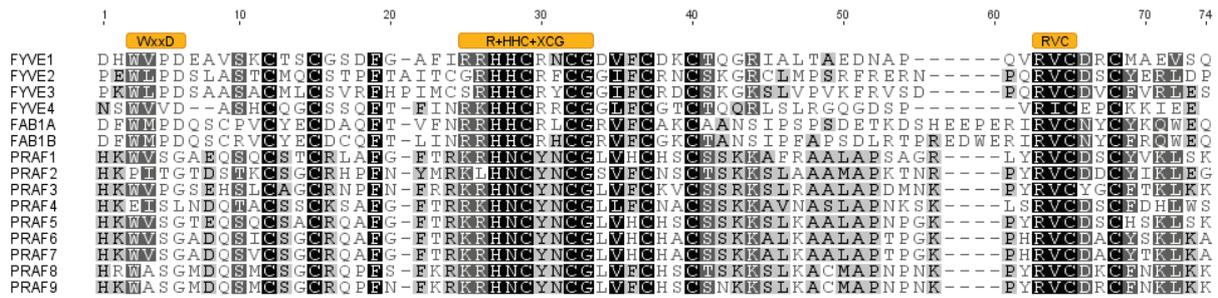
Figure 41. *Arabidopsis* contains 15 FYVE domain-containing proteins.
Alignment of the 15 FYVE domain proteins performed with the conserved FYVE domain only.

The other big family of FYVE proteins in *Arabidopsis*, the PRAF family, is also mainly characterized in respect to their RCC domain, rather than the FYVE domain. PRAF proteins contain additional PH and RCC (Regulator of Chromosome Condensation) domains and are plant-specific (van Leeuwen et al., 2004). RCC domains catalyse guanine nucleotide exchange from GTP to GDP in concert with Rab GTPases. The only described PRAF protein of *Arabidopsis* is PRAF8/UVR8 (Kliebenstein et al., 2002). The *uvr8-1 (UV resistance locus 8-1)* mutant is hypersensitive to UV-B light.

FYVE1 is unique among the *Arabidopsis* FYVE proteins. The only known domains are the FYVE domain and a coiled-coil domain, both located at the C-terminus. The coiled-coil domain is probably necessary for protein-protein interaction and dimerization of proteins. Even though, it was not yet shown if FYVE1 can self-dimerize or not.

The FYVE domains of *Arabidopsis* proteins vary in their amino acid sequence with only the three major motifs of the FYVE domain and highly conserved single amino acids, mostly cysteins, remaining of high similarity as can be seen by the general consensus sequence of the HMM logo of the FYVE domain (Figure 41).

The closest homologs of FYVE1 in the *Arabidopsis* proteome, compared by the FYVE domain, are FYVE4 (AT1G61690), FAB1B (AT3G14270) and FAB1A (AT4G33240) with 41 %, 38 % and 37 % identity, respectively, followed by FYVE2 (AT3G43230) and FYVE3 (AT1G29800) with 35 % identity. The PRAF proteins are more distant to FYVE1 with an identity of 29 to 35 % (Figure 42).
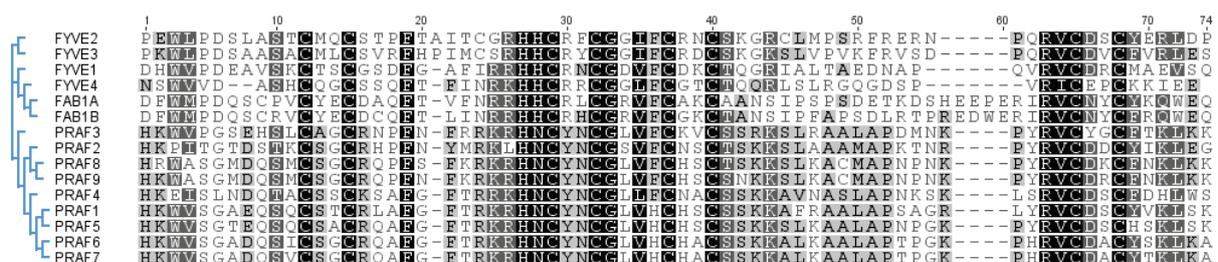
Figure 42. FYVE4, FAB1A and FAB1B are the closest homologs of FYVE1 in *Arabidopsis*.
Relationship of *Arabidopsis* FYVE proteins according to FYVE domain protein sequence. Alignment of the 15 FYVE domain proteins performed with the conserved FYVE domain only.

The relationship of FYVE domain proteins in *Arabidopsis* can also be seen in the phylogenetic tree (Figure 43). Proteins of *class I-IV* group together in one branch, the PRAF proteins (*class V*) form another branch. The FAB proteins (*class I*) are closely related to FYVE4 (*class III*). FYVE2 and FYVE3 are close homologs (*class II*).

The FYVE1 protein has orthologs in other plant species. The FYVE domain and coiled-coil region of FYVE1 are conserved among different plant species, as well as a big part of the amino acid sequence (200 aa; aa 238- 446) upstream of the FYVE domain, hinting at a conserved function of this part of the protein. The middle domain comprises a domain of unknown function or low confidence. In contrast, the N-terminal region (aa 1-237) of FYVE1 seems to be highly variable and of less importance, since it was even deleted in the *Vitis vinifera* protein.

The three characteristic motifs of FYVE domains are conserved across kingdoms. This is also true for the FYVE domain of *Arabidopsis* FYVE1. On the contrary, the highly variable, low complexity N-terminal part of FYVE1 does not seem to have any similar sequences in all but the plant kingdom. FYVE1 homologs in other species are only identified due to the FYVE domain. There are no homologs of high identity of FYVE1 in the human, mouse, drosophila or yeast proteomes. In the plant kingdom, chlorophytes also have no clear homolog to FYVE1. Only embryophytes seem to have evolved the variable, N-terminal protein sequence of the FYVE1 protein. This may hint to a unique function of the N-terminal part in plant development.
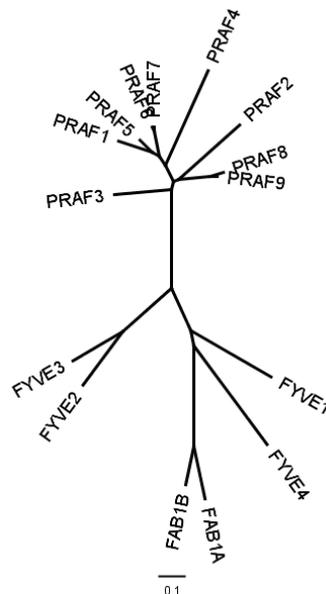
Figure 43. The FYVE domain of FYVE1 is closest related to FYVE4, FAB1A and FAB4B. Phylogenetic tree of all *Arabidopsis* FYVE proteins (FYVE domains only).

4.2.4 FYVE1 acts as an effector protein at late endosomes

The fusion protein sGFP-FYVE1 is mainly localized to the cytosol, to the nucleus (but not the nucleolus) and endosomal vesicles. These results were verified by the work of Barberon et al. (2014), who also showed cytosolic and nuclear localization signals of a FYVE1-mCitrine fusion protein. Both fusion constructs indicate, that N-terminal as well as C-terminal fusion constructs of FYVE1 are viable. They further point out, that the detected intracellular vesicles may be late endosomes in root tip cells and in differentiated root cells. This conclusion was confirmed by treatment of roots with the PI3-kinase inhibitor Wortmannin (Wm), which induced swelling of the FYVE1-positive vesicles, a characteristic of late endosomes. Additionally, FYVE1-mCitrine was colocalizing with the late endosome marker RabF2a and the artificial FYVE domain of HRS (2xFYVE$_{HRS}$), which is binding to PI(3)P and recruited to late endosomes. The colocalization study presented in this work, also showed an overlapping signal with the late endosome marker ARA7. The high frequency of colocalizing signals between the endocytosis marker protein clathrin (CLC) and sGFP-FYVE1 could represent a subpopulation of CLC-positive late endosomes (Ito et al., 2012). Clathrin is a TGN and EE marker protein, but it can also colocalize with the multivesicular endosomes (MVE) specific protein ARA6, marking a subset of late endosomes. This phenomenon was mostly observed in elongating root epidermal cells.

To further define the localization of FYVE1, colocalization of FYVE1 with other RAB GTPases of *Arabidopsis* would be an interesting topic for further experiments. ARA6 (RABF1) and Rab7-like GTPases (AtRABG3f) would be interesting candidates and are known MVB/LE, prevacuole and vacuole markers.

4.2.5 FYVE1 is an essential regulator of vacuolar protein transport

The function of FYVE1 in vacuolar protein transport is already essential in *Arabidopsis* seeds and embryo development. The mis-secretion of the vacuolar cargo protein GFP-CT24 showed that in the *fyve1-1* loss-of-function mutant proteins targeted to the protein storage vacuoles (PSVs) were accumulating in the extracellular space and proper targeting to the PSVs was impaired. Moreover, the PSVs in the *fyve1-1* mutant were of smaller size than in the wild-type embryos. These results were confirmed by the work of Gao and co-workers (Gao et al., 2015). Proteins that were destined to the vacuole for storage purposes were secreted by the default secretion pathway of the cell for proteins without proper targeting signals. This secretion phenotype was also shown for the vacuolar trafficking mutants *vsr1* and *mag1/vps29* (Fuji et al., 2007). This links the function of FYVE1 to the role of the major *Arabidopsis* vacuolar sorting receptor VSR1, which is involved in the vacuolar sorting of storage proteins into PSVs and LVs (Hinz et al., 1999; Shimada et al., 2003; Fuji et

al., 2007). It can be speculated, if FYVE1 plays the role of an essential vacuolar sorting receptor in *Arabidopsis*.

In conclusion, FYVE1 plays an essential role for vacuolar trafficking and PSV biogenesis of *Arabidopsis* maturing seeds and embryos. The vacuolar morphology defect of the *fyve1-1* mutant continued during seed germination until the last mutant seedling development stage and finally led to seedling lethality. Vacuole fusion is essential for proper plant growth and further development of the seedling. Smaller vacuolar structures of the *fyve1-1* mutant indicated that vacuolar membranes and vacuole-like vesicles were built, but could not fuse to a proper central vacuole. This suggests, that FYVE1 plays an important role in the formation of large central vacuoles in plant cells. It is yet unclear if these smaller vacuolar structures are pre-vacuoles and belong to the prevacuolar compartment (PVC) or can be categorized as a MVB-like structure.

By analyzing the localization of VESICLE ASSOCIATED MEMBRANE PROTEIN 711 (VAMP711) as a vacuolar membrane marker in the *free1/fyve1-1* mutant Gao et al. also confirmed the findings of this study of the vacuolar phenotype with a different tonoplast marker protein (Gao et al., 2015). VAMP711 marks the vacuolar membrane in cotyledon cells and in the root elongation zone in the wild-type. By analyzing the processing of the exemplary storage proteins 12S globulin and 2S albumin, Gao et al. could also show strong defects of storage protein processing and accumulation of precursors of storage proteins in the *free1/fyve1-1* mutant, indicating a crucial role of FREE1/FYVE1 in transport of proteins destined to the PSVs (Gao et al., 2015). Gao et al. also showed that not only the protein transport to the PSVs was impaired in the *fyve1-1* mutant, but also the transport of proteins to the lytic vacuole (LV). By using a LV-specific cargo protein, spL-RFP, which contains the signal peptide and the vacuolar sorting signal of proricin, it was shown that the cargo protein was secreted to the extracellular space (Gao et al., 2015).

This indicates that FYVE1 plays a general role in vacuolar transport in *Arabidopsis*, functioning *en route* to PSVs in early development as well as in transport to lytic vacuoles during later steps of development.

4.2.6 FYVE1 is necessary for endocytosis and recycling of plasma membrane proteins

The ARF-GEF specific drug Brefeldin A (BFA) blocks secretion, ER to Golgi trafficking, recycling of endocytic cargo proteins to the plasma membrane and transport to MVB/PVC, which leads to accumulation of proteins in the cytosol, in so called BFA compartments or bodies (Geldner et al., 2003). Since BFA affects several steps in endocytosis, the BFA phenotype is linked to general dysfunction of endocytosis and endomembrane trafficking.

BFA itself is not leading to a distinct vacuolar morphology and vacuole fragmentation as seen in the *amsh3*-like mutants. Instead, the vacuole is mirroring the general unhealthy status of the whole plant cell, due to multiple endocytosis defects. This indicates that BFA does not impair homotypic membrane fusion at concentrations to 50 µM. However, a BFA concentration of 100 µg/ml induces aggregation of PVCs in root tip cells of *Arabidopsis* (Tse et al., 2006).

By staining with the endocytosis tracer dye FM4-64 and simultaneous inhibition with BFA, it was shown that endocytosis in general was impaired in the *fyve1-1* mutant. In addition, the pathway of proteins destined to the vacuole was blocked in the *fyve1-1* mutant. There are also BFA-insensitive trafficking pathways described by which the membrane protein PIN2 and tonoplast proteins like TIPs are transported to the vacuole (Rivera-Serrano et al., 2012). It could be possible that by up-regulation of alternative trafficking routes, BFA body aggregation is avoided in the *fyve1-1* mutant.

If the uptake rate of FM4-64 is not altered in the *fyve1-1* mutant (like in the *amsh3* mutant), this would indicate a decreased trafficking rate of endocytic vesicles to BFA compartments. Otherwise the aggregation rate of vesicles could be inhibited, resulting in an increased number of smaller BFA compartments. This led to the conclusion that endocytosis was slower and fusion of endocytic vesicles might be impaired in the *fyve1-1* mutant.

Gao et al. showed in the *free1/fyve1-1* mutant that PIN2-GFP was localized to the plasma membrane, like in the wild-type (Gao et al., 2014). Treatment with the lipophilic endocytosis tracer dye FM4-64 showed that FM4-64 was correctly transported to the vacuolar membrane after 6 hours of incubation. In dark treatments, PIN2-GFP accumulates in the vacuole in the wild-type. In contrast to the wild-type, the *free1/fyve1-1* mutant did not show vacuole accumulation but instead the tonoplast was stained. This showed that in the *free1/fyve1-1* mutant, recycling of the plasma membrane protein PIN2 was impaired.

4.2.7 FYVE1 interactors have diverse functions in *Arabidopsis*

To fully understand the role of FYVE1 in the protein network of a cell, it is necessary to find interaction nodes with other key players in cellular pathways. To identify interaction partners of FYVE1 a yeast two-hybrid screening was conducted in our group. The FYVE domain was deleted in the used construct, since it was expected that its lipid-binding affinity might interfere with the yeast two-hybrid system. The ΔFYVE construct was used in the yeast two-hybrid screen against a library of ~ 8.000 DB (DNA-binding domain) pools (Arabidopsis Interactome Mapping, 2011) and new interaction partners were identified: the SRC Homology 3 (SH3) domain-containing proteins SH3P2 and SH3P3 (Kolb et al., 2015).

The SH3 domain is a well-known protein interaction domain and can be found in proteins playing a role in signaling pathways or protein regulation. There is also an interesting connection to the phospholipid signaling pathway as proteins like the PI3-kinase (PI3K) or phospholipases also contain a SH3 domain. In *Arabidopsis,* there are three homologs of the mammalian SH3-PROTEIN (SH3P) called SH3P1, SH3P2 and SH3P3 (Lam et al., 2001). Gao et al. also showed an interaction between FREE1/FYVE1 and SH3P2 in the yeast two-hybrid system (Gao et al., 2014), verifying our screen results.

SH3P2 is known to associate with the PI3K complex and interacts with the autophagosome marker protein ATG8, regulating the formation of autophagosomes. In the same study, FYVE1 did not interact with ATG8 directly (Gao et al., 2015). Gao et al. could identify in a direct yeast two-hybrid assay that the C-terminal coiled-coil region of FYVE1 was interacting directly with the BAR domain of SH3P2 (Gao et al., 2015). In theory, it would be also possible, that the SH3 domain is interacting with the proline rich region of FYVE1 (Lam et al., 2001). SH3P2 is also found on autophagosomal membranes, which may be the link between fusion of SH3P2 positive autophagosomes with the vacuole via interaction with FYVE1 as the phospholipid targeting partner.

Barberon et al. identified FYVE1 as an interactor of IRON-REGULATED TRANSPORTER 1 (IRT1) in *Arabidopsis* in a yeast two-hybrid screen (Barberon et al., 2014). IRT1 is the main root transporter of *Arabidopsis* and regulates iron-uptake from the soil. The IRT1 protein localizes to the EE/TGN and is constitutively endocytosed in a monoubiquitin- and clathrin-dependent manner. FYVE1 was shown to control IRT1 recycling to the plasma membrane and the polar delivery to the outer plasma membrane domain. Overexpression of FYVE1 led to iron-deficient plants, shorter roots, hypersensitivity to low iron conditions and reduced accumulation of iron. Upon FYVE1 overexpression, the IRT1 transporter is mis-routed from the EE/TGN toward the plasma membrane and accumulates at the plasma membrane in an apolar fashion.

This study showed that FYVE1 acts on the recycling of IRT1 from endosomal compartments back to the plasma membrane. General endocytosis was not affected upon overexpression of FYVE1, indicating that FYVE1 is targeting specific plasma membrane proteins for degradation or recycling. IRT1 recycling and polarisation is not clathrin dependent, not like the PIN proteins, and may therefore be an example for a subgroup of plasma membrane transporters. It would be interesting to investigate the impact of FYVE1 overexpression on PIN proteins and proteins that are clathrin dependent. Barberon et al. further concluded that FYVE1 dependent recycling of PM proteins may indicate a role for LE as a recycling compartment. This theory is further strengthened by the notion that vacuolar sorting receptors and retromer units are identified as being localized to LEs (Barberon et al., 2014).

Table 14. Interactors of *Arabidopsis* FYVE1**.**

Interactor	ATG number	Localization	Method	Reference
IRT1	AT4G19690	EE/TGN	yeast two-hybrid screen, IP	Barberon et al., 2014
VPS23A/ELC (ESCRT-I subunit)	AT3G12400	PVC/MVB	direct Y2H, Co-IP, Fret-AB	Gao et al., 2014
VPS23B/ELC-LIKE (ESCRT-I subunit)	AT5G13860	PVC/MVB	direct Y2H, Co-IP, Fret-AB	Gao et al., 2014
SH3 domain-containing protein (SH3P2)	AT4G34660	CCV	direct Y2H	Gao et al., 2014; Kolb et al., 2015
SH3 domain-containing protein (SH3P3)	AT4G18060	CCV	ΔFYVE yeast two-hybrid screen	Gao et al., 2014; Kolb et al., 2015

Gao et al. showed specific interaction of FREE1/FYVE1 with the ESCRT-I subunits VPS23A/ELC and VPS23B/ELC-LIKE (Gao et al., 2014). FYVE1 was neither interacting with the other two subunits of the ESCRT-I complex, VPS28 and VPS37, nor with any components of the ESCRT-II, ESCRT-III or VPS4/SKD1 complexes. FYVE1 is a specific ESCRT-I interaction partner and was shown to colocalize with both VPS23 proteins at PVC/MVBs. Domain analysis of this specific interaction partners showed, that the N-terminal proline-rich region of FYVE1 contained PTAP-like tetrapeptide motifs of VPS23 interaction partners. Additionally, Gao et al. showed in this publication via high-resolution gel filtration chromatography that FREE1/FYVE1 was incorporated in and in complex with the plant ESCRT-I machinery. These results implicate that FYVE1 is a unique plant-specific ESCRT component and essential for MVB formation.

4.2.8 FYVE1 is required for proper autophagic degradation

Since the ESCRT machinery is required for autophagy, it would be also possible that FYVE1/FREE1 has a supposed role in this pathway. Gao et al. analyzed the *free1/fyve1-1* mutant via TEM and found that the mutant accumulated autophagosomes, additionally to cells lacking a central vacuole. Gao et al. investigated this theory further and analyzed the localization of the autophagosome marker AUTOPHAGY-RELATED GENE/PROTEIN 8 (ATG8). The authors showed that in the *free1/fyve1-1* mutant ATG8-positive compartments were accumulating, whereas in the wild-type autophagosomes mainly obtained a cytosolic localization, and concluded that this was a result of defects in membrane fusion of endosomes or autophagosomes and vacuoles (Gao et al., 2015). Even though FYVE1 was not directly interacting with ATG8, Gao et al. showed direct interaction between FYVE1 and the autophagy-regulating protein SH3P2 (Gao et al., 2014).

SH3P2 associates with the PI3K complex and interacts directly with ATG8, thereby regulating the formation of autophagosomes. Via immunoprecipitation with ATG6 Gao et al. could show the interaction of ATG6 in complex with FYVE1 and SH3P2, thereby showing the

formation of a PI3K complex together with FYVE1. To prove this theory Gao et al. investigated the localization of the two marker proteins VACUOLAR SORTING RECEPTOR (VSR) and ATG8 and performed a VSR immunofluorescence labeling. In wild-type cells, autophagosomes accumulated in the vacuolar lumen, but in the *fyve1* mutant autophagosomes did not reach the vacuole. Proving that the fusion of MVBs to the vacuole was impaired without FYVE1. Via its interaction with SH3P2, FYVE1 is playing a role as a unique autophagy regulator.

The deubiquitinating enzyme AMSH1, a homolog of *Arabidopsis* AMSH3, was also shown to play a role in autophagy (Katsiarimpa et al., 2013). AMSH1 interacts with the ESCRT-III subunit VPS2.1. The *amsh1-1* mutant shows an autophagy related phenotype after five days of dark treatment, which involves early senescence and hypersensitivity to nutrient starvation. AMSH1 and the ESCRT-III subunit VPS2.1 are necessary for autophagic degradation.

4.2.9 FYVE1 is involved in membrane fusion

All evidence considered, FYVE1 acts as a regulator for membrane fusion events in a number of plant trafficking pathways.

In endocytosis and intracellular protein trafficking, FYVE1 is an important effector protein at late endosomes, where it interacts with SH3P2 and two subunits of the ESCRT-I complex (VPS23A and VPS23B), contributing to correct maturation of late endosomes and formation of MVBs. Ultimately, FYVE1 influences the transport of proteins destined to the vacuole via fusion of endosomal vesicles and vacuoles. In autophagy, FYVE1 may interact with SH3P2, leading to fusion of autophagosomes with MVBs or the vacuole.

FYVE1 is attracted to specific phospholipids at membranes and interacts with other proteins. Thereby, FYVE1 acts as a scaffolding protein for multiprotein complexes and plays a role in lipid signaling of plants.

Even though, open questions regarding FYVE1 remain: Do FYVE1 and AMSH3 interact directly? What other proteins interact with FYVE1? Which protein domains are important for protein-protein interaction? Why does FYVE1 localize to the nucleus? To find answers to these questions will be the subject of future research in this topic.
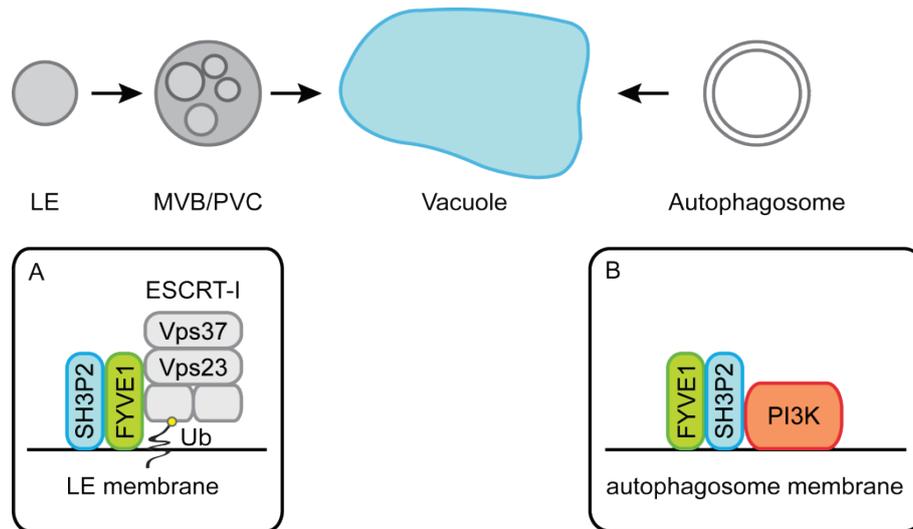
Figure 44. FYVE1 interacts with SH3P2 and ESCRT-I at late endosomes and with SH3P2 at autophagosomes.
(A) At late endosomes, FYVE1 was shown to interact with SH3P2 at the endosomal membrane. Additionally, FYVE1 can also interact with two subunits of the ESCRT-I complex, VPS23A and VPS23B (shown as Vps23). The ESCRT-I complex binds to an ubiquitinated cargo protein via its subunit Mvb12. **(B)** Autophagic material is transported to the vacuole by autophagosomes, which fuse with late endosomes or directly with the vacuole. At the autophagosomal membrane, FYVE1 is interacting with SH3P2. SH3P2 interacts with ATG proteins and the PI3K complex, which phosphorylates membrane phospholipids. LE: late endosome; MVB: multivesicular body; PVC: prevacuolar compartment; PI3K: phosphoinositol-3-kinase; Ub: Ubiquitin.

4.3 Conclusion

In this work, I isolated and characterized the *vfd1* mutant, identified the causative gene locus *FYVE1* and analyzed the FYVE1 protein. With this analysis, I brought the at that time uncharacterized protein in context to the endocytic membrane trafficking pathway and showed that FYVE1 is involved in endocytosis, vacuolar transport and endocytic degradation. Thereby, the two main objectives of this study - (1) to isolate a novel type of *vacuolar fusion defective* mutant and (2) to analyze the molecular function of the gene product of the causative gene - were achieved.

The overall purpose of this work was to utilize a forward genetic mutant screen to identify new factors in the AMSH3-related pathways in the model organism *Arabidopsis thaliana* and to characterize the mutants according to defects in vacuole fusion and intracellular trafficking.

I identified, established and characterized the *vacuolar fusion defective* (*vfd*) *1* mutant that showed the same seedling and vacuole phenotype as the previously described *amsh3* mutant. The *vfd1* was also affected in degradation of ubiquitinated proteins, even though AMSH protein levels were not subject to change. The characterization of *vfd1* showed that the *amsh3*-like phenotype is generated not only by mutations in the *AMSH3* gene locus. This indicates, that the *amsh3*-like phenotype is a general phenotype of vacuole fusion and intracellular trafficking defects. The *vfd* mutant lines may include interesting and yet undescribed genes relevant for vacuole biogenesis and endocytosis and further characterization of the *VFD* genes will help our understanding of the molecular players involved in both processes. Moreover, the *vfd* mutant lines could include unknown AMSH interacting factors.

The characterization of the *vfd1* mutant led to the discovery of the FYVE domain-containing protein FYVE1, a novel factor in plant vacuole biogenesis. I analyzed two knockout mutants of the *FYVE1* gene, *fyve1-1* and *vfd1*/*fyve1-2*, which showed the *vfd* specific and *amsh3*-like phenotypes. The lipid-binding protein FYVE1 is involved in vacuole fusion and endocytosis, and is ultimately essential for plant development. The localization of the fusion protein sGFP-FYVE1 showed that FYVE1 localized to late endosomes (MVB/PVC). This links the function of FYVE1 with the endocytosis related ESCRT-machinery and AMSH3, which are also localized to this endosomal compartment. FYVE1 is also involved in the biosynthetic pathway of *de novo* synthesized proteins targeted to the vacuole.

Taken together, FYVE1 is an important effector protein in the molecular network of intracellular trafficking. FYVE1 interacts with other proteins, binds to specific phospholipids at endosomal organelles and by this, FYVE1 leads other proteins to their membrane destination. This work delivers new insights into the interplay between endocytosis, the regulation of vacuole morphology and lipid signaling in plants by describing FYVE1 as an essential protein.

5. References

Abas, L., R. Benjamins, N. Malenica, T. Paciorek, J. Wisniewska, J. C. Moulinier-Anzola, T. Sieberer, J. Friml and C. Luschnig (2006). Intracellular trafficking and proteolysis of the Arabidopsis auxin-efflux facilitator PIN2 are involved in root gravitropism. Nat Cell Biol **8** (3): 249-256.

Agee, A. E., M. Surpin, E. J. Sohn, T. Girke, A. Rosado, B. W. Kram, C. Carter, A. M. Wentzell, D. J. Kliebenstein, H. C. Jin, O. K. Park, H. Jin, G. R. Hicks and N. V. Raikhel (2010). MODIFIED VACUOLE PHENOTYPE1 is an Arabidopsis myrosinase-associated protein involved in endomembrane protein trafficking. Plant Physiol **152** (1): 120-132.

Ahmed, S. U., M. Bar-Peled and N. V. Raikhel (1997). Cloning and subcellular location of an Arabidopsis receptor-like protein that shares common features with protein-sorting receptors of eukaryotic cells. Plant Physiol **114** (1): 325-336.

Arabidopsis Interactome Mapping, C. (2011). Evidence for Network Evolution in an Arabidopsis Interactome Map. Science (New York, N.Y.) **333** (6042): 601-607.

Aubert, S., E. Gout, R. Bligny, D. Marty-Mazars, F. Barrieu, J. Alabouvette, F. Marty and R. Douce (1996). Ultrastructural and biochemical characterization of autophagy in higher plant cells subjected to carbon deprivation: control by the supply of mitochondria with respiratory substrates. J Cell Biol **133** (6): 1251-1263.

Avila, E. L., J. Zouhar, A. E. Agee, D. G. Carter, S. N. Chary and N. V. Raikhel (2003). Tools to study plant organelle biogenesis. Point mutation lines with disrupted vacuoles and high-speed confocal screening of green fluorescent protein-tagged organelles. Plant Physiol **133** (4): 1673-1676.

Barberon, M., G. Dubeaux, C. Kolb, E. Isono, E. Zelazny and G. Vert (2014). Polarization of IRON-REGULATED TRANSPORTER 1 (IRT1) to the plant-soil interface plays crucial role in metal homeostasis. Proc Natl Acad Sci U S A **111** (22): 8293-8298.

Battey, N. H., N. C. James, A. J. Greenland and C. Brownlee (1999). Exocytosis and endocytosis. Plant Cell **11** (4): 643-660.

Becker, B. (2007). Function and evolution of the vacuolar compartment in green algae and land plants (Viridiplantae). Int Rev Cytol **264** 1-24.

Bethke, P. C. and R. L. Jones (2000). Vacuoles and prevacuolar compartments. Curr Opin Plant Biol **3** (6): 469-475.

Bolte, S., C. Talbot, Y. Boutte, O. Catrice, N. D. Read and B. Satiat-Jeunemaitre (2004). FM-dyes as experimental probes for dissecting vesicle trafficking in living plant cells. J Microsc **214** (Pt 2): 159-173.

Bowers, K. and T. H. Stevens (2005). Protein transport from the late Golgi to the vacuole in the yeast Saccharomyces cerevisiae. Biochim Biophys Acta **1744** (3): 438-454.

Bradford, M. M. (1976). A rapid and sensitive method for the quantitation of microgram quantities of protein utilizing the principle of protein-dye binding. Anal Biochem **72** 248-254.

Chen, X., N. G. Irani and J. Friml (2011). Clathrin-mediated endocytosis: the gateway into plant cells. Curr Opin Plant Biol **14** (6): 674-682.

Clough, S. J. and A. F. Bent (1998). Floral dip: a simplified method for Agrobacterium-mediated transformation of Arabidopsis thaliana. Plant J **16** (6): 735-743.

Cutler, S. R., D. W. Ehrhardt, J. S. Griffitts and C. R. Somerville (2000). Random GFP::cDNA fusions enable visualization of subcellular structures in cells of Arabidopsis at a high frequency. Proc Natl Acad Sci U S A **97** (7): 3718-3723.

Debeaujon, I. and M. Koornneef (2000). Gibberellin requirement for Arabidopsis seed germination is determined both by testa characteristics and embryonic abscisic acid. Plant Physiol **122** (2): 415-424.

Dhonukshe, P., F. Aniento, I. Hwang, D. G. Robinson, J. Mravec, Y. D. Stierhof and J. Friml (2007). Clathrin-mediated constitutive endocytosis of PIN auxin efflux carriers in Arabidopsis. Curr Biol **17** (6): 520-527.

Dove, S. K., K. Dong, T. Kobayashi, F. K. Williams and R. H. Michell (2009). Phosphatidylinositol 3,5-bisphosphate and Fab1p/PIKfyve underPPIn endo-lysosome function. Biochem J **419** (1): 1-13.

Dumas, J. J., E. Merithew, E. Sudharshan, D. Rajamani, S. Hayes, D. Lawe, S. Corvera and D. G. Lambright (2001). Multivalent endosome targeting by homodimeric EEA1. Mol Cell **8** (5): 947-958.

Ebine, K., Y. Okatani, T. Uemura, T. Goh, K. Shoda, M. Niihama, M. T. Morita, C. Spitzer, M. S. Otegui, A. Nakano and T. Ueda (2008). A SNARE complex unique to seed plants is required for protein storage vacuole biogenesis and seed development of Arabidopsis thaliana. Plant Cell **20** (11): 3006-3021.

Efe, J. A., R. J. Botelho and S. D. Emr (2005). The Fab1 phosphatidylinositol kinase pathway in the regulation of vacuole morphology. Curr Opin Cell Biol **17** (4): 402-408.

Fuji, K., T. Shimada, H. Takahashi, K. Tamura, Y. Koumoto, S. Utsumi, K. Nishizawa, N. Maruyama and I. Hara-Nishimura (2007). Arabidopsis vacuolar sorting mutants (green fluorescent seed) can be identified efficiently by secretion of vacuole-targeted green fluorescent protein in their seeds. Plant Cell **19** (2): 597-609.

Gao, C., M. Luo, Q. Zhao, R. Yang, Y. Cui, Y. Zeng, J. Xia and L. Jiang (2014). A unique plant ESCRT component, FREE1, regulates multivesicular body protein sorting and plant growth. Curr Biol **24** (21): 2556-2563.

Gao, C., X. Zhuang, Y. Cui, X. Fu, Y. He, Q. Zhao, Y. Zeng, J. Shen, M. Luo and L. Jiang (2015). Dual roles of an Arabidopsis ESCRT component FREE1 in regulating vacuolar protein transport and autophagic degradation. Proc Natl Acad Sci U S A **112** (6): 1886-1891.

Gao, X. Q., C. G. Li, P. C. Wei, X. Y. Zhang, J. Chen and X. C. Wang (2005). The dynamic changes of tonoplasts in guard cells are important for stomatal movement in Vicia faba. Plant Physiol **139** (3): 1207-1216.

Gattolin, S., M. Sorieul and L. Frigerio (2010). Tonoplast intrinsic proteins and vacuolar identity. Biochem Soc Trans **38** (3): 769-773.

Gaullier, J. M., A. Simonsen, A. D'Arrigo, B. Bremnes, H. Stenmark and R. Aasland (1998). FYVE fingers bind PtdIns(3)P. Nature **394** (6692): 432-433.

Geldner, N., N. Anders, H. Wolters, J. Keicher, W. Kornberger, P. Muller, A. Delbarre, T. Ueda, A. Nakano and G. Jurgens (2003). The Arabidopsis GNOM ARF-GEF mediates endosomal recycling, auxin transport, and auxin-dependent plant growth. Cell **112** (2): 219-230.

Grefen, C., N. Donald, K. Hashimoto, J. Kudla, K. Schumacher and M. R. Blatt (2010). A ubiquitin-10 promoter-based vector set for fluorescent protein tagging facilitates temporal stability and native protein distribution in transient and stable expression studies. Plant J **64** (2): 355-365.

Hara-Nishimura, I., T. Shimada, K. Hatano, Y. Takeuchi and M. Nishimura (1998). Transport of storage proteins to protein storage vacuoles is mediated by large precursor-accumulating vesicles. Plant Cell **10** (5): 825-836.

Hartley, J. L., G. F. Temple and M. A. Brasch (2000). DNA cloning using in vitro site-specific recombination. Genome Res **10** (11): 1788-1795.

Hayakawa, A. and N. Kitamura (2000). Early endosomal localization of hrs requires a sequence within the proline- and glutamine-rich region but not the FYVE finger. J Biol Chem **275** (38): 29636-29642.

Herman, E. M. and B. A. Larkins (1999). Protein storage bodies and vacuoles. Plant Cell **11** (4): 601-614.

Herman, P. K. and S. D. Emr (1990). Characterization of VPS34, a gene required for vacuolar protein sorting and vacuole segregation in Saccharomyces cerevisiae. Mol Cell Biol **10** (12): 6742-6754.

Hershko, A. and A. Ciechanover (1992). The ubiquitin system for protein degradation. Annu Rev Biochem **61** 761-807.

Hinz, G., S. Hillmer, M. Baumer and I. I. Hohl (1999). Vacuolar storage proteins and the putative vacuolar sorting receptor BP-80 exit the golgi apparatus of developing pea cotyledons in different transport vesicles. Plant Cell **11** (8): 1509-1524.

Hirano, T., T. Matsuzawa, K. Takegawa and M. H. Sato (2011). Loss-of-function and gain-of-function mutations in FAB1A/B impair endomembrane homeostasis, conferring pleiotropic developmental abnormalities in Arabidopsis. Plant Physiol **155** (2): 797-807.

Isono, E., A. Katsiarimpa, I. K. Muller, F. Anzenberger, Y. D. Stierhof, N. Geldner, J. Chory and C. Schwechheimer (2010). The deubiquitinating enzyme AMSH3 is required for intracellular trafficking and vacuole biogenesis in Arabidopsis thaliana. Plant Cell **22** (6): 1826-1837.

Ito, E., M. Fujimoto, K. Ebine, T. Uemura, T. Ueda and A. Nakano (2012). Dynamic behavior of clathrin in Arabidopsis thaliana unveiled by live imaging. Plant J **69** (2): 204-216.

Iwaki, T., M. Onishi, M. Ikeuchi, A. Kita, R. Sugiura, Y. Giga-Hama, Y. Fukui and K. Takegawa (2007). Essential roles of class E Vps proteins for sorting into multivesicular bodies in Schizosaccharomyces pombe. Microbiology **153** (Pt 8): 2753-2764.

Jauh, G. Y., T. E. Phillips and J. C. Rogers (1999). Tonoplast intrinsic protein isoforms as markers for vacuolar functions. Plant Cell **11** (10): 1867-1882.

Kalinowska, K., M. K. Nagel, K. Goodman, L. Cuyas, F. Anzenberger, A. Alkofer, J. Paz-Ares, P. Braun, V. Rubio, M. S. Otegui and E. Isono (2015). Arabidopsis ALIX is required for the endosomal localization of the deubiquitinating enzyme AMSH3. Proc Natl Acad Sci U S A **112** (40): E5543-5551.

Karasawa, S., T. Araki, T. Nagai, H. Mizuno and A. Miyawaki (2004). Cyan-emitting and orange-emitting fluorescent proteins as a donor/acceptor pair for fluorescence resonance energy transfer. Biochem J **381** (Pt 1): 307-312.

Kato, T., M. T. Morita, H. Fukaki, Y. Yamauchi, M. Uehara, M. Niihama and M. Tasaka (2002). SGR2, a phospholipase-like protein, and ZIG/SGR4, a SNARE, are involved in the shoot gravitropism of Arabidopsis. Plant Cell **14** (1): 33-46.

Katsiarimpa, A., F. Anzenberger, N. Schlager, S. Neubert, M. T. Hauser, C. Schwechheimer and E. Isono (2011). The Arabidopsis deubiquitinating enzyme AMSH3 interacts with ESCRT-III subunits and regulates their localization. Plant Cell **23** (8): 3026-3040.

Katsiarimpa, A., K. Kalinowska, F. Anzenberger, C. Weis, M. Ostertag, C. Tsutsumi, C. Schwechheimer, F. Brunner, R. Huckelhoven and E. Isono (2013). The deubiquitinating enzyme AMSH1 and the ESCRT-III subunit VPS2.1 are required for autophagic degradation in Arabidopsis. Plant Cell **25** (6): 2236-2252.

Katsiarimpa, A., A. Munoz, K. Kalinowska, T. Uemura, E. Rojo and E. Isono (2014). The ESCRT-III-interacting deubiquitinating enzyme AMSH3 is essential for degradation of ubiquitinated membrane proteins in Arabidopsis thaliana. Plant Cell Physiol **55** (4): 727-736.

Kirsch, T., N. Paris, J. M. Butler, L. Beevers and J. C. Rogers (1994). Purification and initial characterization of a potential plant vacuolar targeting receptor. Proc Natl Acad Sci U S A **91** (8): 3403-3407.

Kliebenstein, D. J., J. E. Lim, L. G. Landry and R. L. Last (2002). Arabidopsis UVR8 regulates ultraviolet-B signal transduction and tolerance and contains sequence similarity to human regulator of chromatin condensation 1. Plant Physiol **130** (1): 234-243.

Klionsky, D. J., P. K. Herman and S. D. Emr (1990). The fungal vacuole: composition, function, and biogenesis. Microbiol Rev **54** (3): 266-292.

Kolb, C., M. K. Nagel, K. Kalinowska, J. Hagmann, M. Ichikawa, F. Anzenberger, A. Alkofer, M. H. Sato, P. Braun and E. Isono (2015). FYVE1 is essential for vacuole biogenesis and intracellular trafficking in Arabidopsis. Plant Physiol **167** (4): 1361-1373.

Koncz, C. and J. Schell (1986). The promoter of T_L-DNA gene 5 controls the tissue-specific expression of chimaeric genes carried by a novel type of *Agrobacterium* binary vector. Molecular and General Genetics MGG **204** (3): 383-396.

Koornneef, M., L. Bentsink and H. Hilhorst (2002). Seed dormancy and germination. Curr Opin Plant Biol **5** (1): 33-36.

Laemmli, U. K. (1970). Cleavage of structural proteins during the assembly of the head of bacteriophage T4. Nature **227** (5259): 680-685.

Lam, B. C., T. L. Sage, F. Bianchi and E. Blumwald (2001). Role of SH3 domain-containing proteins in clathrin-mediated vesicle trafficking in Arabidopsis. Plant Cell **13** (11): 2499-2512.

Laxmi, A., J. Pan, M. Morsy and R. Chen (2008). Light plays an essential role in intracellular distribution of auxin efflux carrier PIN2 in Arabidopsis thaliana. PLoS One **3** (1): e1510.

Lee, Y., E. S. Kim, Y. Choi, I. Hwang, C. J. Staiger, Y. Y. Chung and Y. Lee (2008). The Arabidopsis phosphatidylinositol 3-kinase is important for pollen development. Plant Physiol **147** (4): 1886-1897.

Leitner, J., J. Petrasek, K. Tomanov, K. Retzer, M. Parezova, B. Korbei, A. Bachmair, E. Zazimalova and C. Luschnig (2012). Lysine63-linked ubiquitylation of PIN2 auxin carrier protein governs hormonally controlled adaptation of Arabidopsis root growth. Proc Natl Acad Sci U S A **109** (21): 8322-8327.

Martinoia, E., S. Meyer, A. De Angeli and R. Nagy (2012). Vacuolar transporters in their physiological context. Annu Rev Plant Biol **63** 183-213.

Marty, F. (1999). Plant vacuoles. Plant Cell **11** (4): 587-600.

Meijer, H. J., C. P. Berrie, C. Iurisci, N. Divecha, A. Musgrave and T. Munnik (2001). Identification of a new polyphosphoinositide in plants, phosphatidylinositol 5-monophosphate (PtdIns5P), and its accumulation upon osmotic stress. Biochem J **360** (Pt 2): 491-498.

Meijer, H. J., N. Divecha, H. van den Ende, A. Musgrave and T. Munnik (1999). Hyperosmotic stress induces rapid synthesis of phosphatidyl-D-inositol 3, 5-bisphosphate in plant cells. Planta **208** (2): 294-298.

Meijer, H. J. and T. Munnik (2003). Phospholipid-based signaling in plants. Annu Rev Plant Biol **54** 265-306.

Misra, S. and J. H. Hurley (1999). Crystal structure of a phosphatidylinositol 3-phosphate-specific membrane-targeting motif, the FYVE domain of Vps27p. Cell **97** (5): 657-666.

Morita, M. T., T. Kato, K. Nagafusa, C. Saito, T. Ueda, A. Nakano and M. Tasaka (2002). Involvement of the vacuoles of the endodermis in the early process of shoot gravitropism in Arabidopsis. Plant Cell **14** (1): 47-56.

Moriyasu, Y. and Y. Ohsumi (1996). Autophagy in Tobacco Suspension-Cultured Cells in Response to Sucrose Starvation. Plant Physiol **111** (4): 1233-1241.

Munnik, T. and E. Nielsen (2011). Green light for polyphosphoinositide signals in plants. Curr Opin Plant Biol **14** (5): 489-497.

Munnik, T. and C. Testerink (2009). Plant phospholipid signaling: "in a nutshell". J Lipid Res **50 Suppl** S260-265.

Munnik, T. and J. E. Vermeer (2010). Osmotic stress-induced phosphoinositide and inositol phosphate signalling in plants. Plant Cell Environ **33** (4): 655-669.

Nakagawa, T., T. Kurose, T. Hino, K. Tanaka, M. Kawamukai, Y. Niwa, K. Toyooka, K. Matsuoka, T. Jinbo and T. Kimura (2007). Development of series of gateway binary vectors, pGWBs, for realizing efficient construction of fusion genes for plant transformation. J Biosci Bioeng **104** (1): 34-41.

Nebenführ, A., C. Ritzenthaler and D. G. Robinson (2002). Brefeldin A: deciphering an enigmatic inhibitor of secretion. Plant Physiol **130** (3): 1102-1108.

Nishimura, T., N. Matano, T. Morishima, C. Kakinuma, K. Hayashi, T. Komano, M. Kubo, M. Hasebe, H. Kasahara, Y. Kamiya and T. Koshiba (2012). Identification of IAA transport inhibitors including compounds affecting cellular PIN trafficking by two chemical screening approaches using maize coleoptile systems. Plant Cell Physiol **53** (10): 1671-1682.

Nishizawa, K., N. Maruyama, R. Satoh, Y. Fuchikami, T. Higasa and S. Utsumi (2003). A C-terminal sequence of soybean beta-conglycinin alpha' subunit acts as a vacuolar sorting determinant in seed cells. Plant J **34** (5): 647-659.

Oude Weernink, P. A., M. López de Jesús and M. Schmidt (2007). Phospholipase D signaling: orchestration by PIP(2) and small GTPases. Naunyn-Schmiedeberg's Archives of Pharmacology **374** 399-411.

Piper, R. C., A. A. Cooper, H. Yang and T. H. Stevens (1995). VPS27 controls vacuolar and endocytic traffic through a prevacuolar compartment in Saccharomyces cerevisiae. J Cell Biol **131** (3): 603-617.

Rivera-Serrano, E. E., M. F. Rodriguez-Welsh, G. R. Hicks and M. Rojas-Pierce (2012). A small molecule inhibitor partitions two distinct pathways for trafficking of tonoplast intrinsic proteins in Arabidopsis. PLoS One **7** (9): e44735.

Robinson, D. G. and G. Hinz (1997). Vacuole biogenesis and protein transport to the plant vacuole: A comparison with the yeast and the mammalian lysosome. Protoplasma **197** 1-25.

Robinson, D. G., G. Hinz and S. E. Holstein (1998). The molecular characterization of transport vesicles. Plant Mol Biol **38** (1-2): 49-76.

Rojo, E., C. S. Gillmor, V. Kovaleva, C. R. Somerville and N. V. Raikhel (2001). VACUOLELESS1 is an essential gene required for vacuole formation and morphogenesis in Arabidopsis. Dev Cell **1** (2): 303-310.

Sanderfoot, A. A. and N. V. Raikhel (1999). The specificity of vesicle trafficking: coat proteins and SNAREs. Plant Cell **11** (4): 629-642.

Sanmartin, M., A. Ordonez, E. J. Sohn, S. Robert, J. J. Sanchez-Serrano, M. A. Surpin, N. V. Raikhel and E. Rojo (2007). Divergent functions of VTI12 and VTI11 in trafficking to storage and lytic vacuoles in Arabidopsis. Proc Natl Acad Sci U S A **104** (9): 3645-3650.

Schneeberger, K., S. Ossowski, C. Lanz, T. Juul, A. H. Petersen, K. L. Nielsen, J. E. Jorgensen, D. Weigel and S. U. Andersen (2009). SHOREmap: simultaneous mapping and mutation identification by deep sequencing. Nat Methods **6** (8): 550-551.

Schnell, J. D. and L. Hicke (2003). Non-traditional functions of ubiquitin and ubiquitin-binding proteins. J Biol Chem **278** (38): 35857-35860.

Schulz-Vogt, H. N. (2006). Vacuoles. Inclusions in Prokaryotes. J. M. Shively, Springer. **1**.

Shahriari, M., C. Keshavaiah, D. Scheuring, A. Sabovljevic, P. Pimpl, R. E. Hausler, M. Hulskamp and S. Schellmann (2010). The AAA-type ATPase AtSKD1 contributes to vacuolar maintenance of Arabidopsis thaliana. Plant J **64** (1): 71-85.

Shimada, T., K. Fuji, K. Tamura, M. Kondo, M. Nishimura and I. Hara-Nishimura (2003). Vacuolar sorting receptor for seed storage proteins in Arabidopsis thaliana. Proc Natl Acad Sci U S A **100** (26): 16095-16100.

Shimada, T., Y. Koumoto, L. Li, M. Yamazaki, M. Kondo, M. Nishimura and I. Hara-Nishimura (2006). AtVPS29, a putative component of a retromer complex, is required for the efficient sorting of seed storage proteins. Plant Cell Physiol **47** (9): 1187-1194.

Simonsen, A., R. Lippe, S. Christoforidis, J. M. Gaullier, A. Brech, J. Callaghan, B. H. Toh, C. Murphy, M. Zerial and H. Stenmark (1998). EEA1 links PI(3)K function to Rab5 regulation of endosome fusion. Nature **394** (6692): 494-498.

Singer, S. J. and G. L. Nicolson (1972). The fluid mosaic model of the structure of cell membranes. Science **175** (4023): 720-731.

Spitzer, C., F. C. Reyes, R. Buono, M. K. Sliwinski, T. J. Haas and M. S. Otegui (2009). The ESCRT-related CHMP1A and B proteins mediate multivesicular body sorting of auxin carriers in Arabidopsis and are required for plant development. Plant Cell **21** (3): 749-766.

Stenmark, H. and R. Aasland (1999). FYVE-finger proteins--effectors of an inositol lipid. J Cell Sci **112 (Pt 23)** 4175-4183.

Stenmark, H., R. Aasland, B. H. Toh and A. D'Arrigo (1996). Endosomal localization of the autoantigen EEA1 is mediated by a zinc-binding FYVE finger. J Biol Chem **271** (39): 24048-24054.

Surpin, M., H. Zheng, M. T. Morita, C. Saito, E. Avila, J. J. Blakeslee, A. Bandyopadhyay, V. Kovaleva, D. Carter, A. Murphy, M. Tasaka and N. Raikhel (2003). The VTI family of SNARE proteins is necessary for plant viability and mediates different protein transport pathways. Plant Cell **15** (12): 2885-2899.

Tan, X., L. I. Calderon-Villalobos, M. Sharon, C. Zheng, C. V. Robinson, M. Estelle and N. Zheng (2007). Mechanism of auxin perception by the TIR1 ubiquitin ligase. Nature **446** (7136): 640-645.

Tse, Y. C., S. W. Lo, S. Hillmer, P. Dupree and L. Jiang (2006). Dynamic response of prevacuolar compartments to brefeldin a in plant cells. Plant Physiol **142** (4): 1442-1459.

Ueda, T., T. Uemura, M. H. Sato and A. Nakano (2004). Functional differentiation of endosomes in Arabidopsis cells. Plant J **40** (5): 783-789.

Ueda, T., M. Yamaguchi, H. Uchimiya and A. Nakano (2001). Ara6, a plant-unique novel type Rab GTPase, functions in the endocytic pathway of Arabidopsis thaliana. EMBO J **20** (17): 4730-4741.

Uemura, T., H. Kim, C. Saito, K. Ebine, T. Ueda, P. Schulze-Lefert and A. Nakano (2012). Qa-SNAREs localized to the trans-Golgi network regulate multiple transport pathways and extracellular disease resistance in plants. Proc Natl Acad Sci U S A **109** (5): 1784-1789.

Uemura, T., T. Ueda, R. L. Ohniwa, A. Nakano, K. Takeyasu and M. H. Sato (2004). Systematic analysis of SNARE molecules in Arabidopsis: dissection of the post-Golgi network in plant cells. Cell Struct Funct **29** (2): 49-65.

van Leeuwen, W., L. Okresz, L. Bogre and T. Munnik (2004). Learning the lipid language of plant signalling. Trends Plant Sci **9** (8): 378-384.

van Leeuwen, W., J. E. Vermeer, T. W. Gadella, Jr. and T. Munnik (2007). Visualization of phosphatidylinositol 4,5-bisphosphate in the plasma membrane of suspension-cultured tobacco BY-2 cells and whole Arabidopsis seedlings. Plant J **52** (6): 1014-1026.

Vernoud, V., A. C. Horton, Z. Yang and E. Nielsen (2003). Analysis of the small GTPase gene superfamily of Arabidopsis. Plant Physiol **131** (3): 1191-1208.

Walsby, A. E. and B. W. Nichols (1969). Lipid composition of heterocysts. Nature **221** (5181): 673-674.

Weigel, D. and J. Glazebrook (2002). Arabidopsis: A Laboratory Manual. Cold Spring Harbor, New York, Cold Spring Harbor Laboratory Press.

Weisman, L. S. and W. Wickner (1992). Molecular characterization of VAC1, a gene required for vacuole inheritance and vacuole protein sorting. J Biol Chem **267** (1): 618-623.

Whitley, P., S. Hinz and J. Doughty (2009). Arabidopsis FAB1/PIKfyve proteins are essential for development of viable pollen. Plant Physiol **151** (4): 1812-1822.

Winter, V. and M. T. Hauser (2006). Exploring the ESCRTing machinery in eukaryotes. Trends Plant Sci **11** (3): 115-123.

Wywial, E. and S. M. Singh (2010). Identification and structural characterization of FYVE domain-containing proteins of Arabidopsis thaliana. BMC Plant Biol **10** 157.

Yamamoto, A., D. B. DeWald, I. V. Boronenkov, R. A. Anderson, S. D. Emr and D. Koshland (1995). Novel PI(4)P 5-kinase homologue, Fab1p, essential for normal vacuole function and morphology in yeast. Mol Biol Cell **6** (5): 525-539.

Yamazaki, M., T. Shimada, H. Takahashi, K. Tamura, M. Kondo, M. Nishimura and I. Hara-Nishimura (2008). Arabidopsis VPS35, a retromer component, is required for vacuolar protein sorting and involved in plant growth and leaf senescence. Plant Cell Physiol **49** (2): 142-156.

Zhang, C., G. R. Hicks and N. V. Raikhel (2014). Plant vacuole morphology and vacuolar trafficking. Front Plant Sci **5** 476.

Zheng, H., G. F. von Mollard, V. Kovaleva, T. H. Stevens and N. V. Raikhel (1999). The plant vesicle-associated SNARE AtVTI1a likely mediates vesicle transport from the trans-Golgi network to the prevacuolar compartment. Mol Biol Cell **10** (7): 2251-2264.

Zouhar, J., E. Rojo and D. C. Bassham (2009). AtVPS45 is a positive regulator of the SYP41/SYP61/VTI12 SNARE complex involved in trafficking of vacuolar cargo. Plant Physiol **149** (4): 1668-1678.

Acknowledgments

I would like to recognize my PhD supervisor, PD Dr. Erika Isono, for giving me the opportunity to join her research group for this challenging project. I appreciate her work teaching me all new techniques and guiding the project into the right direction.

I would like to thank Prof. Dr. Claus Schwechheimer for being my thesis supervisor, scientific advice and for his general support of the lab.

I would like to acknowledge my thesis committee members Prof. Dr. Brigitte Poppenberger and Prof. Dr. Ralph Hückelhoven.

Furthermore I convey my gratitude to the Deutsche Forschungsgemeinschaft (DFG) for funding my thesis project and the Sonderforschungsbereich SFB 924. The students' initiative was the best opportunity to organize and live science with other young researchers. I would not miss these three years of networking and science community experience. Altogether, the SFB924 made my PhD so much more fun and memorable.

I would like to thank Petra Wick and Rita Kaindl for their kindness and support in organizational matters.

I would like to express my gratitude to my lab colleagues Anthi Katsiarimpa, Maike Nagel, Kamila Kalinowska and Franziska Anzenberger for their help in all matters of PhD time. I would like to say thank you to our lab students Tina and Teresa for helping in the daily lab routine.

I would like to thank Inês Barbosa, Benjamin Weller and Alexander Steiner for their helpful advice and scientific discussions about PINs, membrane proteins and confocal microscopy.

My thanks to Dr. Melina Zourelidou for her helpful advice and sharing material (seeds, PIN vectors and bacterial stocks).

Many thanks also to Dr. Balaji Enugutti and PD Dr. Farhah Assaad for helping to set-up the molecular mapping of the *fyve1-1* mutant and to Dr. Pascal Falter-Braun and Angela Alkofer for help with the yeast two-hybrid system.

I would like to thank all the past and present lab members of the Schwechheimer lab for the great time: especially Emmanouil Bastakis, Ulrich Lutz, Quirin Ranftl, Ourania Lantzouni, René Richter, Dr. Eri Ogiso-Tanaka and Dr. Hiromasa Shikata.

A big hug goes to all the members of the Botany Allstars of the Grill and Hückelhoven labs.

I am grateful to my parents that they are backing me all the way in my academical career. For giving me courage and bliss, for his continuing support and love, I would like to thank Florian.

Ingolstadt, 28.02.2017

Appendix

Table 15. Chemicals used in this study.

Name	Supplier
2-/β-Mercaptoethanol	Roth, Karlsruhe
2,4-Dichlorophenoxyacetic acid (2,4-D)	Sigma-Aldrich, Munich
5-Bromo-4-chloro-3-indolyl phosphate (BCIP)	Applichem, Darmstadt
6-BA (6-Benzylaminopurine)	Duchefa, Haarlem, The Netherlands
Acetic acid	Roth, Karlsruhe
Acrylamid Rotiphorese Gel 30 (37, 5:1)	Roth, Karlsruhe
Agar, bacteriological	Applichem, Darmstadt
Agarose	Peqlab Biotechnologie, Erlangen
Ammonium nitrate (NH_4NO_3)	Applichem, Darmstadt
Ammonium peroxydisulfate (APS)	Roth, Karlsruhe
Ammonium sulfate ($N_2H_8SO_4$)	Applichem, Darmstadt
Ampicillin (Amp)	Roth, Karlsruhe
Basta	Bayer, Dormagen
Brefeldin A (BFA)	Sigma-Aldrich, Munich
Bromophenol blue	Roth, Karlsruhe
Boric Acid (H_3BO_3)	Roth, Karlsruhe
Bovine serum albumin (BSA)	Roth, Karlsruhe
Calcium chloride ($CaCl_2$)	Applichem, Darmstadt
Calcium chloride dihydrate ($CaCl_2 \cdot 2H_2O$)	Roth, Karlsruhe
Calcium hydrogen phosphate dihydrate ($CaHPO_4 \cdot 2H_2O$)	Roth, Karlsruhe
Calcium hypochlorite ($Ca(ClO)_2$)	Roth, Karlsruhe
Carbenicillin (Carb)	Duchefa, Haarlem, The Netherlands
Chloramphenicol	Roth, Karlsruhe
Chloroform	Roth, Karlsruhe
Cobalt(II) chloride hexahydrate ($CoCl_2 \cdot 6H_2O$)	Roth, Karlsruhe
Coomassie Brilliant Blue R-250 (CBB)	Applichem, Darmstadt
Copper sulfate heptahydrate ($CuSO_4 \cdot 5H_2O$)	Applichem, Darmstadt
D-Mannitol	Applichem, Darmstadt
Desoxyribonucleoside triphosphate (dNTPs)	Fermentas, St. Leon-Rot
Dexamethasone (DEX)	Sigma-Aldrich, Munich
Dimethylformamide (DMF)	Roth, Karlsruhe
Dimethyl sulfoxide (DMSO)	Roth, Karlsruhe
Disodium phosphate dihydrate ($Na_2HPO_4 \cdot 2H_2O$)	Applichem, Darmstadt
Dithiothreitol (DTT)	Sigma-Aldrich, Munich
Ethanol (EtOH)	Roth, Karlsruhe
Ethidium bromide (EtBr)	Roth, Karlsruhe
Ethylenediaminetetraacetic acid (EDTA)	Applichem, Darmstadt
FM4-64	Invitrogen, Darmstadt
Formaldehyde	Roth, Karlsruhe
Gamborg B5 Vitamins	Duchefa, Haarlem, The Netherlands
Gentamycin sulfate (Gen)	Duchefa, Haarlem, The Netherlands
Glycerol/Glycerine	Applichem, Darmstadt
Glycine	Applichem, Darmstadt
Glucose (D-)	Applichem, Darmstadt
Hydrochloric acid (HCl)	Sigma-Aldrich, Munich
Hygromycine B (Hygro)	Sigma-Aldrich, Munich
Iron(II) sulfate heptahydrate ($Fe(II)SO_4 \cdot 7H_2O$)	Applichem, Darmstadt
Isopropanol (2-Propanol, IPA)	Roth, Karlsruhe
Kanamycine (Kan)	Applichem, Darmstadt
Magnesium chloride ($MgCl_2$)	Applichem, Darmstadt
Magnesium sulfate heptahydrate ($MgSO_4 \cdot 7H_2O$)	Applichem, Darmstadt
Manganese(II) dichloride ($MnCl_2$)	Applichem, Darmstadt
MES (2-(N-morpholino)ethanesulfonic acid)	Roth, Karlsruhe
Methanol	Roth, Karlsruhe
MG132	Enzo Life Sciences, Lörrach

Monosodium phosphate (monohydrate) (NaH$_2$PO$_4$(H$_2$O))	Applichem, Darmstadt
MOPS (3-(N-morpholino)propanesulfonic acid)	Sigma-Aldrich, Munich
Murashige & Skoog Medium (MS)	Duchefa, Haarlem, The Netherlands
Myo-Inositol	Applichem, Darmstadt
Nicotinamide	Applichem, Darmstadt
Nitro blue tetrazolium (NBT)	Applichem, Darmstadt
Polyethylene glycol 4000 (PEG 4000)	Applichem, Darmstadt
Phenol	Roth, Karlsruhe
Plant agar	Duchefa, Haarlem, The Netherlands
Phenylmethylsulfonyl fluoride (PMSF)	Applichem, Darmstadt
Phosphoric acid (H$_3$PO$_4$)	Applichem, Darmstadt
Potassium acetate (KCH$_3$COO)	Roth, Karlsruhe
Potassium chloride (KCl)	Applichem, Darmstadt
Potassium dihydrogen phosphate (KH$_2$PO$_4$)	Applichem, Darmstadt
Potassium iodide (KI)	Applichem, Darmstadt
Potassium hydroxide (KOH)	Applichem, Darmstadt
Potassium nitrate (KNO$_3$)	Applichem, Darmstadt
Powdered milk	Applichem, Darmstadt
Protease Inhibitor Complete EDTA-free	Roche Diagnostics, Mannheim
Pyridoxin/HCl	Applichem, Darmstadt
Rifampicine (Rif)	Duchefa, Haarlem, The Netherlands
Sodium bi-/hydrogen carbonate (NaHCO$_3$)	Roth, Karlsruhe
Sodium carbonate (Na$_2$CO$_3$)	Roth, Karlsruhe
Sodium chloride (NaCl)	Roth, Karlsruhe
Sodium dodecyl sulfate (SDS)	Applichem, Darmstadt
Sodium hydrogen phosphate (NaH2PO4 H2O)	Roth, Karlsruhe
Sodium molybdate (Na$_2$MoO$_4$•2H$_2$O)	Applichem, Darmstadt
Silwet L-77	Roth, Karlsruhe
Spectinomycine (Spec)	Duchefa, Haarlem, The Netherlands
Sucrose	Roth, Karlsruhe
Tetramethyl ethylene diamine (TEMED)	Roth, Karlsruhe
Tetracycline (Tet)	Duchefa, Haarlem, The Netherlands
Thiamin/HCl (Vit B1)	Duchefa, Haarlem, The Netherlands
Tris (2-Amino-2-hydroxymethyl-propane-1,3-diol, THAM)	Applichem, Darmstadt
Triton X-100	Applichem, Darmstadt
Tryptone	Applichem, Darmstadt
Tween 20	Applichem, Darmstadt
Xylose (D-(+))	Roth, Karlsruhe
Yeast extract	Roth, Karlsruhe
Zinc sulfate heptahydrate (ZnSO$_4$•7H$_2$O)	Roth, Karlsruhe

Table 16. Materials and enzymes used in this study.

Name	Supplier
Millipore PVDF Membrane	Merck-Millipore, Darmstadt
Hybond ECL Nitrocellulose Membrane	GE Healthcare, Freiburg
Bio-Rad Protein Assay	Bio Rad Laboratories, Munich
Cellulase "ONOZUKA" R-10	Yakult, Japan
Complete EDTA free inhibitor cocktail	Roche, Mannheim
Gateway BP Clonase II Enzyme Mix	Invitrogen, Darmstadt
Gateway LR Clonase II Enzyme Mix	Invitrogen, Darmstadt
GeneRuler 1 kb DNA ladder	Fermentas, St. Leon-Rot
iTaq Universal SYBR Green Supermix	Bio-Rad Laboratories, Munich
JetStar 2.0 Plasmid Purification System	Genomed, Löhne
Macerozyme R-10	Yakult, Japan
QIAEX II Gel Extraction Kit	QIAGEN, Hilden
Restriction Endonuclease *Mae* III	Roche Diagnostics, Mannheim
M-MuLV Reverse Transcriptase	Fermentas, St. Leon-Rot
NucleoSpin RNA Plant Kit	Macherey-Nagel, Düren
PageRuler Plus Prestained Protein Ladder	Fermentas, St. Leon-Rot
Plasmid Miniprep Kit I	Peqlab Biotechnologie, Erlangen

Phusion High-Fidelity DNA Polymerase	New England BioLabs, Frankfurt am Main
rDNase	Macherey-Nagel, Düren
Restriction enzymes	Fermentas, St. Leon-Rot
RNaseA	Roth, Karlsruhe
Super Signal West Femto Maximum Sensitivity Substrate	Thermo Fisher Scientific, Bonn
Taq DNA Polymerase	Schwechheimer Lab, Freising
T4 DNA Ligase	Fermentas, St. Leon-Rot
Whatman paper (3 mm)	Roth, Karlsruhe
Wizard SV Gel and PCR Clean-Up System	Promega, Mannheim

Table 17. Vectors used in this study.

Vectors	Description	Reference
	Entry clones	
pDONR207	Gateway DONR, Gen^R	Invitrogen, Darmstadt
	Plant expression vectors	
pGWB414	Gateway Destination vector	Nakagawa et al. (2007)
pUBC-GFP-DEST	Gateway Destination vector	Grefen et al. (2010)
pUBN-GFP-DEST	Gateway Destination vector	Grefen et al. (2010)

Table 18. Plasmids used in this study.

Name	Description	Vectors
pCK32	pENTRY-FYVE1	pDONR207
pCK35	p35S::FYVE1	pGWB414
pCK47	pENTRY-N-FYVE1	pDONR207
pCK48	pENTRY-FYVE1-C	pDONR207
pCK51	pUBQ10::sGFP-FYVE1	pUBN-GFP-DEST
pCK52	pUBQ10::FYVE1-sGFP	pUBC-GFP-DEST
GFP-CT24	Expression vector	Nishizawa et al. (2003)

Table 19. Primers used in this study.

Primer	Description	Sequence 5'-3'
Primers for cloning		
CK40	35S::FYVE fw for GW Cloning	GGGGACAAGTTTGTACAAAAAAGCAGGCTATGCAACAGGGAGATTAC
CK41	35S::FYVE rv for GW Cloning	GGGGACCACTTTGTACAAGAAAGCTGGGTTCAATGTGCGCTAACGAG
CK131	attB Primer FYVE fw N-terminal for GW Cloning	GGGGACAAGTTTGTACAAAAAAGCAGGCTTGCAACAGGGAGATTAC
CK132	attB Primer FYVE rv C-terminal for GW Cloning	GGGGACCACTTTGTACAAGAAAGCTGGGTAATGTGCGCTAACGAG
EI1	GW Adapter Primer fw	GGGGACAAGTTTGTACAAAAAAGCAGGCT
EI2	GW Adapter Primer rv	GGGGACCACTTTGTACAAGAAAGCTGGGT
Primers for Genotyping		
CK46	FYVE 500 bp upstream fw	GGAATGTGAGCCTGCA
CK47	FYVE 500 bp downstream rv	GGACAACAGACTACATGAAAAG
CK48	FYVE 500 bp upstream fw	GCCAAGGAAACCACTG
CK49	FYVE 500 bp downstream rv	CCAATCAGACATCAGTAGGA
EI40	EI40 AMSH3 GeTy FW	AAGGCAATGGGTTGCACCCAAGTCAGAGAT

EI41	EI41 AMSH3 GeTy RV		CTGCTTTGGGATTATGAGAGTAGTGATATG	
EI511	Genotyping Primer RIKEN fw		GCGACATCACTAAACCC	
EI512	Genotyping Primer RIKEN rv		AACCCACCAACATAAGAAC	
p745	p745 AMSH3 Genotypisierung FW		AACGTCCGGAATGTGTTATTAAGTTGTC	
Ds5-2a	Genotyping Primer RIKEN LB		TCCGTTCCGTTTTCGTTTTTTAC	

Primers for map-based cloning

Name	Chr	Positi on [Mb]	FW Primer	RV Primer
NGA63	1	3,55	ACCCAAGTGATCGCCACC	AACCAAGGCACAGAAGCG
NGA692	1	28,84	AGCGTTTAGCTCAACCCTAG G	TTTAGAGAGAGAGAGCGCGG
CIW12	1	9,62	AGGTTTTATTGCTTTTCACA	CTTTCAAAAGCACATCACA
CIW1	1	18,36	ACATTTTCTCAATCCTTACTC	GAGAGCTTCTTTATTTGTGAT
NGA111	1	27,35	TGTTTTTTAGGACAAATGGCG	CTCCAGTTGGAAGCTAAAGGG
NT7I23	1	0,43	GTGTCCTTTTTTCTCAACGAT G	CATGCACGTACGATTTGTTTAA C
NF7G19	1	2,85	TCGTTGAAAACGATTAGATTG G	TTCAAAAATCGTGAGATGAAAT G
F16J7-TRB	1	3,83	TGATGTTGAGATCTGTGTGCA G	GTGTCTTGATACGCGTCGAT
T16N11	1	5,37	TTGACTGACCATTCTTATTCG TGCG	ACAAAAGGCAAAGTGGCAATA GAGG
NGA392	1	9,83	GGTGTTAAATGCGGTGTTC	TTGAATAATTTGTAGCCATG
T27K12-SP6	1	15,92	GGAGGCTATACGAATCTTGA CA	GGACAACGTCTCAAACGGTT
NGA128	1	20,63	ATCTTGAAACCTTTAGGGAGG G	GGTCTGTTGATGTCGTAAGTC G
CER452630	2	7,56	CAGTCCTCATCTTGTTTGTTT AACGGTCC	TCGTGGAAAGTATTCTTCTGTG TCCGATAC
NGA168	2	16,29	GAGGACATGTATAGGAGCCT CG	TCGTCTACTGCACTGCCG
NGA162	3	4,60	CTCTGTCACTCTTTTCCTCTG G	CATGCAATTTGCATCTGAGG
NGA6	3	23,03	ATGGAGAAGCTTACACTGATC	TGGATTTCTTCCTCTCTTCAC
CER453787	4	9,10	AGGATCCAACGGTCGATTCT CGCTAG	GTGGGTTCTTCCCAAGATTCC CCTC
CER451534	4	14,60	GCCCAGAGGAAGAAGAGCAA ACTAGC	TGGGAATTCATGAGAGAATAT GTGGGAC
CER457348	5	1,40	GGAAAACAATGAAATTGAAAG AAACGAGAG	AAACATGAAGAGAATCTTTGG AGCGAAG
22441	5	22,44	CTTTGGCGATCTTTCCTCCC	CCGGTTGAGCATCAAAGTCC

SNP Sequencing Primers

CK92	FYVE1 SNP fw II (gDNA specific)	CGATCACCGATTCAGC
CK93	FYVE1 SNP rv II (gDNA specific)	GGGGACATTACCTGACAA

Primers for *AMSH3* gene locus sequencing

CK7	Amsh3 Intron Primer fw	GCGGACAATTCAGGGTAA
CK8	Amsh3 Intron Primer rv	CGGCTGAGACATCTGATC
CK9	Amsh3 Intron2 fw	GGTAAGGATAAAAGTATCTC
CK10	Amsh3 Intron2 rv	GAGATACTTTTATCCTTACC
CK11	Amsh3 Intron5 fw	GGATGATCATTGAGAC
CK12	AMSH3 Exon 4 rv Primer	GGCCACTCAACAGCA
CK13	AMSH3 Intron 4 rv Primer	GGAAAAGGCATTGCTG

Primers for Sequencing

CK86	Seqprimer FYVE fw	GCAACCGTAGCTGGTC
CK87	Seqprimer FYVE rv	CCATCGCCATAGGAAT
CK104	(A) 35S-FYVE CDS fw	GGCTGAGACTTATGGACAA
CK105	(A) 35S-FYVE UTR rv	GAGCTCTAAGCGCTGC
CK106	(A) 35S-FYVE ATG fw	ATGCAACAGGGAGATTACA
CK107	(A) 35S-FYVE CDS rv	CCAATCTGACAAAGAACATC
35S fw	35S Promoterregion	CCCCCACTATCCTTCGCAAGACCC
pDONR201 fw	GW cloning	TCGCGTTAACGCTAGCATGGATCTC
pDONR201 rv	GW cloning	GTAACATCAGAGATTTTGAGACAC

Primers for qRT-PCR

ACT8 fw	Actin 8 fw	ATTCAGATGCCCAGAAGTCTTGTTC
ACT8 rv	Actin 8 rv	GCAAGTGCTGTGATTTCTTTGCTCA
PIN1 fw	PIN1 2stp 3	TCATCGTCTTTGTTACCGAAACT
PIN1 rv	PIN1 2stp 5	CCTCCAGGGGAATAGTAACGACA
PIN2 qRT fw	qRT-PIN2 fw Primer	GGCGAAGAAAGCAGGAAGA
PIN2 qRT rv	qRT-PIN2 rv Primer	GGTGGGTACGACGGAACA
EI541	FYVE1 qRT trunc FW	GCAACAGGGAGATTACAATTCG
EI542	FYVE1 qRT trunc RV	TCGGAGTAGGATTTTGAAATTGA
EI543	FYVE1 qRT FW	GAGAACATCACAAGATGCGAAA
EI544	FYVE1 qRT RV	GCTTCAATGTCTACCGGAGTCT

Primers were ordered at Sigma-Aldrich, Munich.

Table 20. Antibodies used in this study.

Primary antibodies

Name	Dilution	Origin	Reference
Anti-AMSH1	1:1000	rabbit	Katsiarimpa et al. (2013)
Anti-AMSH3	1: 2500	rabbit	Isono et al. (2010)
Anti-CDC2	1: 5000	rabbit	Santa Cruz Biotechnology, Heidelberg
Anti-FYVE1 (Serum 2)	1: 1000	rabbit	Eurogentec S.A., Belgium In this study
Anti-GFP	1: 2000	rabbit	Invitrogen, Darmstadt
Anti-H$^+$-ATPase	1: 2000	rabbit	Agrisera, Sweden
Anti-PIN1	1: 2000	sheep	Willige et al. (2011)
Anti-Ubiquitin (P4D1)	1: 2000	mouse	Cell Signaling Technology, USA
Anti-UGPase	1: 2000	rabbit	Agrisera, Sweden
Anti-V-ATPase	1: 2000	rabbit	Agrisera, Sweden

Secondary antibodies

Name	Dilution	Origin	Reference
Anti-rabbit IgG AP	1: 5000	goat	Sigma-Aldrich, Munich
Anti-rabbit HRP	1: 1000	goat	Sigma-Aldrich, Munich
Anti-mouse HRP	1: 2000	goat	Thermo Fisher Scientific, Bonn
Anti-goat HRP/POD	1: 1000	rabbit	Sigma-Aldrich, Munich
Anti-chicken HRP	1: 12000	rabbit	Sigma-Aldrich, Munich

Table 21. Transgenic and mutant plants used in this study.

Arabidopsis wild-type

Wild-type	Abbreviation/alias
Columbia	Col-0
Landsberg *erecta*	L*er*-0
Nossen	No-0

Arabidopsis EMS mutant lines

Name	Screen number (M2)	Ecotype	Reference
vfd1/fyve1-2	#343.36	Col-0 (GFP::δ-TIP)	This thesis; Barberon et al. (2014); Kolb et al. (2015).
vfd2	#505.9	Col-0 (GFP::δ-TIP)	This thesis.
vfd3	#621.30	Col-0 (GFP::δ-TIP)	This thesis.
vfd4	#230.13	Col-0 (GFP::δ-TIP)	This thesis.
vfd5	#327.1	Col-0 (GFP::δ-TIP)	This thesis.
vfd6	#124.15	Col-0 (GFP::δ-TIP)	This thesis.
vfd7	#202.2	Col-0 (GFP::δ-TIP)	This thesis.
vfd8	#229.13	Col-0 (GFP::δ-TIP)	This thesis.
vfd9	#251.8	Col-0 (GFP::δ-TIP)	This thesis.
vfd10	#379.13	Col-0 (GFP::δ-TIP)	This thesis.
vfd11	#399.4	Col-0 (GFP::δ-TIP)	This thesis.
vfd12	#444.7	Col-0 (GFP::δ-TIP)	This thesis.
vfd13	#491.2	Col-0 (GFP::δ-TIP)	This thesis.

Arabidopsis mutant lines

Name		Ecotype	Locus	Reference
amsh1-1	CSHL_ET8678	Col-0	AT1G48790	Katsiarimpa et al. (2014)
amsh3-1	WiscDsLox412D09	Col-0	AT4G16144	Isono et al. (2010)
fyve1-1	15-1960-1; pst18264	No-0	AT1G20110	This thesis; Barberon et al. (2014);

Arabidopsis transgenic lines

Line	Abbreviaton	Ecotype	Reference
GFP::δ-TIP		Col-0	Cutler et al. (2000)
amsh1 (DEX:35S:AMSH1)		Col-0	Isono, Freising
amsh2 (DEX:35S:AMSH2)		Col-0	Isono, Freising
WT/p35S::FYVE1	WT/pCK35	Col-0 (GFP::δ-TIP)	This thesis; Kolb et al. (2015)
vfd1/p35S::FYVE1	*vfd1*/pCK35	Col-0 (GFP::δ-TIP)	This thesis; Kolb et al. (2015)
WT/pUBQ10::GFP-FYVE1	WT/pCK51 GFP-FYVE1	No-0	This thesis; Barberon et al. (2014); Kolb et al. (2015)
fyve1-1/ pUBQ10::GFP-FYVE1	*fyve1-1*/pCK51	No-0	This thesis; Barberon et al. (2014); Kolb et al. (2015)
WT/GFP-CT24		No-0	This thesis; Kolb et al. (2015)
fyve1-1/GFP-CT24		No-0	This thesis; Barberon et al. (2014)
RFP- ARA7		Col-0	Ueda et al. (2004)
CLC-mKO		Col-0	Karasawa et al. (2004)
RFP- SYP61		Col-0	Uemura et al. (2012)
pin1/pPIN1::PIN1-RFP	PIN1-RFP	Col-0	Melina Zourelidou, unpublished
pPIN2::PIN2-GFP	PIN2-GFP	Col-0	Abas et al. (2006) Zourelidou, Freising

---

Table 22. List of used software.

Name	Version	Company
Microsoft Office	2007	Microsoft, Unterschleißheim
ImageJ	2.0.0	NIH, Bethesda, USA
cellSens Dimension		Olympus, Hamburg
Geneious Pro	5.3.6	Biomatters Ltd., New Zealand
Fluoview		Olympus, Hamburg
Adobe Photoshop CS3 Extended	10.0	Adobe Systems, München
Adobe Illustrator CS3	13.0.0	Adobe Systems, München
EndNote	X7.1	Thomson Reuters, München

Table 23. ESCRT complexes and subunits and their homologs and synonyms in budding yeast, human and Arabidopsis. Modified after Winter and Hauser, 2006.

ESCRT complex	Yeast	Mammals	Plants
ESCRT-0	Vps27p/Sst4p	HRS/HGS	TOM1-like?
	Hse1p	STAM1,2	
ESCRT-I	Vps23p/Stp22p/Sst6p	VPS23/TSG101	VPS23A,B (putative)
	Vps28p	VPS28	VPS28A,B (putative)
	Vps37p/Srn2p	VPS37A,B,C,D	VPS37A,B (putative)
	Mvb12p	MVB12a/MVBB/UBAP1	
ESCRT-II	Vps22p/Snf8p/Dot2p	VPS22/EAP30	VPS22 (putative)
	Vps25p	VPS25/EAP20	
	Vps36p	VPS36/EAP45	VPS36 (putative)
ESCRT-III	Vps2p/Did4p/Chm2p	VPS2A,B/CHMP2A,B	VPS2.1, 2.2, 2.3
	Vps20p/Chm6p	VPS20/CHMP6	
	Vps24p	VPS24/CHMP3	VPS24.1, 24.2
	Vps32p/Snf7p	SNF7A,B,C/CHMP4A,B,C	
	Vps60p/Chm5p	VPS60/CHMP5	
	Vps46p/Did2p/Chm1p	DID2A,B/CHMP7,CHMP1A,B	CHMP1A,B
	Ist1p	IST1	
Vps4-Vta1	Vps4p	SKD1,2/VPS4A,B	VPS4/SKD1
	Vta1p	VTA1/LIP5	
DUBs	Doa4p/UBPs	UBPY	
	AMSH/Sst2	AMSH	AMSH1, AMSH3
		AMSH-LP	

Table 24. List of all custom generated and used primers.

Primer	Sequence 5'-3'	Description
CK1	AAAAAGCAGGCTTGGCGACGAGAAGACGTAC	attB1 fw Primer for N-terminal tag fusion (adapter PCR), RabG3a.1
CK2	AGAAAGCTGGGTTCAGCAAGCGCAACCACC	attB2 rv Primer for N-terminal tag fusion (adapter PCR), RabG3a.1
CK3	AAAAAGCAGGCTTGGCTTCTCGGCGG	attB1 fw Primer for N-terminal tag fusion (adapter PCR), RabG3c.1
CK4	AGAAAGCTGGGTTTAGCATTCGCACCCAGTTG	attB2 rv Primer for N-terminal tag fusion (adapter PCR), RabG3c.1
CK5	AAAAAGCAGGCTTGCCTTCTCGTAGAAGAA	attB1 fw Primer for N-terminal tag fusion (adapter PCR), RabG3e.1
CK6	AGAAAGCTGGGTTCAGCATTCACATCCTGTTG	attB2 rv Primer for N-terminal tag fusion (adapter PCR), RabG3e.1
CK7	GCGGACAATTCAGGGTAA	Amsh3 Intron Primer fw
CK8	CGGCTGAGACATCTGATC	Amsh3 Intron Primer rv
CK9	GGTAAGGATAAAAGTATCTC	Amsh3 Intron2 fw
CK10	GAGATACTTTTATCCTTACC	Amsh3 Intron2 rv
CK11	GGATGATCATTGAGAC	Amsh3 Intron5 fw
CK12	GGCCACTCAACAGCA	AMSH3 Exon 4 rv Primer
CK13	GGAAAAGGCATTGCTG	AMSH3 Intron 4 rv Primer
CK14	GGTCTAGAATGCCGATCAGAAACATCG	TipF XbaI modified for Gamma-TIP CDS fw
CK15	GGGGATCCGTAGTCTGTGGTTGGGAGC	TipR BamHI modified for Gamma-TIP CDS rv
CK16	AAAAAGCAGGCTTGGAAAAAACAAAGC	attB1 fw Primer for N-terminal tag fusion (adapter PCR), RabG1
CK17	AGAAAGCTGGGTTCAGCATGAACAACGGC	attB2 rv Primer for N-terminal tag fusion (adapter PCR), RabG1
CK18	AAAAAGCAGGCTTGGATTCTTTGAAG	attB1 fw Primer for N-terminal tag fusion (adapter PCR), RabG2
CK19	AGAAAGCTGGGTTCAGCAAGCACAACC	attB2 rv Primer for N-terminal tag fusion (adapter PCR), RabG2+RabG3b
CK20	AAAAAGCAGGCTTGTCGACGCGAAGACG	attB1 fw Primer for N-terminal tag fusion (adapter PCR), RabG3b
CK21	AAAAAGCAGGCTTGTCTTCTCGCCGGAGAG	attB1 fw Primer for N-terminal tag fusion (adapter PCR), RabG3d
CK22	AGAAAGCTGGGTTTAGCATTCACACCC	attB2 rv Primer for N-terminal tag fusion (adapter PCR), RabG3d+RabG3f
CK23	AAAAAGCAGGCTTGCCGTCCCGTAGACG	attB1 fw Primer for N-terminal tag fusion (adapter PCR), RabG3f
CK24	AAGGGGGTACCATTGTACCGGGATTCTTTG	pFYVE-KpnI fw (endogenes Konstrukt)
CK25	AAGGGGTCGACCGCTGAATCGGTGATC	pFYVE-SalI rv (endogenes Konstrukt)

CK26	AAGG<u>GTCGAC</u>ATGTACCCATACGACGTTCCT	3xHA-ECFP-SalI fw (endogenes Konstrukt)
CK27	AAGG<u>CCATGG</u>CTTGTACAGCTCGTCCATG	3xHA-ECFP-NcoI rv (endogenes Konstrukt)
CK28	AAGG<u>CCATGG</u>TTGCAACAGGGAGATTACA	FYVEter-NcoI fw (endogenes Konstrukt)
CK29	AAGG<u>GAGCTC</u>GGTACACCATTGTAGCACAG	FYVEter-SacI rv (endogenes Konstrukt)
CK30	AAGG<u>GGTACC</u>GTGGAACGCATCGCT	pENTH-KnpI fw (endogenes Konstrukt)
CK31	AAGG<u>GTCGAC</u>GAAGGTAATCAAATCTGGTAAC	pENTH-SalI rv (endogenes Konstrukt)
CK32	AAGG<u>GTCGAC</u>TACCCATACGACGTTCCT	3xHA-ECFP-SalI fw (endogenes Konstrukt)
CK33	AAGG<u>CCATGG</u>TTA CTTGTACAGCTCGTCCATG	3xHA-ECFP-NcoI rv (endogenes Konstrukt)
CK34	AAGG<u>CCATGG</u>TTGCAACTTGATCAGATTCA	ENTHter-NcoI fw (endogenes Konstrukt)
CK35	AAGG<u>CTGCAG</u>CCAATAAATTTTCACCATGC	ENTHter-PstI rv (endogenes Konstrukt)
CK36	AAGG<u>GGTACC</u>GTGGCTGCTGGCTC	pVAMP724-KnpI fw (endogenes Konstrukt)
CK37	AAGG<u>GTCGAC</u>GAGTCGCCACCGAGTAT	pVAMP724-SalI rv (endogenes Konstrukt)
CK38	AAGG<u>CCATGG</u>TTGGGTCAAGAATCGTTTAT	VAMP724ter-NcoI fw (endogenes Konstrukt)
CK39	AAGG<u>CTGCAG</u>TGCAAAGCTGTGTTGC	VAMPter-PstI rv (endogenes Konstrukt)
CK40	GGGG<u>ACAAGT TTGTAC</u>**AAAAAA**GCAGGCT**ATG**CAACAGGGAGATTAC	35S::FYVE fw für GW Cloning
CK41	GGGG<u>ACCAC</u>**TTTGTA**CAAGAAAGCTGGGT**TCA**ATGTGCGCTAACGAG	35S::FYVE rv für GW Cloning
CK42	GGGG<u>ACAAGT TTGTAC</u>**AAAAAA**GCAGGCT**ATG**AAGCTGTGGAAACGG	35S::ENTH fw für GW Cloning
CK43	GGGG<u>ACCAC</u>**TTTGTA**CAAGAAAGCTGGGT**TTA**GAAGGTAATCAAATC	35S::ENTH rv für GW Cloning
CK44	GGGG<u>ACAAGT TTGTAC</u>**AAAAAA**GCAGGCT**ATG**GGTCAAGAATCGTTT	35S::AtVAMP724 fw für GW Cloning
CK45	GGGG<u>ACCAC</u>**TTTGTA**CAAGAAAGCTGGGT**TCA**ATCCGTGCAATTAAA	35S::AtVAMP724 rv für GW Cloning
CK46	GGAATGTGAGCCTGCA	FYVE 500 bp upstream Genotypisierungsprimer fw
CK47	GGACAACAGACTACATGAAAAG	FYVE 500 bp downstream Genotypisierungsprimer rv
CK48	GCCAAGGAAACCACTG	FYVE 500 bp upstream Genotypisierungsprimer fw
CK49	CCAATCAGACATCAGTAGGA	FYVE 500 bp downstream Genotypisierungsprimer rv
CK50	GCATGAAACCGTGTGG	ENTH 500 bp upstream Genotypisierungsprimer fw
CK51	GCGAGATCTTCTCCTTGA	ENTH 500 bp downstream Genotypisierungsprimer rv
CK52	CCAGTAGCCAGAAGATCTCA	ENTH 500 bp upstream Genotypisierungsprimer fw
CK53	CCAGCTTCTTGTGCG	ENTH 500 bp downstream Genotypisierungsprimer rv
CK54	GGGAGAGATTGAAAGCAA	ENTH Homolog 500 bp upstream Genotypisierungsprimer fw
CK55	CCATGAAGAAGCATTAAGG	ENTH Homolog 500 bp downstream Genotypisierungsprimer rv
CK56	CCACAAAACATCCAGATTC	CK56 At1g61690 fw

		Genotypisierungsprimer SALK
CK57	CGTTCAAAATTCCAAGATT	CK57 At1g61700 rv Genotypisierungsprimer SALK
CK58	GCAGCCTCTAGTTCCTTCT	CK58 At1g61690 fw Genotypisierungsprimer SALK
CK59	CGCGATCTTTAGATTCTTAGTT	CK59 At1g61690 rv Genotypisierungsprimer SALK
CK60	CGGACAGAACTAAATCGAA	CK60 WiscDsLoxHs161_10G fw
CK61	GCCCGTAAGGAGTGTAATT	CK60 WiscDsLoxHs161_10G rv
CK64	ATGTTGGAGAAGATCGGA	RT-PCR Primer fw für FYVE Homolog CDS
CK65	TCAACTTGAAGCAAGAGC	RT-PCR Primer rv für FYVE Homolog CDS
CK68	GATTCATCGTCTCCGTG	RT-PCR Primer fw für ENTH Homolog CDS
CK69	CGAAAATCTCCCATTTGT	RT-PCR Primer rv für ENTH Homolog CDS
CK70	GGGTCCCAAAATCATACA	Seq Primer fw pJET-FYVEgen+ter Mitte 1
CK71	CCCAATCCTTTTTTCTTCT	Seq Primer fw pJET-FYVEgen+ter Mitte 2
CK72	CCCTTCTCAAAGTAAGTGCT	RT-PCR Primer rv für FYVE Homolog CDS II
CK73	CCGAAATCTGAACCACA	Seq Primer fw pJET-FYVEgen+ter Mitte 3
CK74	GCAGATCATCAGTTTCTCC	SALK_041152 Seq fw, SALK_044496C fw
CK75	GCTGCTTCAAGAACACAA	SALK_041152 Seq rv, SALK_044496C rv
CK76	GGCTCCGTCAAGTACAC	SALK_082448 Seq fw, SALK_082430 Seq fw
CK77	CCCCAACTCTTCCATCT	SALK_082448 Seq rv, SALK_082430 Seq rv
CK78	GGTTGGCATTTTATCATTG	XCP2 Exon1 fw
CK79	CCTTGCGTAGACCTCC	XCP2 Exon1 rv
CK80	GCAGAGTTCGCTTACAGG	XCP2 Exon2 fw
CK81	CGAAGACACTGTAAGATGCT	XCP2 Exon2 rv
CK82	GCACACATCCACCCTATT	ZIB Exon1 fw
CK83	CGCATCAAGCTCATCTC	ZIB Exon1 rv
CK84	GCTCAGAGGTGTTGTTTG	ZIB Exon2 fw
CK85	CCACCATCGCCACT	ZIB Exon2 rv
CK86	GCAACCGTAGCTGGTC	Seqprimer FYVE fw
CK87*	CCATCGCCATAGGAAT	Seqprimer FYVE rv (* non functional)
CK88	CCATTGCTCATCAGACC	Seqprimer RDR1 fw
CK89	GGATTCCCTAATGGTGTG	Seqprimer RDR1 rv
CK90	GGATTGTCATGTGCCTTA	Seqprimer MATE fw
CK91	CCAAAATGTGAAGGCAT	Seqprimer MATE rv
CK92	CGATCACCGATTCAGC	Seqprimer FYVE SNP fw II (gDNA spezifisch)
CK93	GGGGACATTACCTGACAA	Seqprimer FYVE SNP rv II (gDNA spezifisch)
CK94	ATGGCTCTTTCTTCACCTT	XCP2 ATG fw
CK95	GCCGCTATAGAACTGGAA	XCP2 Exon3 rv
CK96	GGAGCGATCACACTTCA	MATE Promotor fw

CK97	CGTTTCCATGTTTAACCAT	MATE Exon2 rv
CK98	GCCAGTTCACGTCACTT	EAP Exon1 fw
CK99	CTCAAAAGTGGCTGACTTAA	EAP Promotor rv
CK100	GGATGCTCGGTTGTTG	TCP Exon5 fw
CK101	CGATATCCAAGGTGCC	TCP Exon8 rv
CK102	GGTGTTTGATGATTTAGGC	TCP Intron3 fw
CK103	CCTGCATTTGAATTGCT	TCP Exon5 rv
CK104	GGCTGAGACTTATGGACAA	(A) 35S-FYVE CDS fw
CK105	GAGCTCTAAGCGCTGC	(A) 35S-FYVE UTR rv
CK106	ATGCAACAGGGAGATTACA	(A) 35S-FYVE ATG fw
CK107	CCAATCTGACAAAGAACATC	(A) 35S-FYVE CDS rv
CK108	ATGGGAGACGCAGAGA	MATE RT-PCR Primer ATG fw
CK109	TTACGTTCCATAGGCCA	MATE RT-PCR Primer TAA rv
CK110	ATGGAGGAAGATCGTGG	TCP11 RT-PCR Primer ATG fw
CK111	CCTTACAAAGCACCTCCA	TCP11 RT-PCR Primer Exon5 rv
CK112	ATGTCTCCTAACTACTCCTTCTTC	EAP RT-PCR Primer ATG fw
CK113	TTAGCATTTATTAGACGAGAATCC	EAP RT-PCR Primer TAA rv
CK114	GGATACCAGTCCGACAAC	SNP UBC34 fw
CK115	CCAAACCATTATCCTCAATT	SNP UBC34 rv
CK116	GGTTTCAGTGTTGGCTC	SNP AAE1 fw
CK117	CGTGTTTCCTCTGAAGAC	SNP AAE1 rv
CK118	GGAACTTGCGAGATGC	SNP XCP2 fw
CK119	GCTTTAATTTCTTCATGGTTG	SNP XCP2 rv
CK120	GGTGAAAAGCTCATTGG	SNP ZIB fw
CK121	GGTGTACCTCCAACGG	SNP ZIB rv
CK122	GGATCCGTCCTGTGC	SNP BYPASS fw
CK123	GCTCCTCCAACGCC	SNP BYPASS rv
CK124	GGTTGATAACGCACAACA	SNP SMO2 fw
CK125	CCTCGTCTTCATGGAGA	SNP SMO2 rv
CK126	GGAGGCTGATGATGAAG	SNP ENTH fw
CK127	GGACTCGGATCCATGT	SNP ENTH rv
CK128	GGTTGTGGACACAGCA	SNP EAP fw
CK129	GCATTGCAACAACAAGTAC	SNP EAP rv
CK130	GCAGAAGAACGGCATC	RT-PCR B tag fw
CK131	GGGG<u>ACAAGT TTGTAC</u>**AAAAAA**GCAGGCT**TG**CAACAGGGAGATTAC	attB Primer FYVE fw N-terminal für GW Cloning
CK132	GGGG<u>ACCAC</u>**TTTGTA**CAAGAAAGCTGGGT**A**ATGTGCGCTAACGAG	attB Primer FYVE rv C-terminal für GW Cloning
CK133	GCATGGACGAGCTGTAC	RT-PCR B tag II fw
CK134	GGTTCCGCCGATTAC	SNP Seq MaeIII fw
CK135	GG**<u>GTCGAC</u>**ATGGTGAGCAAGGGC	B1 EYFP SalI fw (endogenes Konstrukt)
CK136	GG**<u>CCATGG</u>**CTTGTACAGCTCGTCCAT	B1 EYFP NcoI rv (endogenes Konstrukt)
CK140	GGCATTACTCAACCTATTAACAGGCTTTAT	Y2H ΔFYVE Teil 1 rv
CK141	ATAAAGCCTGTTAATAGGTTGAGTAATGCC	Y2H ΔFYVE Teil 2 fw
CK143	GGGG<u>ACAAGT TTGTAC</u>**AAAAAA**GCAGGCTGTACCGGGATTCTTTGC	GW FYVE promotor fw

| CK144	ATCTCCCTGTTGCATCGCTGAATCGGTGATCG	Overlap PCR proFYVE rv
CK145	CGATCACCGATTCAGCG**ATG**CAACAGGGAGAT	Overlap PCR FYVE ATG fw
CK146	**AAGCGGGTAGGAAGATCAATGTGCGCTAAC**	Overlap PCR FYVE TGA-ter rv
CK147	**GTTAGCGCACATTGATCTTCCTACCCGCTT**	Overlap PCR FYVE TGA-ter fw
CK148	GGGG<u>ACCAC</u>**TTTGTA**CAAGAAAGCTGGGT GAAAGGAAAGCTTAAAAATTTG	GW FYVE ter rv
CK149	GGGG<u>ACCAC</u>**TTTGTA**CAAGAAAGCTGGGT **ATGTGCGCTAACG**	GW FYVE CDS no stop rv
CK150	GGACGATCCATTAGCTTTT	RT-PCR pCK51 fw
CK151	GGTTCAATGTGCGCTAA	RT-PCR pCK51 rv
CK152	GGAAACCACTGGCAG	RT-PCR pCK52 fw
CK153	CCATGCCGAGAGTGAT	RT-PCR pCK52 rv
CK154	GGGCTGTTTTTCCCA	Actin2 RT-PCR Primer fw
CK155	GGCCTTGGAGATCCA	Actin2 RT-PCR Primer rv
CK156	CGAGTGTGATGACGAGAC	PIN2 Exon5 Primer fw
CK157	CCATAGAAAGGTTTTGGAGA	SYP43 Exon3 Primer rv
CK158	CGCACACATCACCATAC	SYP43 Exon8 Primer rv
CK159	GGCGAGGAGCTGTTC	GFP fw
CK160	GCCCTCAAAATTGAAGAC	CT24 rv
CK161	GGCGAAGAGCTGATTAAG	RFP fw
CK162	CCCCAGTTTGCTAGGG	RFP rv
CK163	GGTAGGAAGATCAATGTGC	RT-PCR rv FYVE1 Stop
CK164	CCAGAGGTTTGATGCTG	RT-PCR rv RIKEN mut
CK165	CTGATACGGAGCAGTAGAATC	RT-PCR rv EMS mut
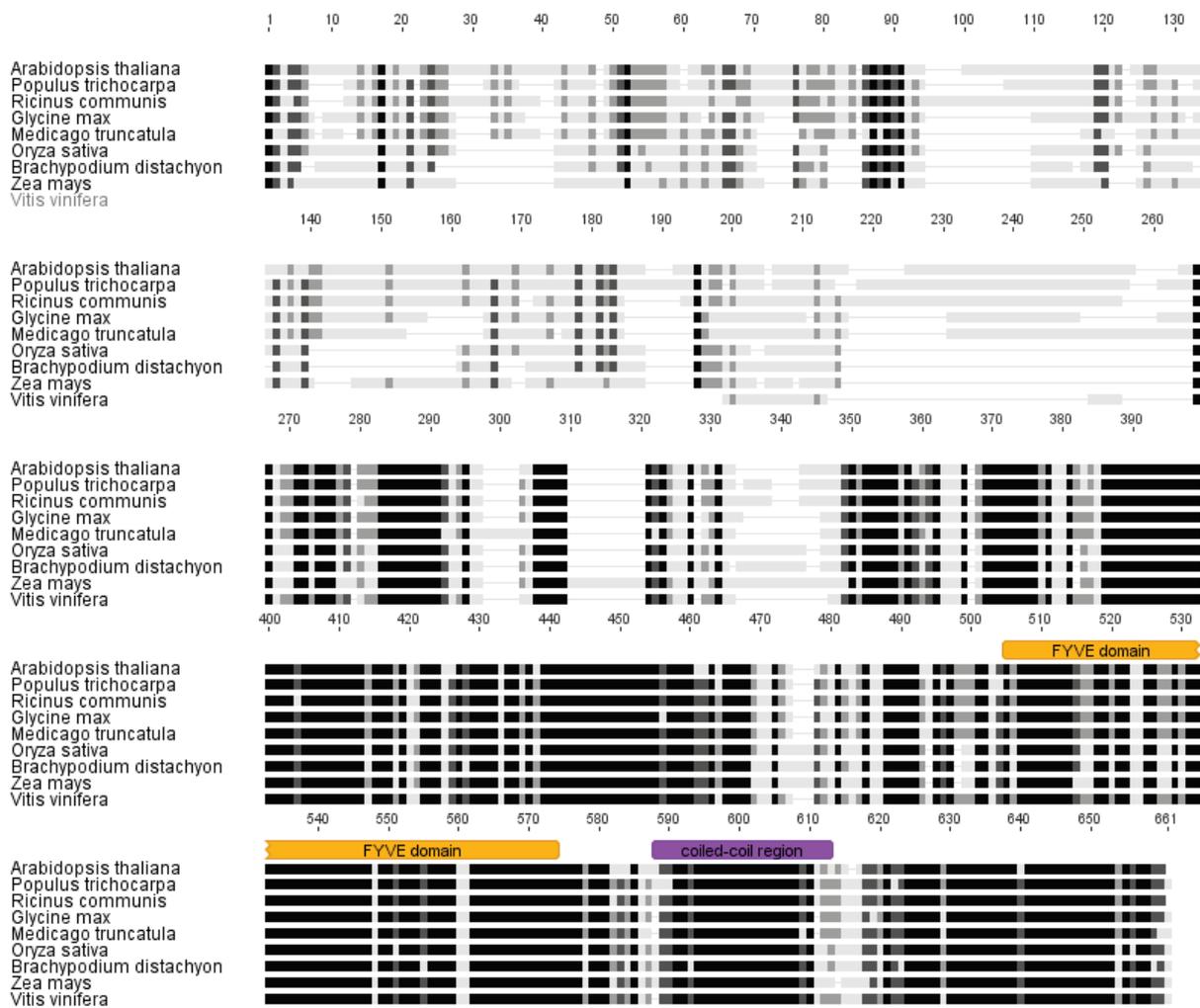
Figure 45. FYVE1 is a unique FYVE domain-containing protein in plants.

Curriculum Vitae

Cornelia Kolb

Persönliche Daten

Adresse	Bachstr. 4, 85139 Wettstetten
Staatsangehörigkeit	deutsch
Geburtsdatum und -ort	28.11.1984 in Ingolstadt, Deutschland

Bildungsgang

seit 02/2016	**Arbeitsvermittlerin im Arbeitgeber-Service** Agentur für Arbeit, Ingolstadt
06/2015 - 10/2015	**Fachseminar** "Life Science Management" ATV Ausbildung Training Vernetzung GmbH, München
05/2011 – 10/2014	**Doktorandin (Wissenschaftliche Mitarbeiterin)** „Identification and characterization of *vacuole fusion defective* (*vfd*) mutants" Prof. Dr. Claus Schwechheimer, Systembiologie der Pflanzen, Wissenschaftszentrum Weihenstephan, Technische Universität München
06/2009 – 03/2010	**Diplomarbeit** „Entwicklung von Transformationsvektoren zur Induzierung von RNA-Interferenz in der Kieselalge *Phaeodactylum tricornutum*" Prof. Dr. Peter Kroth, Pflanzen-Ökophysiologie, Universität Konstanz
10/2004 – 03/2010	**Diplomstudium** im Fach **Biologie** Fachbereich Biologie, Universität Konstanz Studienschwerpunkte: Pflanzenphysiologie, Phytopathologie, Ökotoxikologie, Molekulare Mikrobiologie
06/2004	**Allgemeine Hochschulreife** (Abitur) Christoph-Scheiner-Gymnasium, Ingolstadt

Persönliche Fähigkeiten

Sprachkenntnisse	Deutsch (Muttersprache) Englisch (Verhandlungssicher) Japanisch (Grundkenntnisse) Russisch (Grundkenntnisse) Latein (Großes Latinum)
Sonstige	Ersthelfer am Lehrstuhl für Systembiologie (11/2013 - 10/2014)

Engagement

05/2011 – 10/2014	Mitglied im **Organisationskomitee der Studenteninitiative** des Sonderforschungsbereichs SFB924 (Deutsche Forschungsgemeinschaft)

Curriculum Vitae

Cornelia Kolb

Publikationen

Kolb, C.; Nagel, M.-K.; Kalinowska, K.; Hagmann, J.; Ichikawa, M.; Anzenberger, F.; Alkofer, A.; Sato, M. H.; Schmid, M.; Falter-Braun, P.; Isono, E.:
FYVE1 is essential for vacuole biogenesis and intracellular trafficking in *Arabidopsis thaliana* (Plant Physiology 2015)

Barberon, M.; Dubeaux, G.; Kolb, C.; Isono, E.; Zelazny, E.; Vert, G.:
Polarization of IRON-REGULATED TRANSPORTER 1 (IRT1) to the plant-soil interface plays crucial role in metal homeostasis (PNAS 2014)

Wettstetten, den 28.02.2017

Cornelia Kolb